



HAL
open science

A review of coarse mineral dust in the Earth system

Adeyemi Adebiyi, Jasper F Kok, Benjamin J Murray, Claire L Ryder,
Jan-Berend W Stuut, Ralph A Kahn, Peter Knippertz, Paola Formenti,
Natalie M Mahowald, Carlos Pérez García-Pando, et al.

► To cite this version:

Adeyemi Adebiyi, Jasper F Kok, Benjamin J Murray, Claire L Ryder, Jan-Berend W Stuut, et al.. A review of coarse mineral dust in the Earth system. *Aeolian Research*, 2023, 60, pp.100849. 10.1016/j.aeolia.2022.100849 . hal-03917173

HAL Id: hal-03917173

<https://hal.science/hal-03917173>

Submitted on 1 Jan 2023

HAL is a multi-disciplinary open access archive for the deposit and dissemination of scientific research documents, whether they are published or not. The documents may come from teaching and research institutions in France or abroad, or from public or private research centers.

L'archive ouverte pluridisciplinaire **HAL**, est destinée au dépôt et à la diffusion de documents scientifiques de niveau recherche, publiés ou non, émanant des établissements d'enseignement et de recherche français ou étrangers, des laboratoires publics ou privés.



Invited Review Article



A review of coarse mineral dust in the Earth system

Adeyemi Adebisi^{a,*}, Jasper F. Kok^b, Benjamin J. Murray^c, Claire L. Ryder^d,
Jan-Berend W. Stuut^{e,f}, Ralph A. Kahn^g, Peter Knippertz^h, Paola Formentiⁱ, Natalie
M. Mahowald^j, Carlos Pérez García-Pando^{k,l}, Martina Klose^h, Albert Ansmann^m, Bjørn
H. Samsetⁿ, Akinori Ito^o, Yves Balkanski^p, Claudia Di Biagioⁱ, Manolis N. Romanias^q,
Yue Huang^b, Jun Meng^b

^a Department of Life and Environmental Sciences, University of California, Merced, CA, USA

^b Department of Atmospheric and Oceanic Sciences, University of California, Los Angeles, CA, USA

^c School of Earth and Environment, University of Leeds, Leeds LS2 9JT, United Kingdom

^d Department of Meteorology, University of Reading, Reading RG6 6BB, United Kingdom

^e NIOZ-Royal Netherlands Institute for Sea Research, Texel, The Netherlands

^f VU – Vrije Universiteit Amsterdam, Faculty of Science, Department of Earth Sciences, The Netherlands

^g Earth Sciences Division, NASA Goddard Space Flight Center, Greenbelt, MD, USA

^h Karlsruher Institut für Technologie, Institut für Meteorologie und Klimaforschung, Karlsruhe, Germany

ⁱ Université Paris Cité and Univ Paris Est Creteil, CNRS, LISA, F-75013 Paris, France

^j Earth and Atmospheric Sciences Department, Cornell University, Ithaca, NY, USA

^k Barcelona Supercomputing Center, Barcelona, Spain

^l ICREA, Catalan Institution for Research and Advanced Studies, Barcelona, Spain

^m Leibniz Institute for Tropospheric Research, Leipzig, Germany

ⁿ CICERO Center for International Climate Research, Oslo, Norway

^o Yokohama Institute for Earth Sciences, JAMSTEC, Yokohama, Kanagawa 236-0001, Japan

^p Laboratoire des Sciences du Climat et de l'Environnement, CEA-CNRS-UVSQ, IPSL, Gif-sur-Yvette, France

^q Institut Mines-Télécom Nord Europe, Univ. Lille, Center for Energy and Environment, F-59000 Lille, France

ARTICLE INFO

Keywords:

Mineral dust

Coarse dust

Size distribution

Climate

Earth system

ABSTRACT

Mineral dust particles suspended in the atmosphere span more than three orders of magnitude in diameter, from $<0.1 \mu\text{m}$ to more than $100 \mu\text{m}$. This wide size range makes dust a unique aerosol species with the ability to interact with many aspects of the Earth system, including radiation, clouds, hydrology, atmospheric chemistry, and biogeochemistry. This review focuses on coarse and super-coarse dust aerosols, which we respectively define as dust particles with a diameter of $2.5\text{--}10 \mu\text{m}$ and $10\text{--}62.5 \mu\text{m}$. We review several lines of observational evidence indicating that coarse and super-coarse dust particles are transported farther than previously expected and that the abundance of these particles is substantially underestimated in current global models. We synthesize previous studies that used observations, theories, and model simulations to highlight the impacts of coarse and super-coarse dust aerosols on the Earth system, including their effects on dust-radiation interactions, dust-cloud interactions, atmospheric chemistry, and biogeochemistry. Specifically, coarse and super-coarse dust aerosols produce a net positive direct radiative effect (warming) at the top of the atmosphere and can modify temperature and water vapor profiles, influencing the distribution of clouds and precipitation. In addition, coarse and super-coarse dust aerosols contribute a substantial fraction of ice-nucleating particles, especially at temperatures above $-23 \text{ }^\circ\text{C}$. They also contribute a substantial fraction to the available reactive surfaces for atmospheric processing and the dust deposition flux that impacts land and ocean biogeochemistry by supplying important nutrients such as iron and phosphorus. Furthermore, we examine several limitations in the representation of coarse and super-coarse dust aerosols in current model simulations and remote-sensing retrievals. Because these limitations substantially contribute to the uncertainties in simulating the abundance and impacts of coarse and super-coarse dust aerosols, we offer some recommendations to facilitate future studies. Overall, we conclude that an accurate

* Corresponding author.

E-mail address: aaadebiyi@ucmerced.edu (A. Adebisi).

<https://doi.org/10.1016/j.aeolia.2022.100849>

Received 23 August 2022; Received in revised form 27 November 2022; Accepted 29 November 2022

Available online 16 December 2022

1875-9637/© 2022 The Author(s). Published by Elsevier B.V. This is an open access article under the CC BY license (<http://creativecommons.org/licenses/by/4.0/>).

representation of coarse and super-coarse properties is critical in understanding the impacts of dust aerosols on the Earth system.

1. Introduction

Mineral dust or desert dust aerosols are suspended soil particles in the atmosphere (Choobari et al., 2014; Knippertz and Stuut, 2014). They account for more than two-thirds of the global aerosol mass and approximately one-quarter of the solar radiation extinguished by all aerosol particles in the atmosphere (e.g., Textor et al., 2006; Kinne et al., 2006). As a result, mineral dust aerosols produce key impacts on several critical aspects of the Earth system (Jickells et al., 2005; Goudie and Middleton, 2006; Shao et al., 2011; Knippertz and Todd, 2012; Kok et al., 2012; Knippertz and Stuut, 2014; Kok et al., 2022). One such impact is that dust affects the climate system through the absorption and scattering of shortwave and longwave radiation (Tegen et al., 1996; Miller et al., 2014). At the top of the atmosphere, this interaction results in negative dust direct radiative effect (DRE; i.e., dust cools the climate system) in the shortwave and positive dust DRE (i.e., dust warms the climate system) in the longwave spectrum (Claquin et al., 1998; Satheesh and Ramanathan, 2000; Kok et al., 2017; Di Biagio et al., 2020; Adebisi and Kok, 2020). Another key impact is that dust affects the distribution and lifetime of clouds and precipitation because it can act as a cloud- or ice-nucleating particle (DeMott et al., 2003; Atkinson et al., 2013; Cziczo et al., 2013; Storelvmo, 2017; Hawker et al., 2021). Furthermore, dust can also alter atmospheric chemistry through its interaction with trace gases that ultimately might influence the lifetime and concentration of atmospheric greenhouse gases, such as methane and ozone (Dentener et al., 1996; Usher et al., 2003; Gaston, 2020), as well as the concentration and radiative impacts of anthropogenic aerosols (Karydis et al., 2016; Klingmüller et al., 2020). Once deposited to the surface, dust particles can stimulate biogeochemical activity in marine and terrestrial ecosystems (Jickells et al., 2005). Specifically, iron- and phosphorus-containing dust minerals can increase primary productivity, which in turn can influence the uptake of carbon dioxide from the atmosphere (Jickells et al., 2005; Mahowald et al., 2009; Jickells et al., 2014). In addition, dust particles can speed up the ocean carbon cycle by ballasting organic material towards the seafloor, thus increasing carbon export efficiency (Alldredge and Silver, 1988; van der Jagt et al., 2018).

All these various dust impacts on the Earth's system depend critically

on the size distribution of dust particles in the atmosphere. Dust sizes span more than three orders of magnitude, from $<0.1 \mu\text{m}$ to more than $100 \mu\text{m}$ in diameter (Mahowald et al., 2014; van der Does et al., 2018a; Ryder et al., 2019). Because the properties of these dust particles are size-dependent, most studies separate dust particles into different classes – broadly defined as *fine* and *coarse* dust (Whitby, 1978; Seinfeld and Pandis, 2006) – which could produce distinct impacts on the Earth system (Mahowald et al., 2014). For example (see Fig. 1), coarse dust absorbs more shortwave radiation, which could cause more atmospheric heating than fine dust (Otto et al., 2011; Ryder et al., 2018). Since coarse dust also has a substantial radiative impact in the longwave spectrum, the overall ratio of the coarse-to-fine dust in the atmosphere could determine whether dust exerts a net positive or negative direct radiative effect on the global climate system (Kok et al., 2017; Di Biagio et al., 2020; Adebisi and Kok, 2020). In addition, coarse dust dominates the deposited dust mass, especially near dust sources, and the delivery of micro-nutrients into the marine and terrestrial ecosystems, consequently influencing its biogeochemistry (Jickells et al., 2005; Yu et al., 2015). Despite the influence of dust size distribution on dust impacts, there are inconsistencies in the terminology and the diameter range currently attributed to different dust size classes across the literature (Whitby, 1978; WHO, 2006; Seinfeld and Pandis, 2006; Mahowald et al., 2014; Maynard et al., 2017).

Furthermore, dust size influences the emission and transport processes in the global dust cycle (e.g., Drakaki et al., 2022; Meng et al., 2022). The conventional pathway of dust emission primarily occurs when strong surface winds force sand particles with diameters of about or greater than $\sim 75 \mu\text{m}$ into ballistic trajectories in a process called *saltation* (Bagnold, 1941; Shao, 2001; Kok et al., 2012). The impact of these saltating particles on the surface breaks soil aggregates into smaller dust aerosols that are ejected back into the atmosphere (Marticorena and Bergametti, 1995; Shao, 2008; Kok, 2011a). These ejected dust aerosols undergo short-term or long-term suspension and get transported between a few meters to thousands of kilometers, depending on particle size and environmental conditions (Pye, 1987; Shao, 2008; Kok et al., 2012). Since larger particles experience greater gravitational fall speeds than smaller particles (e.g., Seinfeld and Pandis, 2006), the potential for the long-range transport of coarse dust particles likely

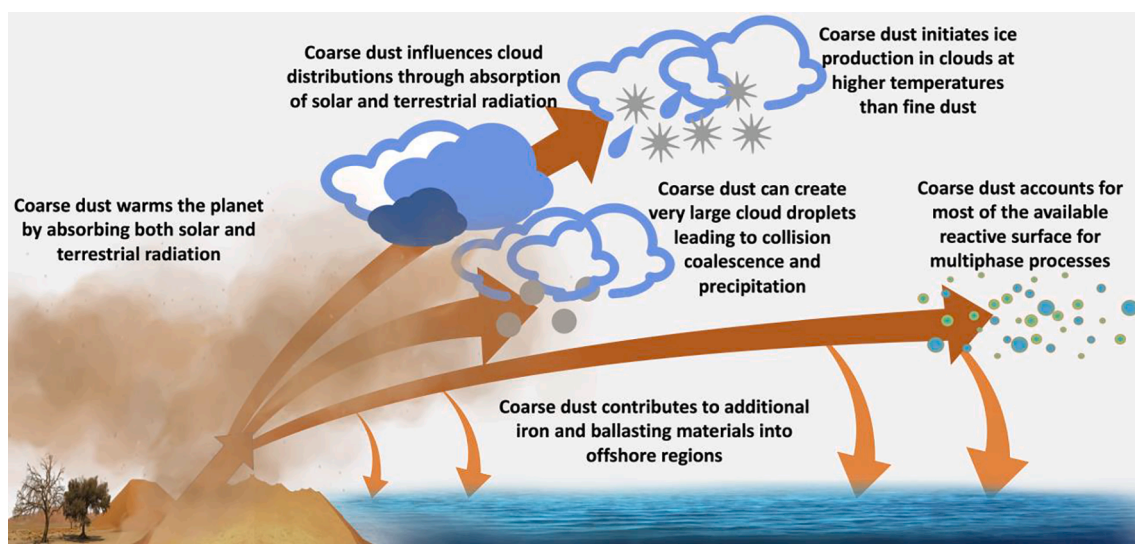


Fig. 1. Coarse dust (and super-coarse dust) impacts several aspects of the Earth system, including radiation, clouds, precipitation, atmospheric chemistry, and biogeochemistry (see details in Section 4).

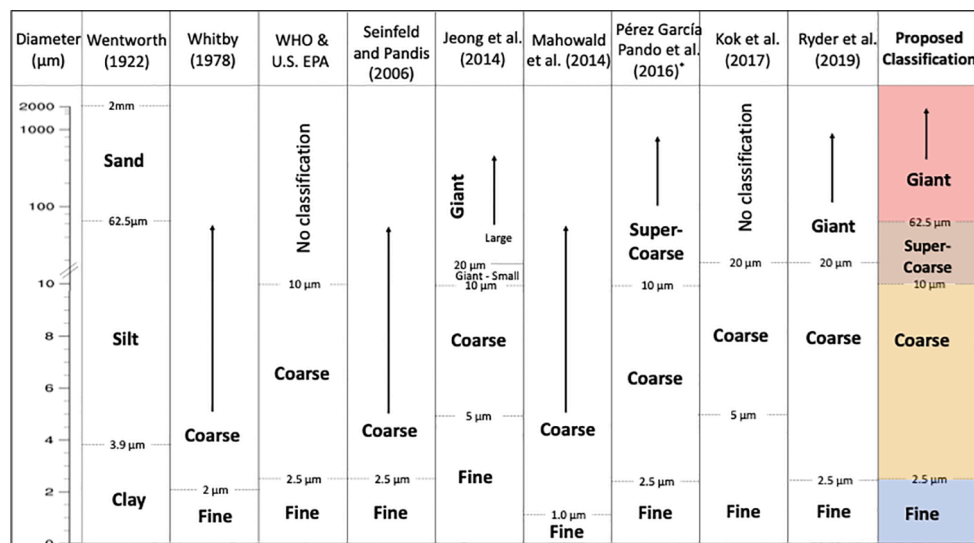


Fig. 2. Classification of dust sizes used in different studies. The last column shows the dust size classification and the geometric diameter range proposed by this review article. Note that the vertical scale is linear up to 10 µm but logarithmic afterward. Also, the WHO and U.S. EPA classifications use aerodynamic diameter for fine (PM_{2.5}) and coarse aerosols (PM₁₀), which respectively correspond to geometric diameters of ~ 1.7 and ~ 7 µm (e.g., Huang et al., 2021).

depends on favorable environmental conditions (van der Does et al., 2018a; Adebisi and Kok, 2020). These environmental conditions include strong prevailing winds in the free troposphere, strong convection, atmospheric instability, and turbulence within the boundary layer or the elevated dust layer (Ansmann et al., 2009; Knippertz and Todd, 2012; Rosenberg et al., 2014; Garcia-Carreras et al., 2015; Gasteiger et al., 2017). In addition, the shape and potential orientation of dust particles and possibly the electrification of the dust layer can also help reduce the gravitational settling speed, potentially aiding the long-range transport of coarse dust (Nicoll et al., 2011; Renard et al., 2018; Huang et al., 2020; Mallios et al., 2020).

Regardless of the conditions responsible for its long-range transport, several observational studies have indicated that there are more coarse dust aerosols in the atmosphere than represented in climate models (Betzer et al., 1988; Kandler et al., 2009; Ryder et al., 2013b, a; Jeong et al., 2014; Ansmann et al., 2017; Gasteiger et al., 2017; van der Does et al., 2018a; Adebisi and Kok, 2020). For example, dust particles up to about 30 µm were measured by aircraft-based instruments during a field campaign in the Caribbean after being transported for thousands of kilometers from the Sahara desert (Weinzierl et al., 2017). Other observational evidence, such as that taken close to the surface of the ocean, also shows that dust particles with a diameter greater than 75 µm are deposited over the North Atlantic and Pacific Oceans (Betzer et al., 1988; Jeong et al., 2014; van der Does et al., 2016, 2018a). Such long-range transport of coarse dust particles cannot be accounted for using a simple Stokes settling theory in most current climate models (Ansmann et al., 2017; Weinzierl et al., 2017; van der Does et al., 2018a). In addition, there are several reasons why particles larger than 10 µm in diameter are systematically excluded in the previous generation of climate models (e.g., Zender et al., 2003). For example, these reasons included (1) an emphasis on shortwave radiation and on aerosol-cloud interactions for which coarse dust has historically not been considered important, (2) a lack of observations compared to the thousands of stations that measure PM₁₀ (particulate matter, PM ≤ 10 µm aerodynamic diameter), and (3) a reduction in computational load since coarse particles had previously been assumed to travel much less distance than fine mode aerosols (e.g., Woodward, 2001; Mahowald et al., 2011). Because most climate models poorly represent coarse dust particles, a recent study estimated that more than three-quarters of particles larger than 5 µm in diameter are likely missing in climate models (Adebisi and Kok, 2020). This bias in the representation of simulated

dust aerosols suggests that coarse dust aerosols may have a substantially greater impact on the Earth system than previously understood (e.g., Fig. 1).

Therefore, we examine the current state of understanding of coarse dust aerosols and provide comprehensive documentation of the impacts they have on the Earth system. In addition, we also document the strengths of observing coarse dust particles and the limitations in modeling them. Although Mahowald et al. (2014) were the first to provide a review of dust size distribution, and other reviews, such as Jickells et al. (2005), Goudie and Middleton (2006), Shao et al. (2011), Kok et al. (2012), and Knippertz and Todd (2012), focused on other aspects of the dust cycle, none have focused specifically on coarse aerosols in the Earth system. We organize this review article as follows. In Section 2, we provide a comprehensive review of how dust size classes have historically been represented in the literature. To allow for consistency in future studies, we propose a uniform classification for coarse dust particles, making a justification for diameters between 2.5 µm and 10 µm. We extend this definition to include *super-coarse* and *giant* dust particles as particles with diameters between 10 and 62.5 µm and above 62.5 µm, respectively (Fig. 2). Except when otherwise noted, we, therefore, focus this review on the coarse and super-coarse dust aerosols. Consequently, in Section 3, we review the multiple lines of evidence that indicate that coarse to giant dust aerosols are more abundant in the atmosphere than accounted for in current models. Section 4 reviews the impacts of coarse and super-coarse dust aerosols on dust-radiation interactions, dust-cloud interactions, atmospheric chemistry, and biogeochemistry. Finally, Section 5 reviews the limitations in observations and modeling of coarse and super-coarse dust aerosols. We provide a summary and recommendations with key areas for future research in Section 6.

2. Representation of dust particle sizes

Although a dust particle size is characterized by its radius or diameter, a collection of dust particles is described by a dust size distribution, which is the distribution of particle numbers, surface area, volume, or mass over a particular diameter range (Seinfeld and Pandis, 2006). Because size distribution is an important dust property, its representation is critical for dust processes, such as the effects of dust on atmospheric chemistry depend primarily on the surface area distribution, and the biogeochemical effects of dust depend on the mass (or volume) size

distribution (Mahowald et al., 2014). Despite its importance, there have also been inconsistencies in the diameter range and terminologies used to classify dust particle sizes (Whitby, 1978; Seinfeld and Pandis, 2006; Mahowald et al., 2014). Part of the reason for this inconsistency in terminologies is the different ways dust diameters can be defined and measured (Reid et al., 2003a; Formenti et al., 2011b; Huang et al., 2021). In this section, we describe the representation of dust diameter types and propose a new size classification for atmospheric dust particles. Specifically, we propose new terminologies and diameter ranges to define fine, coarse, super-coarse, and giant dust in the atmosphere.

2.1. Dust diameter types

Different types of diameters have been used to describe aerosol particles in the atmosphere, including dust aerosols. This is, in part, because different measurement techniques and different disciplines describe particles using an “equivalent” diameter that is based on the properties or behaviors of the particles in a given system (Hinds, 1999; Kulkarni et al., 2011). For example, some aerosol measurement techniques utilize the particle settling velocity or scattering properties to quantify the state of the aerosols and thus define an equivalent diameter relative to these properties (Kulkarni et al., 2011). By definition, the equivalent diameter is the diameter of a sphere that corresponds to the same size of a particle with a specific property or behavior (Seinfeld and Pandis, 2006). Examples of equivalent diameters are aerodynamic equivalent diameter, mobility equivalent diameter, optical diameter, projected-area equivalent diameter, and volume-equivalent or geometric diameter.

Of these examples, four diameter types are commonly used for measurements and studies of atmospheric dust, namely the aerodynamic equivalent, optical equivalent, area-equivalent, and volume-equivalent (or geometric) diameters (Reid et al., 2003a; Formenti et al., 2011b; Mahowald et al., 2014; Huang et al., 2021). First, the aerodynamic equivalent diameter describes the diameter of a sphere with a standard density (1000 kg m^{-3}) that has the same terminal velocity as an irregularly-shaped dust particle settling under the influence of gravity (Hinds, 1999). Aerodynamic diameter is used to describe the behavior of particles in the respiratory tract (Maynard et al., 2017). Consequently, the World Health Organization (WHO) and other air-quality agencies around the world use aerodynamic diameter to define the air quality standards for pollution, namely the PM_{2.5} and PM₁₀, defined as particulate matter (PM) with an aerodynamic diameter < 2.5 and 10 μm , respectively (Suess et al., 1976; EPA, 1987, 1997; WHO, 2006). Second, the optical equivalent diameter is the diameter of a calibration sphere with given optical properties that scatter the same amount of radiation into a particular direction as an irregularly-shaped dust particle (Formenti et al., 2011b; Mahowald et al., 2014). The optical diameter is commonly used in optical particle counters – an instrument that utilizes light-scattering techniques to measure the dust size distribution. Third, the area-equivalent diameter is the diameter of a circle with the same area as an irregularly-shaped dust particle projected on a two-dimensional (2-D) image (Hinds, 1999; Reid et al., 2003a; Kandler et al., 2007; Huang et al., 2020). The area-equivalent is commonly measured using electron and light microscopy on particles collected on filters (e.g., Reid et al., 2003a; Kandler et al., 2007; Chou et al., 2008). Finally, the volume-equivalent or geometric diameter describes the diameter of a sphere with the same volume as an irregularly-shaped dust particle (Hinds, 1999). Although difficult to obtain, previous studies have used shadowing techniques to measure the third dimension and combined it with the area-equivalent information to obtain the geometric (volume-equivalent) diameter (Anderson et al., 1996; Okada et al., 2001; Reid et al., 2003a). Unlike the aerodynamic equivalent, optical equivalent, or projected-area equivalent diameter, the volume equivalent or geometric diameter is the primary diameter type used in dust modeling (Mahowald et al., 2014).

For the same dust particle, values of these diameter types could differ

widely, and the conversion from one diameter type to another is not straightforward (Reid et al., 2003a; Huang et al., 2021). This is, in part, because dust particles are usually assumed to be spherical, whereas measurements have shown that dust is highly aspherical, with typical particle length-to-width (aspect ratio) and height-to-width ratios often deviating from unity (Okada et al., 2001; Kandler et al., 2007; Chou et al., 2008; Huang et al., 2020). Furthermore, because irregularly-shaped dust particles have different aerodynamic, optical, and geometric properties than spherical particles, accurate conversion between one diameter type to another is important (Huang et al., 2021). For example, when a dust particle is represented as a triaxial ellipsoid, its drag force is higher than when the same dust is represented as a volume-equivalent sphere (Huang et al., 2020; Mallios et al., 2020). This difference in asphericity contributes to why a dust particle described by the aerodynamic diameter is, on average, 45 % larger than the same dust particle described by the geometric diameter (Huang et al., 2021). In addition, the conversion between aerodynamic diameter and geometric diameter also depends on the difference between the dust density and the density of water (Hinds, 1999). Furthermore, knowledge of dust’s index of refraction and dust shape is important for converting optical diameter to other diameter types. Thus, uncertainties in dust asphericity, dust density, and index of refraction can lead to errors in converting from one diameter type to another, particularly for coarse dust particles (e.g., Huang et al., 2021).

Since most dust modeling studies define dust in terms of its geometric diameter, we similarly use geometric diameter to represent dust particle size for the remainder of this article unless otherwise stated.

2.2. Classification of dust particle sizes

In addition to the differences in the diameter types used to describe dust particles, there are inconsistencies in the terminologies used to describe the diameter range of different dust size classes. This inconsistent terminology in the literature makes it more difficult to compare different studies of dust impacts that depend on size. Thus, a new dust size classification is required to facilitate easy comparison in future studies.

The classification of dust sizes was introduced in the early 1900s and was mostly popularized in geology, especially in sedimentology (Wentworth, 1922). Most studies of that era separated sand from dust particles and further separated dust particles into silt and clay particles based on their *grain* sizes (Grabau, 1913; Udden, 1914; Baker, 1920). For example, Baker (1920) defined sand particles as particles between 100 and 2000 μm and put the boundary between silt and clay particles at 10 μm . Wentworth (1922) presented the collective state of knowledge prior to the early 1900s and provided a generalized classification that defined sand particles between 62.5 and 2000 μm and the boundary between silt and clay dust particles at 3.9 μm (Friedman and Sanders, 1978 later provided a modified version).

Although dust particles were classified by grain sizes in geology, in the atmospheric sciences, the term dust referred to one of the aerosol species in the atmosphere. Because of this identification as an aerosol species, the dust size terminologies used in atmospheric sciences were related to the broad aerosol size modes defined as *fine* and *coarse* aerosol modes (Seinfeld and Pandis, 2006; Whitby, 1978). The fine mode was further subdivided into the Aitken (or nucleation) and accumulation modes. Earlier studies on aerosol size distributions mostly attributed the origin of this classification to the differences in aerosol formation processes and chemical composition (Willeke and Whitby, 1975; Whitby, 1978; Hering and Friedlander, 1982; Heintzenberg, 1989; John et al., 1990). These studies argued that condensation and coagulation processes that can accumulate particles together produced fine-mode aerosols, while mechanical processes, such as dust emission, produced coarse-mode aerosols (Whitby, 1978). As a result, dust particles were initially associated with coarse modes, although subsequent studies clarified that they also exist in the fine mode.

There have been widespread inconsistencies in the definition of the boundary diameter that separated the fine and coarse modes (e.g., Heintzenberg, 1989; John et al., 1990; Kulkarni et al., 2011). Before the late 1970 s, most studies defined this boundary at 2 μm (Danes, 1954; Heintzenberg, 1989; Spurny, 1998; Walton, 1954; Whitby, 1978; Willeke and Whitby, 1975). Subsequent studies re-defined the boundary diameter between fine and coarse modes to be at 1 μm (Friedlander, 2000; Mahowald et al., 2014; Ansmann et al., 2017), 2.5 μm (Seinfeld and Pandis, 2006; Zhang et al., 2013; Pérez García-Pando et al., 2016), 4 μm (e.g., Rajot et al., 2008), or at 5 μm (Kok et al., 2017; Adebisi and Kok, 2020). In addition to differences in the exact diameter between fine and coarse mode aerosols, additional discrepancies arise from differences in how that diameter was measured. As part of setting air quality standards for atmospheric aerosols, the WHO and the U.S. EPA defined fine aerosols as particles with a mean aerodynamic diameter less than or equal to 2.5 μm (also called PM_{2.5}) (EPA, 1997; WHO, 2006; Maynard et al., 2017). This diameter thus effectively separated the fine-mode from coarse-mode aerosol particles for studies involving air quality and human health (e.g., Giannadaki et al., 2014). However, this dust classification in air quality studies was adopted for aerodynamic diameter type, which is different from (and larger than) the geometric diameter commonly used in studies involving dust modeling in the Earth system (Hinds, 1999; Reid et al., 2003a; Huang et al., 2021). While potential conversion between the two diameter types is possible (e.g., Hinds, 1999; Huang et al., 2021), this inconsistency in the definition of dust diameter types further contributed to the confusion in dust size classifications between different research areas.

Similar to the lack of consensus on the boundary diameter separating fine- and coarse-mode dust aerosols, there was also no consensus on the upper limit of coarse-mode particles in atmospheric science. Most definitions of coarse mode do not include an upper diameter limit. For example, Whitby (1978) and Seinfeld and Pandis (2006) arbitrarily defined coarse mode as all particles with a diameter greater than 2 μm and 2.5 μm , respectively, with no upper diameter limit. In contrast, one of the earliest definitions for the upper diameter limit of coarse-mode particles arose from WHO and EPA's air quality standards (EPA, 1987; WHO, 2006; Maynard et al., 2017). These organizations defined coarse-mode particles as particles with an aerodynamic diameter between 2.5 and 10 μm . The 10- μm -diameter upper limit likely informed some studies in the beginning era of dust modeling, leading to the limitation of dust size range to 10 μm in some climate and chemical transport models (Zender et al., 2003; Zhao et al., 2010; Albani et al., 2014). However, 10- μm defined for the aerodynamic diameter differs from 10- μm defined for the geometric diameter. For other studies that involve dust particles larger than 10 μm , different terminologies have been used that further introduce irregularities in the dust size classification. For example, studies have termed particles larger than 10 μm as “large coarse-mode” (Weinzierl et al., 2011), “super-coarse” (Pérez García-Pando et al., 2016), “giant” particles (Jeong et al., 2014), or even “ultra-giant” (Lasher-Trapp et al., 2001). In addition, not all studies use the 10- μm -diameter upper limit for coarse-mode particles, introducing further inconsistencies in the dust size classification. For example, studies have defined the upper limit for coarse-mode particles as 20 μm (Ryder et al., 2019), 37.5 μm (Ryder et al., 2013b), 62.5 μm (Goudie and Middleton, 2001), and 75 μm (Betzer et al., 1988; van der Does et al., 2018a).

Due to these widespread inconsistencies in the definitions of dust size classes, a uniform classification is needed that will allow for consistency in future literature. To this end, we propose the following terminology for the classification of atmospheric dust particles (Fig. 2), with the diameter range defined in terms of geometric diameter (D).

Fine dust ($D < 2.5 \mu\text{m}$) – For this classification, 2.5 μm is the most common diameter range used to define fine-mode aerosols in the atmosphere (e.g., Seinfeld and Pandis, 2006). Therefore, we propose fine dust here as all airborne dust particles with a diameter less than the geometric diameter of 2.5 μm . In addition, the existing sub-class of fine mode aerosols also applies to fine dust – namely, Aitken (or nucleation)

mode dust particles are particles with a diameter $< 0.1 \mu\text{m}$, and accumulation mode dust particles are particles with a diameter between 0.1 and 2.5 μm (Seinfeld and Pandis, 2006). While this dust classification is defined for geometric diameter, it should not be confused with the aerodynamic diameter used to define PM_{2.5} adopted for air quality studies by the WHO and U.S. EPA (EPA, 1987, 1997; WHO, 2006; Maynard et al., 2017), which is equivalent to approximately 1.7 μm geometric diameter.

Coarse dust ($2.5 \leq D < 10 \mu\text{m}$) – We propose the geometric diameter of 10 μm as the upper limit for coarse dust for two reasons. First, many current climate and chemical transport models only account for dust with a diameter of up to 10 μm (Zender et al., 2003; Hurrell et al., 2013; Zhao et al., 2013). Therefore, this classification will allow for comparisons between past and future studies. The second reason we propose a 10- μm geometric diameter as the upper limit of coarse dust is that dust size distributions for particles between ~ 2.5 and 10 μm are commonly scale-invariant – that is, they follow a power-law distribution (Junge, 1963; Gillette et al., 1974; Whitby, 1978; Jaenicke, 1993; Seinfeld and Pandis, 2006; Kok, 2011a). In addition, observational studies have also suggested that normalized distributions of dust particles with a diameter of $< 10 \mu\text{m}$ remain largely unchanged even after days of transport in the atmosphere (Maring et al., 2003; Reid et al., 2008). Similar to our classification of fine dust, we also note here that our classification of coarse dust is based on geometric diameter and not the aerodynamic diameter used to define PM₁₀.

Super-coarse dust ($10 \leq D < 62.5 \mu\text{m}$) – Beyond the generic terminology of atmospheric aerosols (Whitby, 1978), we propose the term “super-coarse” dust for particles with a geometric diameter between 10 and 62.5 μm . We do so for two reasons: first, there is now increasing evidence that dust particles with a diameter greater than 10 μm and up to about 60 μm consistently undergo long-range transport beyond what can be explained by Stokes settling theory alone (Reid et al., 2003a; Clarke et al., 2004; McConnell et al., 2008; Wagner et al., 2009; Johnson and Osborne, 2011; Weinzierl et al., 2011, 2017; Ryder et al., 2018). Second, we propose the super-coarse dust classification and the upper diameter limit of 62.5 μm to be consistent with the grain-size classification of dust emission, which defines the diameter boundary between sand and dust particles at 62.5 μm (Wentworth, 1922; Shao, 2008; Kok et al., 2012).

Giant dust ($D > 62.5 \mu\text{m}$) – Finally, we propose “giant” dust for all atmospheric sand-sized particles with a diameter greater than 62.5 μm . Although giant dust particles have been observed mostly close to dust sources and, in some cases, at distant locations (Betzer et al., 1988; Ryder et al., 2013b; Weinzierl et al., 2017; van der Does et al., 2018a), they are unlikely to consistently undergo the type of long-range transport that is possible for coarse (2.5 – 10 μm) and super-coarse dust (10 – 62.5 μm).

3. Evidence of coarse and super-coarse dust aerosols in the Earth system

Despite the irregularities in the dust size classification and representation, several lines of evidence have indicated that coarse and super-coarse dust aerosols are abundant in the Earth system. This realization has been possible because of the recent progress in measuring the abundance and size distribution of coarse to giant dust particles, at the surface, throughout the atmosphere, and in deposition measurements. Many aspects of observing and measuring dust particles are underpinned by the basic foundations of aerosol measurement science, descriptions of which can be found in ample sources such as Kulkarni et al. (2011) and are not described here. However, several features of dust measurements require different instrumental capabilities and assumptions when processing and interpreting measurement data, and some of these aspects are summarized in this section. Section 3.1 summarizes recent lines of evidence for coarse to giant dust particles from ground-based and deposition measurements, while Section 3.2 examines

Table 1

Evidence of large particles observed since 2006 in the atmosphere and through deposition, in order of measurement date. Only measurement campaigns which measured up to at least 20 μm in diameter are included, and those with measurements in a size mode are noted with the check mark (\checkmark). “NM” indicates Not measured, “ATM” indicates atmospheric measurements, and “DEP” indicates deposition measurements.

References	Field Campaign Name	Measurement Location and Date	Measurement Type and Platform	Measurement upper size limit, μm	Size Modes Detected			
					Fine (<2.5 μm)	Coarse (2.5–10 μm)	Super-Coarse (10–62.5 μm)	Giant (>62.5 μm)
Weinzierl et al. (2009)	SAMUM-1	Morocco, May–June 2006	ATM, Aircraft	100	\checkmark	\checkmark	\checkmark	\checkmark
Formenti et al. (2011)	AMMA	Niger/Benin, June–Jul 2006	ATM, Aircraft	20	\checkmark	\checkmark	\checkmark	NM
Johnson and Osborne (2011)	GERBILS	June 2007, Mali, Mauritania	ATM, Aircraft	60	\checkmark	\checkmark	\checkmark	NM
Weinzierl et al. (2011)	SAMUM-2	Cape Verde region, Morocco, Jan–Feb 2008	ATM, Aircraft	30	\checkmark	\checkmark	\checkmark	NM
Ryder et al. (2013b,a)	Fennec	Mali, Mauritania, June 2011	ATM, Aircraft	930	\checkmark	\checkmark	\checkmark	\checkmark
Ryder et al. (2013b,a, 2019)	Fennec-SAL	Canary Islands, June 2011	ATM, Aircraft	930	\checkmark	\checkmark	\checkmark	\checkmark
van der Does et al. (2016)	TRAFFIC	North Atlantic, Oct 2012 – Oct 2013	DEP, Submarine traps	2,000	\checkmark	\checkmark	\checkmark	\checkmark
Denjean et al. (2016)	ADRIMED	Mediterranean Sea, Jun–July 2013	ATM, Aircraft	20	\checkmark	\checkmark	\checkmark	NM
Weinzierl et al. (2017)	SALTRACE	Tropical western and eastern Atlantic, Jun–Jul 2013	ATM, Aircraft	60	\checkmark	\checkmark	\checkmark	NM
Renard et al. (2018)	ChArMEX	Mediterranean Sea, June–Aug 2013	ATM, Radiosondes & drifting balloons	100	\checkmark	\checkmark	\checkmark	\checkmark ¹
van der Does et al. (2020)	DUSTTRAFFIC	North Atlantic, Barbados, Oct 2012 – Oct 2014	DEP, Submarine traps, dust buoys on land HiVol	2,000	\checkmark	\checkmark	\checkmark	\checkmark
Varga et al. (2014)		Carpathian Basin, 2013–2014	DEP, On land traps		\checkmark	\checkmark	\checkmark	\checkmark
van der Does et al. (2018a)	DUSTTRAFFIC	North Atlantic, Oct 2013 – Apr 2016	DEP, Submarine traps dust buoys	2,000	\checkmark	\checkmark	\checkmark	\checkmark
Varga (2020)		Carpathian Mountains, 2014–2018	DEP, On land traps	3,000	\checkmark	\checkmark	\checkmark	\checkmark
Ryder et al. (2018)	AER-D	Tropical Eastern Atlantic, Aug 2015	ATM, Aircraft	100	\checkmark	\checkmark	\checkmark	\checkmark
Barkley et al. (2021)		Cayenne, French Guiana, Dec 2015–Mar 2016	ATM, Ground-based High-volume sampler, Filter samples	32	\checkmark	\checkmark	\checkmark	NM
Varga et al. (2021)		Iceland, Apr 2014 – Feb 2020	DEP, On land traps	250	\checkmark	\checkmark	\checkmark	\checkmark

¹ Largest size bin spanned super-coarse and giant modes (30–100 μm).

airborne measurements higher up in the atmosphere. A summary of the studies discussed, including the measurement platforms and size modes measured, is given in Table 1. Although measurements highlighted here are limited in spatial and temporal coverages, with the majority over North Africa and North Atlantic Ocean, they are direct measurements of dust particles and describe the presence of coarse to giant dust particles in the atmosphere. In contrast, retrievals of dust sizes from remote-sensing platforms with continuous spatial or temporal coverages, such as from ground-based AERONET or satellite platforms, are accompanied by large biases and uncertainties (e.g., McConnell et al., 2008; Ryder et al., 2015), and they are not discussed in this section (see Section 5.1).

3.1. Ground-based in-situ and deposition measurements

In many ways, ground-based observations form the basis of the most accessible long-term measurement approach for dust observations. Probably the best-known and longest continuous time series of desert-dust monitoring are the observations and monitoring of Saharan dust on Barbados that were started in 1965 (Delany et al., 1967), and these observations taught us a lot about relationships between environmental conditions in the dust source areas, dust emission, and atmospheric-transport processes. Dust observations in east Asia date back much longer (e.g., Natsagdorj et al., 2003), with dust outbreaks in China and Korea being recorded already in 57 BC (Chun et al., 2008). The

collection of actual aeolian dust for the study of its physical properties and mineralogical- and chemical composition in relation to atmospheric-transported processes was probably described first in Barbados, and many dust-deposition stations have been set up there after, such as in French Guyana (Prospero et al., 1981), Mali (Kaly et al., 2015), Senegal (Skonieczny et al., 2013), Tenerife (Prospero, 1996), Gran Canaria (Torres-Padrón et al., 2002), Crete (Guerzoni and Chester, 1996). In addition, larger programs were set up to monitor dust across regions in southeast Australia (Leys et al., 2008), the central north Atlantic Ocean (Korte et al., 2017), and the Mediterranean (XMed-Dry) (Rizza et al., 2021).

In the late 1970s, it was observed that large dust events transport huge amounts of material into the ocean (Duce et al., 1980), and international efforts were undertaken to study these events. The first actual observations of giant particles were done in the atmosphere and the Pacific Ocean water column during the ADIOS – Asian Dust Input to the Oceanic System experiment in 1986 when during a dust outbreak in eastern Asia, aeolian particles were collected at >10,000 km from its source and measuring >75 μm (Betzer et al., 1988). However, not much attention was paid to these exceptional so-called ‘giant particles’ until recently when van der Does et al. (2018a) and Ryder et al., (2019) showed the presence of such large particles over the Atlantic Ocean across thousands of kilometers from their source as well as at several kilometers altitude in the atmosphere. Similar to the observation of

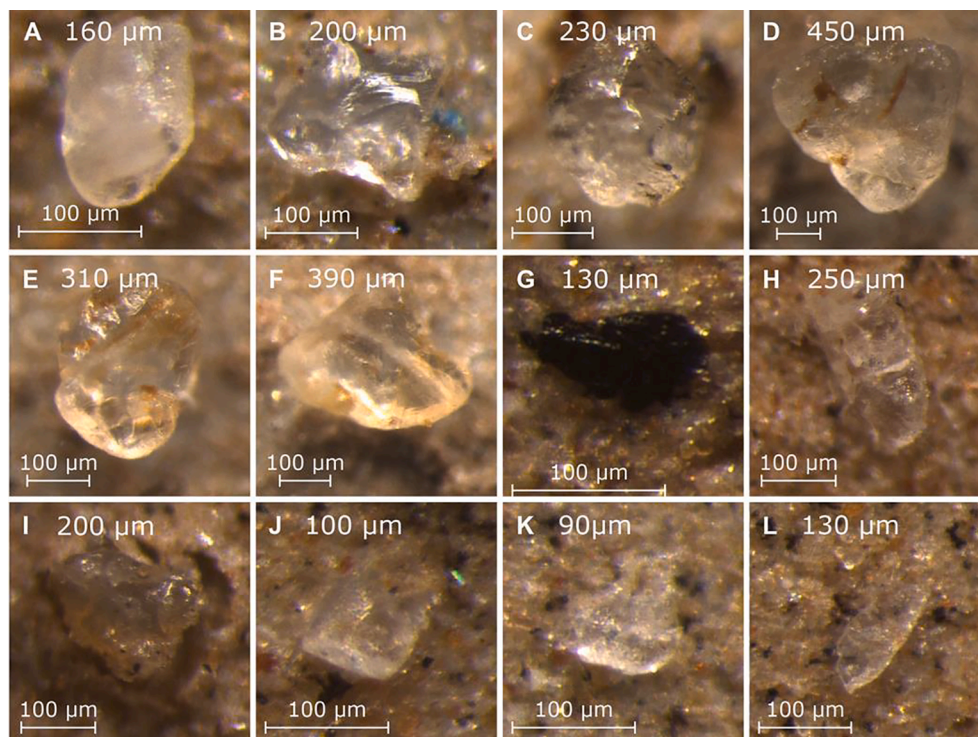


Fig. 3. Giant dust particles collected on an autonomous dust-collecting buoy in the central north equatorial Atlantic Ocean at $\sim 12^{\circ}\text{N}/37^{\circ}\text{W}$, more than 2,000 km from the nearest African coast (adapted with permission from [van der Does et al., 2018a](#)).

Asian dust in the Pacific Ocean ([Betzer et al., 1988](#)), examples of large aeolian dust particles collected at 3 m above sea level, approximately 2400 and 3500 km from the West African coast, are shown in [Fig. 3](#) ([van der Does et al., 2018a](#)). Several mechanisms have been proposed ([van der Does et al., 2018a](#)), such as repeated uplift in convective cells and triboelectric charging of particles causing sustained suspension in the air of particularly quartz particles (see [Section 5.2.2](#)).

Furthermore, other deposition observations of present-day sand-sized Saharan dust were made across the Atlantic Ocean, over Central America, and in other places. For example, across the Atlantic Ocean, these observations were made in sea-bed samples ([Holz et al., 2004](#)) as well as collected with dust collectors above the ocean surface, such as on ships off Northwest Africa (e.g., [Stuut et al., 2005](#)) or mounted on moored surface buoys (e.g., [van der Does et al., 2018a](#)). Time series of dust collected along a transect across the Atlantic Ocean at 12°N showed seasonal changes in dust particle sizes with coarsest-grained material deposited in summer and finest-grained dust in winter ([van der Does et al., 2016](#)). With the use of radiogenic isotopes, the northwest African provenance of these aeolian particles was demonstrated ([van der Does et al., 2018b](#)). In addition, North African super-coarse dust has recently been measured in French Guiana ([Barkley et al., 2021](#)), where a substantial proportion of super-coarse particles were found to be freshwater diatoms, notable for their low density and high asphericity. Moreover, large particles were also observed in Saharan dust events in the Carpathian Basin in 2013 and 2014 ([Varga et al., 2014](#)). The most recent findings of large aeolian particles were reported from Iceland, where in the period between 2008 and 2020, fifteen Saharan-dust events were recorded in satellite and lidar data ([Varga et al., 2021](#)). The Saharan provenance of two of these dust events deposited in Iceland was confirmed by back-trajectory calculations, granulometric (particle-size and -shape distributions) characteristics, and mineralogy and included the occurrence of giant ($>100\ \mu\text{m}$) particles ([Varga et al., 2021](#)). The several observations of these giant particles suggest that they, but also smaller-sized particles such as coarse and super-coarse dust aerosols, are abundant in the atmosphere and likely travel farther distances than

explained by gravitational settling theory (e.g., [Seinfeld and Pandis, 2006](#)).

3.2. Airborne measurements

Airborne observations have the benefit of being the only method allowing in-situ profiling of the vertical distribution of dust particles, including the size distribution, which may be very different from that observed at ground level. The vertical distribution of dust composition, loading, and particle sizes are of key importance in defining the viability of long-range transport and certain impacts of dust, including air quality, radiative effects, and cloud interactions. Therefore, the ability to measure the vertical profile of the dust particle size distribution is of great importance.

3.2.1. Aircraft measurements

Historically, measurements of the full dust size distribution, including coarse and super-coarse dust particles, have often not been made on aircraft. This has occurred due to various factors, including (1) assumptions that coarse mode dust particles simply were not lifted to high altitudes or transported far from dust sources and therefore not even necessary to measure, (2) due to instrumental challenges of measuring coarse particles, and (3) that observations behind inlets and pipework restricting coarse particle concentrations led to incorrect assumptions that substantial coarse dust particles were not present, or were present in low-to-insignificant quantities.

In the last 20 years, there has been significant progress in aircraft observations measuring further into the coarse, super-coarse, and even giant mode dust size range. [Ryder et al. \(2018\)](#) summarize airborne observations from the major dust field campaigns since 2006, highlighting different instrumental upper size limits and restrictions due to inlet size cut-offs. Aircraft inlets are of great value in allowing aerosols to be drawn into the aircraft cabin via pipework, where various measurements of interest can be made. However, it is imperative that attention is paid to the characteristics of the inlet and length of pipework, which

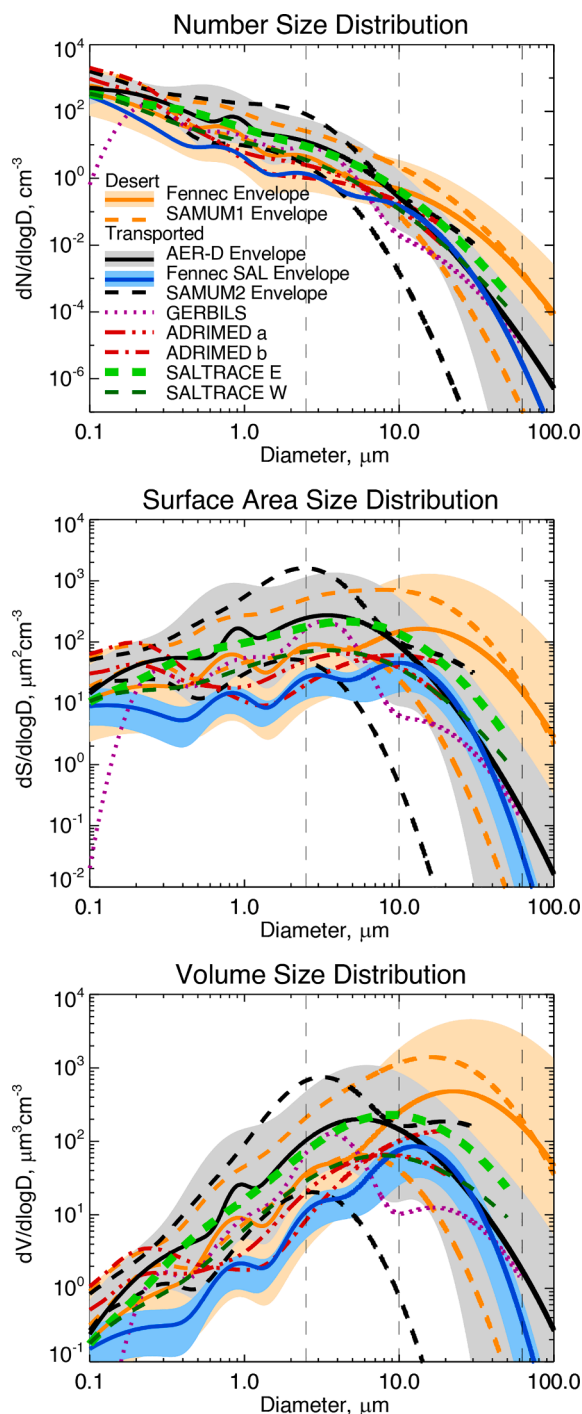


Fig. 4. Lognormal size distributions for recent airborne campaigns measuring Saharan dust extending to sizes larger than 20 μm diameter, shown in number distribution (top), surface area distribution (center), and volume distribution (bottom). Observations close to dust sources are colored orange. Shading represents variability within certain fieldwork campaigns. Lognormal curves are not shown at sizes above which measurements were made. Data are taken shown for Fennec-Sahara (Ryder et al., 2019), SAMUM1 (Weinzierl et al., 2009), AER-D (Ryder et al., 2018), Fennec-SAL (Ryder et al., 2019), SAMUM2 (Weinzierl et al., 2011), GERBILS (Johnson and Osborne, 2011), ADRIMED (ADRIDMED a and b represent dust above 3 km and beneath 3 km, respectively) (Denjean et al., 2016), SALTRACE (SALTRACE E and W represent observations over the eastern vs western Atlantic) (Weinzierl et al., 2017).

impact sampling and transmission efficiency so that any limitations of the measurements made downstream are characterized and accounted for (e.g., Krämer et al., 2013; Sanchez-Marroquin et al., 2019). For example, inlets are typically characterized by the diameter at which passing efficiency is reduced to 50 %, which may vary between 1 and 20 μm (e.g., McConnell et al., 2008; Formenti et al., 2011a; Denjean et al., 2016). However, lengthy pipework inside an aircraft cabin further reduces coarse aerosol transmission, and pipework bends of 90° can prevent the sampling of particles larger than around 1 μm (e.g., Krämer et al., 2013), even if the inlet is able to sample larger particles. For aerosol types where coarse particles are present, such as dust, these processes can severely alter the measured size distribution (e.g., Ryder et al., 2013b, 2013a; their Fig. 3).

To quantify the size distribution of the full-size ranges of dust particles, here we present only airborne dust observations extending up to at least 20 μm diameter and only present observations taken on wing-mounted probes, which do not suffer from inlet and transmission size restrictions (e.g., Ryder et al., 2013b). Observations are taken mostly from optical particle counters, measuring optical diameter from scattering cross sections, which are then converted to geometric diameter by accounting for the likely (or measured, where possible) refractive index of the dust sampled (e.g., see Section 2.1). In many cases, the authors have applied detailed procedures to account for and propagate uncertainties stemming from the non-linear, non-monotonic Mie scattering theory relating scattering cross-section to particle diameter (Rosenberg et al., 2012; Walser et al., 2017). In some cases, optical array probes, which utilize light shadowing techniques and provide a geometric diameter, have also been used in combination with optical particle counters, particularly for the super-coarse and giant modes. This is particularly valuable since optical array probes do not require assumptions about the refractive index or rely on non-linear responses.

We show the dust size distributions from a selection of fieldwork campaigns satisfying the above criteria in Fig. 4. Observations close to desert sources are colored orange, and other observations are as shown in the legend. Size distributions are given as the number, surface area, and volume distributions since each may impact different components of the climate system. Size distributions are shown as combinations of lognormal modes since this provides a straightforward way to summarize the measurements and renders them easily replicable. From Fig. 4, the number concentration decreases as dust particle size increases. However, in terms of surface area and volume distribution, concentrations of dust in the coarse and super-coarse size ranges are high and dominate the dust volume (and, therefore, mass). In terms of surface area, the fine and coarse modes contribute fairly equally, demonstrated by the flat surface area distribution, and there is a drop-off in surface area, which occurs at various diameters through the super-coarse mode. Volume distributions reach a maximum in the super-coarse mode over the desert (orange lines in Fig. 4), and for transported dust, the volume distribution peaks around the lower bound of the super-coarse mode or throughout the coarse mode. Contributions from the giant mode become most significant in terms of volume distribution (as opposed to number or surface area) and contribute most strongly for the desert cases, where the giant mode volume distribution can sometimes exceed that of the other size ranges.

Much variation is seen between different field campaigns (Fig. 4). Observations closest to dust sources over the desert (Fennec and SAMUM1) show the strongest contributions from the super-coarse size range (with volume median diameters, VMD, of 21 and 5–14 μm , respectively) and the size of the peak volume concentration drops with transport away from the sources, with VMDs between 3 and 12 μm for the other campaigns. Variability in dust size over the desert with dust age following uplift also occurs; for example, during Fennec, the effective diameter was found to decrease rapidly with dust age, from 13 to 8 μm for dust within the first 12 h of uplift, down to 6 μm for dust transported for 2 days in the atmosphere (Ryder et al., 2019).

In addition to different transport distances, some variation between

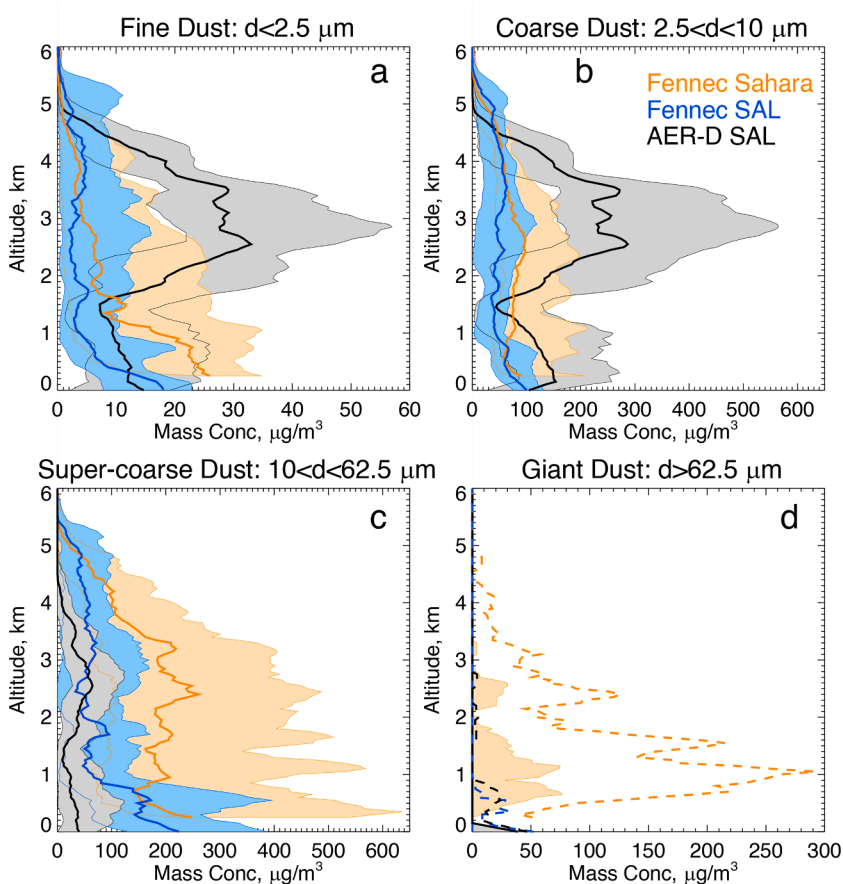


Fig. 5. Vertical distribution of dust mass concentrations in different dust size ranges. (a) fine dust; (b) coarse dust; (c) super-coarse dust; (d) giant dust. Dust density is assumed at 2.65 g cm^{-3} . Data is shown from three airborne field campaigns. Fennec-Sahara over the desert, Fennec-SAL, and AER-D SAL in the Saharan Air Layer over the Canary Islands and Cape Verde Islands, respectively. Solid lines represent medians, and shading bounded by dashed lines represents the 25th to 75th percentiles. Panel d shows the 90th percentile in dashed lines. Note the different x-axis scales for each panel.

different campaign-averaged size distributions can be attributed to sampling dust in different locations (though all sampled North African dust), seasons, and dust originating from different sources. For example, the SAMUM2 size distributions represent wintertime Saharan dust, which remains at low altitudes in the atmosphere and may be impacted by different vertical mixing and deposition to summertime dust, which can be mixed upwards to altitudes of 5–6 km under intense deep boundary layer heating (McConnell et al., 2008; Johnson and Osborne, 2011; Ryder et al., 2013b; Garcia-Carreras et al., 2015). The GERBILS size distributions, although measured over the desert, most likely represented a mixture of aged regional dust and fresher samples (Johnson and Osborne, 2011; Ryder et al., 2019). The ADRIMED data were observed over the Mediterranean and originated from somewhat different sources to the other campaigns shown in Fig. 4 (Denjean et al., 2016).

We show in Fig. 5 how summertime Saharan dust mass concentrations vary vertically from three field campaigns for different size ranges over the Sahara desert compared to the Sahara Air Layer (SAL). In the fine and coarse modes, the structure of the elevated SAL peaking at 2.5 to 3.5 km is strongly evident in AER-D due to the different nature of the size distribution compared to Fennec-Sahara and Fennec-SAL. Super-coarse dust concentrations are higher over the desert (around $200 \mu\text{g m}^{-3}$ up to 3.5 km) compared to transported dust (around $50 \mu\text{g m}^{-3}$ up to 5 km). Under average conditions, very few giant particles were measured, with the median mass of all the campaigns being zero (panel d). However, when the variability encountered is considered, observations up to the 75th percentile over the desert (orange shading) does identify up to $70 \mu\text{g m}^{-3}$ of giant dust at altitudes of around 1 km. When considering variability up to the 90th percentile (dashed orange line), significant mass concentrations of giant dust, up to nearly $300 \mu\text{g m}^{-3}$, are encountered. Notably, the 90th percentile Fennec profile even shows

giant dust concentrations of $10 \mu\text{g m}^{-3}$ just beneath 5 km altitudes. Therefore, this data shows that the giant particles are not consistently present, but under the larger dust loadings, they are present in high mass concentrations and up to high altitudes. The 90th percentiles in the SAL (blue and black dashed lines) demonstrate few giant dust particles in the SAL, other than beneath 1 km – possibly a result of deposition from the overlying SAL.

3.2.2. Observations from unmanned aerial vehicles, radiosondes, and floating balloons

In the past 15 years, technical developments have permitted smaller-sized, lightweight aerosol sensors, which have permitted dust measurements to be carried out on meteorological radiosondes, floating balloons, and unmanned aerial vehicles (UAVs) at a much lower cost than manned research aircraft. Similar to aircraft measurements, this suite of observations also can provide in-situ vertical sampling and, to some extent, horizontal sampling of a limited domain. However, they are generally limited to sampling the meteorology and dust events that overpass a field site location, rather than being able to target specific events and sample larger areas, as is possible with research aircraft.

Renard et al. (2016a, 2016b, 2018) describe the light optical aerosol counter (LOAC), measuring size-resolved dust concentrations between 0.2 and $100 \mu\text{m}$ with an optical particle counter (OPC). The LOAC was mounted on radiosondes or drifting balloons during the Chemistry-Aerosol Mediterranean Experiment (ChArMEX) campaign over the Mediterranean Sea during the summer of 2013, sampling the passage of Saharan dust events. When mounted on radiosondes, LOAC measures the vertical profile of dust as it ascends, while the drifting balloons follow a near-Lagrangian trajectory within the same air mass, enabling it to sample dust size distributions during transport. Renard et al. (2018) frequently observed particles sized larger than $40 \mu\text{m}$ at concentrations

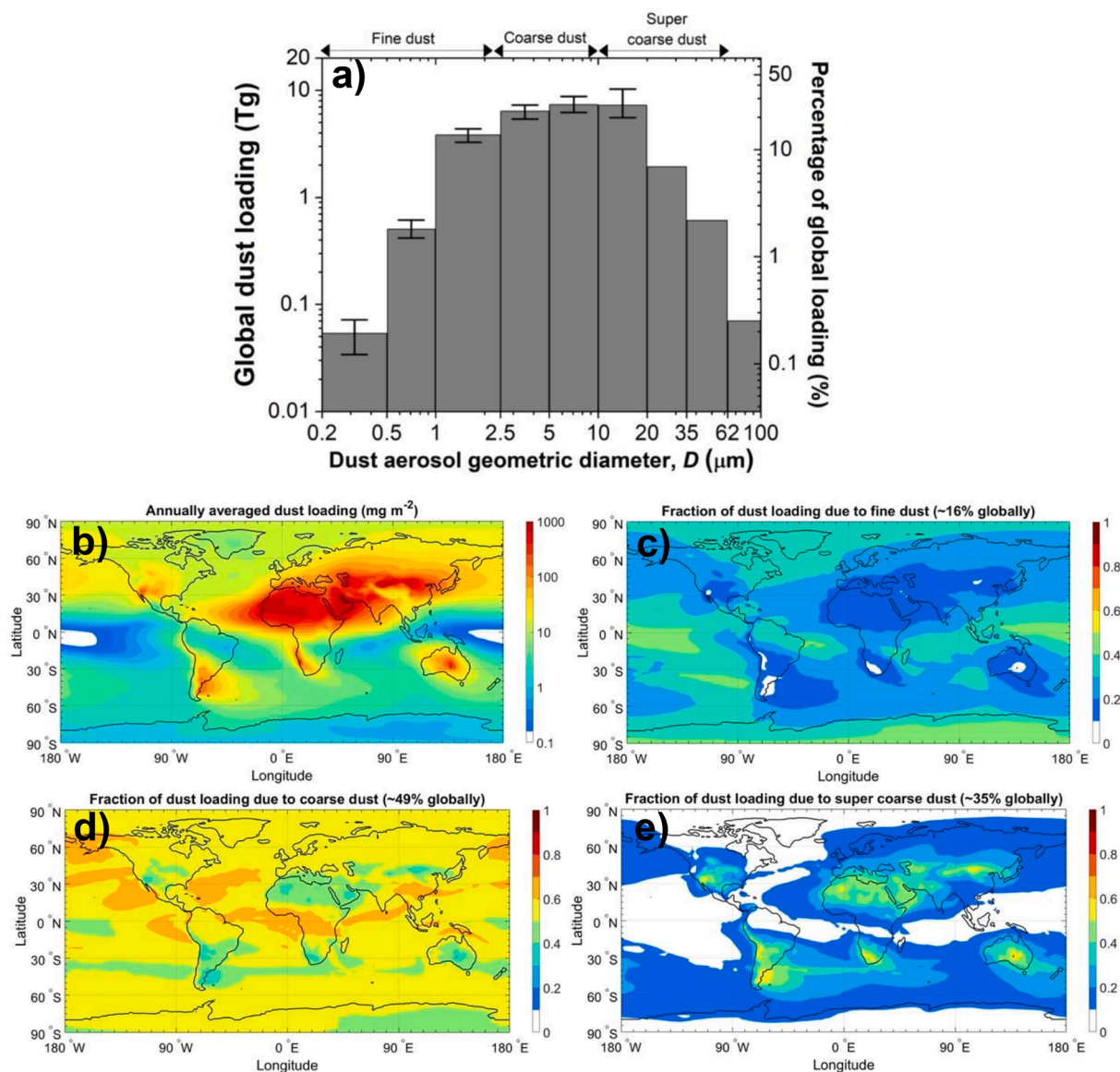


Fig. 6. Dust mass loading resolved by dust diameter. (a) The size-resolved global dust load (Tg, left axis), including the percentage contribution of each size range to global dust loading (%), right axis). The spatial distribution for (b) the annually-averaged bulk dust (0.2–100 μm) column loading in mg m^{-2} and the fraction of bulk dust loading that is (c) fine dust (0.2–2.5 μm diameter), (d) coarse dust (2.5–10 μm), and (e) super-coarse dust (10–62.5 μm). These results use data from the DustCOMM (Adebisi and Kok, 2020; Kok et al., 2021a) for dust up to 20 μm diameter, supplemented with Community Earth System Model simulations for dust up to 100 μm . The results for D greater than 20 μm diameter do not have quantified errors and are uncertain.

above 10^{-4} cm^{-3} at a distance from source regions. Other instruments, such as the Universal Cloud and Aerosol Sounding System (UCASS, Smith et al., 2019), a lightweight OPC which can be deployed on radiosondes, dropsondes, or UAVs to measure size distributions between optical diameters between 0.4 and 17 μm have also been developed and show promising results (Kezoudi et al., 2021a, b).

4. Impacts of coarse and super-coarse dust aerosols on the Earth system

With several pieces of evidence indicating the persistence of coarse to giant dust aerosols in the atmosphere, it follows that their impacts on the Earth's climate system are stronger than previously estimated. Globally, coarse and super-coarse dust aerosols account for a substantial fraction (about 85 %) of the overall dust mass in the atmosphere (Fig. 6). Data from the Dust Constraints from joint Observational-Modeling-experimental analysis (DustCOMM) (Adebisi and Kok, 2020; Kok

et al., 2021a), which is based on a suite of observational constraints combined with an ensemble of model simulations, indicated that the coarse dust mass load (2.5–10 μm in diameter) is approximately 14 Tg (95 % confidence interval: 10–18 Tg). This is more than three times the global fine dust mass load (about 4 Tg, 3–6 Tg) in the atmosphere (Fig. 6a). In comparison, the global mass loads of super-coarse and giant dust are less certain because of the limited availability of airborne measurement constraints. We nonetheless extended the DustCOMM constraints to a particle diameter of 100 μm with Community Earth System Model (CESM) simulations of the ratio of super-coarse and giant dust to dust particles with $D \leq 20 \mu\text{m}$ from Meng et al. (2022). The authors used an improved parameterization of the size distribution of emitted dust that accounts for the emission of super-coarse dust. In addition, they used a dust density reduced by a factor of 10 (250 kg m^{-3}) as a proxy for as-of-yet unclear processes missing from models that likely cause coarse dust to deposit less quickly than observed in nature (Section 5.2). As a result, these simulations were able to match in situ

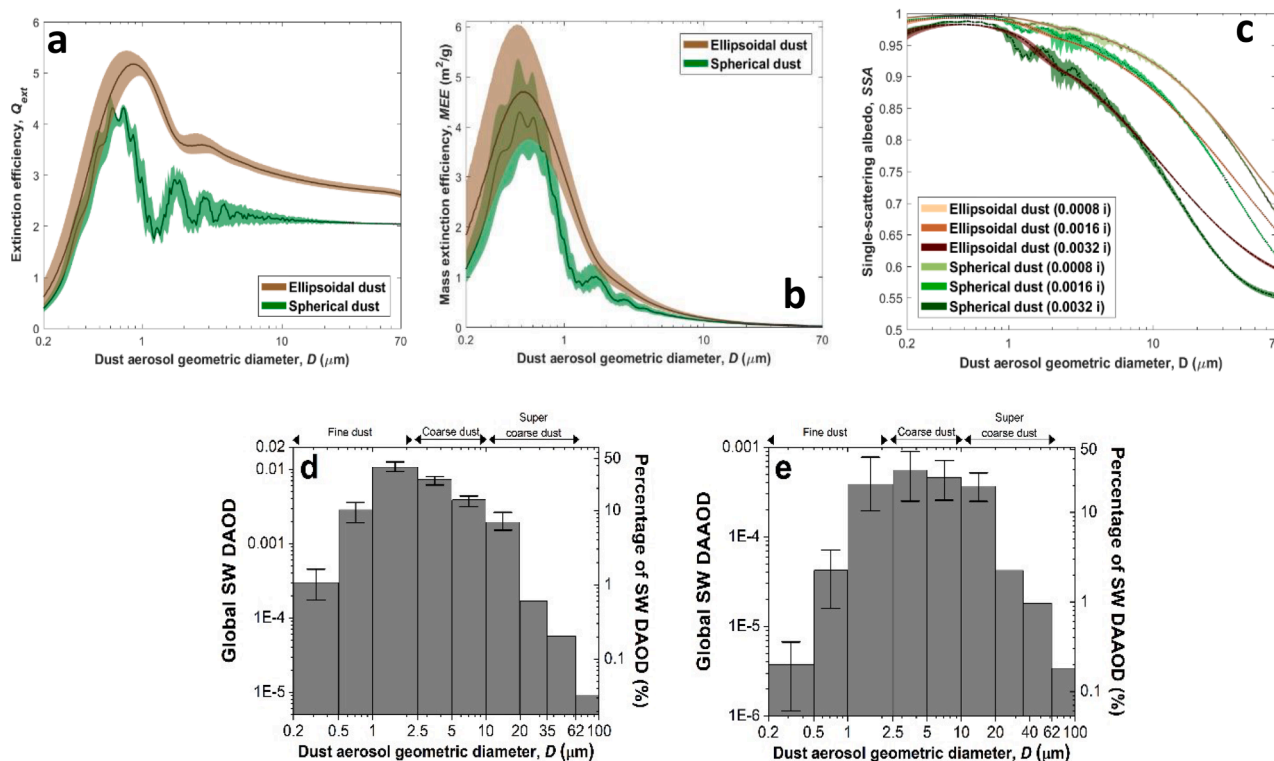


Fig. 7. Size dependence of dust interactions with shortwave (SW) radiation. The size-resolved (a) dust extinction efficiency and (b) mass extinction efficiency for spherical and ellipsoidal dust, (c) the single-scattering albedo for different values of the imaginary index of refraction, (d) the globally averaged SW dust aerosol optical depth (DAOD) wavelength per particle size bin (the median total global SW DAOD is 0.028), and (e) the globally averaged dust absorption aerosol optical depth (DAAOD) per particle size bin (the median total global SW DAAOD is 0.0019). Results for ellipsoidal dust in panels (a), (b), and (c) are after Huang et al. (2022), who combined a database of single-scattering properties (Meng et al., 2010) with constraints on the probability distributions of dust aspect ratio and height-to-width ratio (Huang et al., 2020). These results use a real index of refraction of 1.53 ± 0.03 and an imaginary index of refraction of $\log(k) = -2.75 \pm 0.25$ for panels (a) and (b), which are both based on data compilations in Di Biagio et al. (2019); results for spherical dust were calculated using Mie theory (Mätzler, 2002). Results in panels (d) and (e) used these optical properties of ellipsoidal dust and were obtained from constraints on global size-resolved mass loading for dust aerosols up to $20 \mu\text{m}$ diameter from the DustCOMM data set (Kok et al., 2021a), extended up to a diameter of $100 \mu\text{m}$ using Community Earth System Model simulations by Meng et al. (2022) (also see description at the beginning of Section 4). As such, results beyond $20 \mu\text{m}$ diameter do not have quantified errors and are especially uncertain. The extinction efficiency is defined here as the extinction normalized by the projected area of a sphere with diameter D (Kok et al., 2017). All results are for a wavelength of 550 nm ; error bars and shading denote one standard error.

measurements of super-coarse dust both close to and far from dust source regions (Meng et al., 2022). The estimated super-coarse and giant dust mass loads are approximately 10 Tg and 0.3 Tg , respectively (Fig. 6a).

Although in these model simulations, coarse and super-coarse dust aerosols dominate the global dust mass (Fig. 4 and Fig. 6), their transport and deposition pathways determine their spatial distribution and, eventually, the spatial extent of their impacts on the Earth system. Because coarse dust is transported much farther than super-coarse dust, it can have stronger impacts on the Earth's system. For example, a substantial amount of coarse dust can reach the western parts of the North Atlantic and Pacific Oceans from the Sahara and Asia deserts. In contrast, the amount of super-coarse dust aerosols reaching those locations is very small (Fig. 6c & d). Therefore, the spatial distribution and the eventual spatial extent of dust impacts on the Earth system remain a strong function of dust particle size.

Summarized by the schematics in Fig. 1, here we describe the impacts of coarse and super-coarse dust aerosols on radiation, including the adjustments to dust-radiation interactions (Sections 4.1 and 4.2), the role of coarse and super-coarse dust aerosols as cloud condensation and ice-nucleating particles (Section 4.3), and the impacts on atmospheric chemistry (Section 4.4), and biogeochemistry (Section 4.5).

4.1. Interactions of coarse and super-coarse dust aerosols with radiation

Because of their abundance and wide range of sizes, dust aerosols produce important radiative interactions over a wide spectral range. Indeed, dust aerosols account for about a quarter of aerosol extinction in the shortwave (SW) spectrum (Gliß et al., 2021; Ridley et al., 2016), and dust is the main aerosol species producing extinction and radiative effects in the (LW) spectrum (Dufresne et al., 2002; Heald et al., 2014).

4.1.1. Interactions of coarse and super-coarse dust aerosols with SW radiation

Dust interactions with SW radiation are strongly sensitive to particle size (Fig. 7). Dust with a diameter smaller than the wavelength of visible light ($D \leq \sim 0.5 \mu\text{m}$) is relatively inefficient at producing SW extinction (Fig. 7a) and thus accounts for only a few percent of the dust aerosol optical depth (DAOD) (Fig. 7d). As the diameter increases, its extinction efficiency (the extinction cross-section unit surface area) increases, peaking at approximately double the wavelength of light ($D \sim 1 \mu\text{m}$ for mid-visible light). As dust size increases further, the extinction efficiency declines somewhat. However, because the surface area per unit mass decreases with particle size, the extinction produced per unit dust mass (the mass extinction efficiency) decreases strongly with particle size beyond $D \sim 1 \mu\text{m}$ (Fig. 7b). Nevertheless, if the total dust mass in this size range is large, the total extinction can be much greater and impact the overall DAOD. Consequently, even though coarse and super-coarse

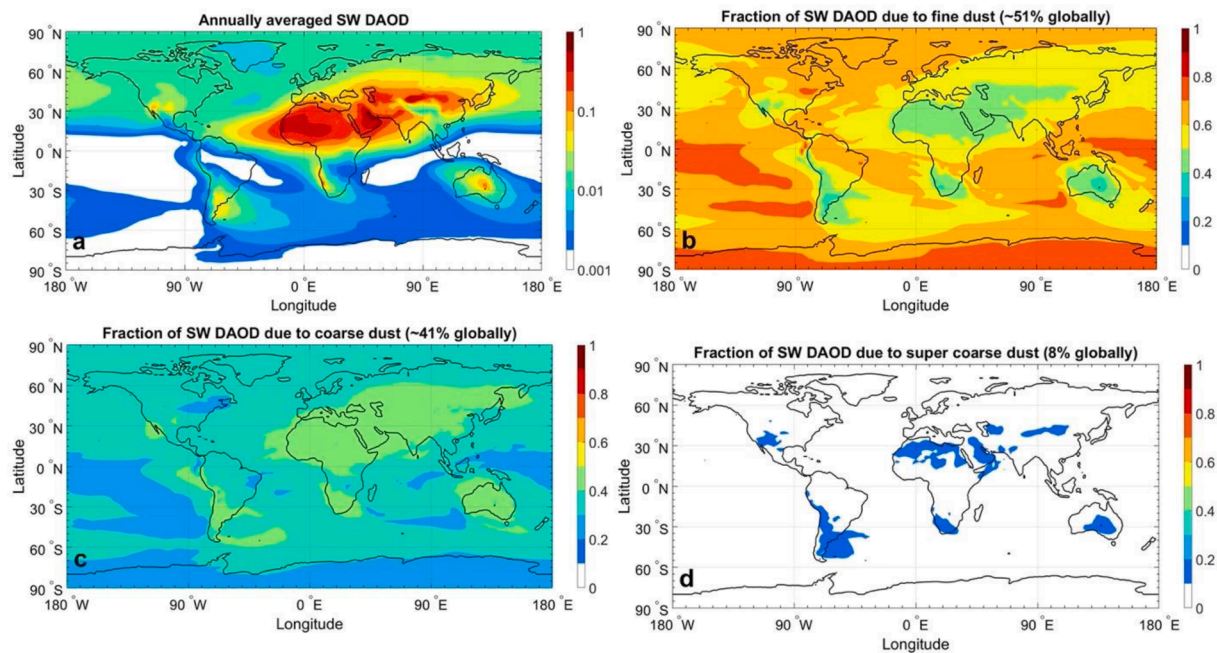


Fig. 8. The contribution of different dust particle size ranges to shortwave (SW) dust aerosol optical depth (DAOD) at 550 nm. Shown are the SW DAOD due to dust of all sizes (a) and the fraction of that DAOD produced by (b) fine ($D \leq 2.5 \mu\text{m}$), (c) coarse ($2.5 < D \leq 10 \mu\text{m}$), and (d) super-coarse ($10 < D \leq 62.5 \mu\text{m}$) dust. Results were obtained by extending DustCOMM constraints on DAOD for dust with $D \leq 20 \mu\text{m}$ with Community Earth System Model simulations of dust out to $100 \mu\text{m}$, as described at the beginning of Section 4 and Fig. 7. The contribution of giant dust (D greater than $62.5 \mu\text{m}$) was $\sim 0.01\%$ of global SW DAOD and is not shown.

dust aerosols account for $\sim 85\%$ of the atmospheric dust mass loading (Fig. 6), they account for only $\sim 50\%$ of DAOD (Fig. 7d).

Dust size also partially determines the fraction of extinguished radiation that is absorbed. The single-scattering albedo (SSA) - the ratio of the scattering to the extinction cross sections - decreases strongly with particle size (Fig. 7c). Fine dust has an SSA close to 1, but as the particle diameter increases relative to the wavelength of light, so does the fraction of extinction that is due to absorption (dust aerosols are a mixture of different minerals whose relative abundances, particle size distribution, shape, surface topography and mixing state influence their effect upon climate; Fig. 7c). This decrease in SSA with sizes is partially offset by the decreasing content of light-absorbing iron oxides with dust aerosol size (Kandler et al., 2009; Caponi et al., 2017; Ryder et al., 2018). Overall, of the order of 5% of dust extinction of SW radiation is due to absorption (Fig. 7b, d), and coarse and super-coarse dust aerosols account for approximately-three-quarters of this absorption (Fig. 7e).

In addition to size, the dust SSA is determined by the imaginary part of the index of refraction (Fig. 7c), which in turn depends on dust mineralogy (Sokolik and Toon, 1999; Perlwitz et al., 2015; Scanza et al., 2015; Di Biagio et al., 2019). Unfortunately, both dust mineralogy itself and the optical properties of the main SW absorbing minerals (iron oxides in the form of goethite and hematite) remain highly uncertain (Gillespie and Lindberg, 1992; Bedidi and Cervelle, 1993; Claquin et al., 1999; Journet et al., 2014; Schuster et al., 2016a). Consequently, the dust absorption aerosol optical depth (DAAOD), which quantifies the globally averaged extinction produced by dust absorption, remains highly uncertain (Fig. 7d). Nevertheless, existing estimates suggest that dust absorption accounts for $\sim 25\%$ of global aerosol absorption optical depth (AAOD) (Buchard et al., 2015; Samset et al., 2018; Sand et al., 2021). This absorption of SW radiation by dust and other aerosol species (black carbon and brown carbon) has important consequences for the Earth system, which include offsetting dust cooling due to SW scattering, reducing the intensity of the hydrological cycle, and stabilizing the atmosphere (Balkanski et al., 2007; Solmon et al., 2008; Samset et al., 2016).

The interactions of dust with SW radiation are enhanced by the substantial asphericity of dust, with the particle length-to-width (the

aspect ratio) and height-to-width ratios substantially different from unity (Okada et al., 2001; Kandler et al., 2007; Chou et al., 2008; Huang et al., 2020). This asphericity increases the surface area for a given volume (or mass) of dust aerosol, which results in enhanced extinction, especially for particle radii in excess of the wavelength of light. Measurements of dust shapes combined with calculations of single-particle scattering properties indicate that asphericity enhances dust mass extinction by $\sim 40\%$ (Kalashnikova and Sokolik, 2004; Kok et al., 2017). Accounting for this enhancement in dust extinction efficiency appears to be important for models to simultaneously match observations of DAOD and surface concentration (Kok et al., 2021a).

The relative contributions of the different dust size range to DAOD change substantially as a function of distance from the major source regions (Fig. 8). This occurs because the lifetime of dust decreases strongly with particle size (Miller et al., 2006; Kok et al., 2017), largely due to increasing gravitational settling speed. As such, coarse and super-coarse dust aerosols are concentrated close to the major source regions (Fig. 6), where they account for the majority of DAOD. But the fractional contribution of coarse and super-coarse dust aerosols to DAOD decreases rapidly with distance from source regions (Fig. 8c, d), such that the contribution of fine dust to DAOD dominates further from source regions (Fig. 8). Because coarse and super-coarse dust aerosols account for around three-quarters of dust absorption of SW radiation, these results also further confirm that semi-direct effects of dust on clouds, as well as effects of dust absorption on precipitation, have the strongest influence around the major source regions (Solmon et al., 2008; Amiri-Farahani et al., 2017) (see also Section 4.2).

4.1.2. Interactions of coarse and super-coarse dust aerosols with LW radiation

Dust is unique among aerosol species in producing interactions with LW radiation that are important to the Earth's radiation budget. Indeed, other aerosol species besides sea salt are too fine to interact substantially with LW radiation, and sea salt is usually confined to the atmospheric boundary layer, such that its small temperature contrast with the surface causes its longwave interactions to produce only a small perturbation of the top-of-atmosphere (TOA) energy balance (Dufresne et al., 2002;

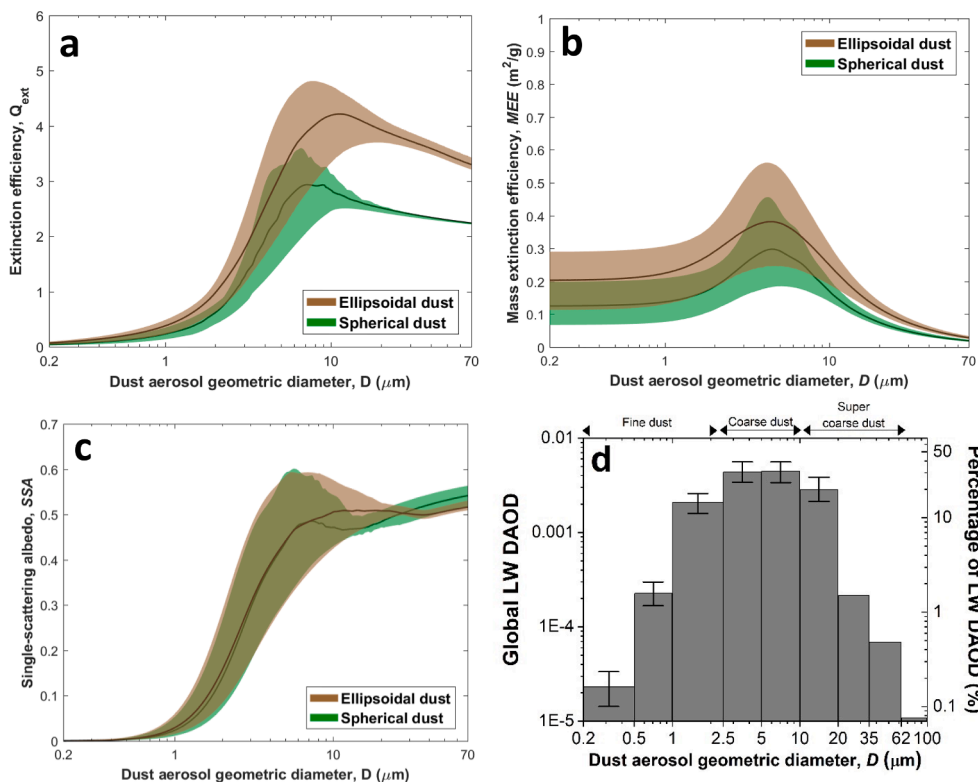


Fig. 9. Size dependence of dust interactions with longwave (LW) radiation. Shown are the size-resolved (a) dust extinction efficiency, (b) mass extinction efficiency, and (c) single-scattering albedo for both spherical and aspherical (ellipsoidal) dust. Also shown is (d) the globally averaged dust aerosol optical depth (DAOD) at 10 μm wavelength per size bin (the median total global LW DAOD is 0.015). The calculations for these figures follow the similar panels in Fig. 7 for dust interactions with shortwave radiation, except that we used a real index of refraction of 1.70 ± 0.20 and an imaginary index of refraction of $\log(k) = 0.41 \pm 0.11$, both based on data compilations of dust optical properties in the LW spectrum reported in Di Biagio et al. (2017).

Heald et al., 2014). The effects of absorption and scattering of LW radiation by dust are mostly relevant in the infrared atmospheric window ($\sim 8\text{--}13 \mu\text{m}$) as the atmosphere is opaque at other infrared wavelengths (Liou, 2002).

As was the case for interactions with SW radiation (Section 4.1),

interactions of dust with LW radiation depend strongly on size. Dust with diameters substantially smaller than the wavelength of infrared radiation is inefficient at producing extinction (Fig. 9a), such that dust with $D < 1 \mu\text{m}$ produces only a few percent of the total DAOD of ~ 0.015 (Kok et al., 2021b) in the LW spectrum (Fig. 9d). As dust size increases,

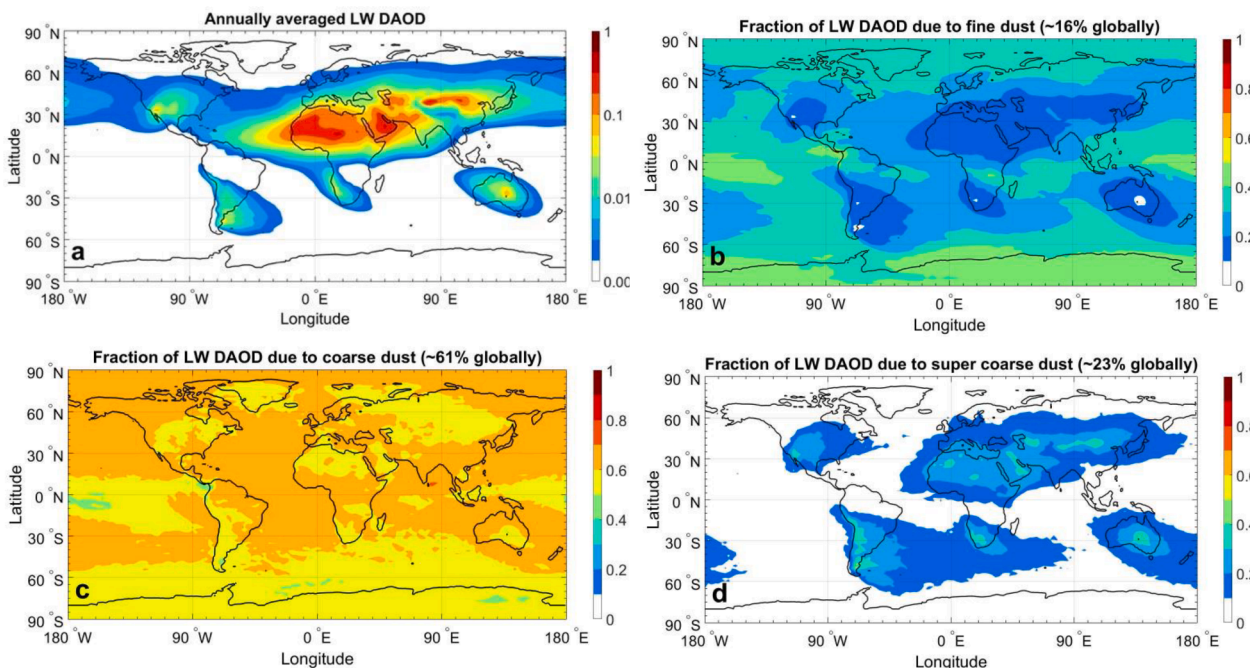


Fig. 10. The contribution of different dust particle size ranges to longwave (LW) dust aerosol optical depth (DAOD) at 10 μm . Shown are the LW DAOD due to dust of all sizes (a) and the fraction of that DAOD produced by (b) fine ($D \leq 2.5 \mu\text{m}$), (c) coarse ($2.5 < D \leq 10 \mu\text{m}$), and (d) super-coarse ($10 < D \leq 62.5 \mu\text{m}$) dust. Results were obtained by extending DustCOMM constraints on DAOD due to dust with $D \leq 20 \mu\text{m}$ with Community Earth System Model simulations of dust out to 100 μm (Meng et al., 2022), using parameters as described in the captions of Fig. 7 and Fig. 9. The contribution of giant dust (D greater than $62.5 \mu\text{m}$) was $\sim 0.02\%$ of global LW DAOD and is not shown.

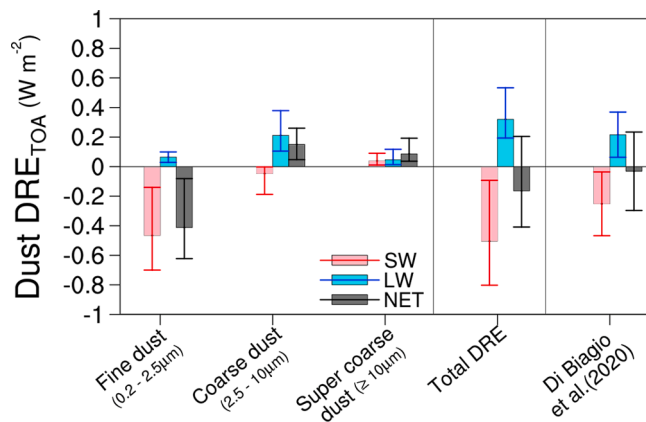


Fig. 11. Global dust direct radiative effect (DRE) resolved by particle size. Shown are the DRE in the shortwave (SW) and longwave (LW) spectra and their sum (NET) for fine, coarse, and super-coarse dust (left three columns) and for all dust from results obtained here and in Di Biagio et al. (2020). Results for dust with $D \leq 20 \mu\text{m}$ are from Adebisi and Kok (2020), and results for D greater than $20 \mu\text{m}$ were obtained by combining our results on SW DAOD (Fig. 7d) with an estimated global DRE per unit SW DAOD of $20 \pm 8 \text{ Wm}^{-2}$ for both SW and LW radiation (Kok et al., 2017). Results from Di Biagio et al. (2020) used a dust size distribution that accounts for coarse and super-coarse dust particles by fitting the data from Kok et al. (2017) and the FENNEC campaign over North Africa (Ryder et al., 2013b, 2013a).

its extinction efficiency increases rapidly, peaking around the $\sim 10 \mu\text{m}$ wavelength of infrared radiation in the atmospheric window (Fig. 9a). Because the ratio of surface area to particle mass decreases with increasing particle size, the mass extinction efficiency peaks at a smaller diameter of $\sim 5 \mu\text{m}$ (Fig. 9b). Consequently, coarse dust ($2.5 \leq D < 10 \mu\text{m}$) is the dominant contributor to LW DAOD; super-coarse dust provides another $\sim 30\%$. As such, coarse and super-coarse dust aerosols account for the bulk of dust extinction of LW radiation, making it critical that global models adequately account for these particles (Fig. 9d).

Both scattering and absorption contribute substantially to the dust extinction of LW radiation, with a single-scattering albedo of around 0.5 (Fig. 9). However, LW scattering interactions are generally not accounted for in global models, which likely causes models to underestimate the radiative effects of dust interactions with LW radiation (Dufresne et al., 2002; Miller et al., 2006; Kok et al., 2017; Di Biagio et al., 2020).

Dust optical properties in the LW spectrum are uncertain because of a dearth of measurements and the substantial spread in measured optical properties between the few published experimental studies (Volz, 1972, 1973; Di Biagio et al., 2014, 2017). Although the real index of refraction in the LW spectrum appears to be relatively constant across dust samples, the imaginary index of refraction appears to vary substantially with dust mineralogy and also varies rapidly with wavelength (Di Biagio et al., 2017). As with SW radiation, dust asphericity enhances the extinction of LW radiation by $\sim 50\%$ (Fig. 9a).

The pattern of LW DAOD is remarkably similar to that of SW DAOD (Fig. 8 & Fig. 10) because the 1–10 μm size range dominates both, accounting for $\sim 80\%$ of SW DAOD and $\sim 65\%$ of LW DAOD (Fig. 7d, Fig. 9d). Nonetheless, fine dust makes only a minor contribution to LW DAOD, except in remote regions like the polar caps, where little coarse dust remains (Fig. 10b). On the other hand, coarse dust accounts for over half of LW DAOD in most of the world (Fig. 10c), and super-coarse dust also contributes approximately a quarter of LW DAOD close to source regions (Fig. 10d), thereby underscoring the need for global aerosol models to account for dust with diameters in excess of $10 \mu\text{m}$ (Ryder et al., 2019; Adebisi and Kok, 2020).

4.1.3. Global direct radiative effect of coarse and super-coarse dust aerosols

Dust size largely determines the relative importance of cooling due to

scattering SW radiation versus warming due to absorbing SW and scattering and absorbing LW radiation (Fig. 7 and Fig. 9). Indeed, fine dust produces substantial extinction in the SW spectrum (Fig. 7a-c), of which only a few percent is due to absorption (Fig. 7e), such that fine dust produces a substantial cooling effect at both the surface and TOA (Fig. 11). Conversely, coarse dust absorbs a larger fraction of extinguished SW radiation and also scatters and absorbs substantially in the LW spectrum, thereby, on balance producing net warming at TOA. Super-coarse dust absorbs an even higher fraction of extinguished SW radiation (Fig. 7e) and also produces substantial extinction in the LW spectrum (Fig. 9d). Super-coarse dust, therefore, also warms at TOA, though its net direct radiative effect is smaller than for coarse dust (Fig. 11) because of lower mass extinction efficiencies in both the SW (Fig. 7b) and LW spectra (Fig. 9b), combined with a smaller mass loading (Fig. 6a). Giant dust has relatively low mass loading and mass extinction efficiencies and does not produce a substantial impact on Earth's global radiation budget.

Because dust direct radiative effects are thus in large part determined by dust size, the global dust direct radiative effect (DRE) is partially determined by the globally averaged dust size distribution (Fig. 11) (Kok et al., 2017; Adebisi and Kok, 2020; Di Biagio et al., 2020). Other important factors that determine the net global dust DRE at TOA include dust mineralogy, the presence of underlying clouds, the surface albedo and emissivity, and the dust plume height (Liao and Seinfeld, 1998; Li et al., 2021). For example, uncertainties in dust mineralogy are important for dust SW DRE (e.g., Li et al., 2021), however model results suggested that, after accounting for coarse and super-coarse dust aerosols, agreement with observation over the North Atlantic requires a less absorptive SW dust refractive index than currently used in models (e.g., Ito et al., 2021a). Because of uncertainties in all these factors (e.g., Kim et al., 2014; Di Biagio et al., 2019; Ryder et al., 2019; Adebisi and Kok, 2020; O'Sullivan et al., 2020), it is still not clear whether the dust DRE net warms or cools the planet (Fig. 11) (Kok et al., 2017; Adebisi and Kok, 2020; Di Biagio et al., 2020; Li et al., 2020). However, it is clear that fine dust tends to cool on a global scale, whereas coarse and super-coarse dust aerosols warm, thereby counteracting this cooling. The exact proportions of fine and coarse dust in our atmosphere are thus critical determinants of the sign and magnitude of the global dust DRE. Furthermore, because atmospheric dust loading has increased substantially over the past century (Mahowald et al., 2010; Hooper and Marx, 2018; Kok et al., 2022) and might change substantially in the future (Stanelle et al., 2014; Kok et al., 2018), narrowing the uncertainty on the global dust size distribution and dust optical properties is critical for improving projections of future climate changes.

4.2. Impacts of coarse and super-coarse dust absorption on clouds and precipitation

Dust aerosols not only affect the global climate system through their direct interactions with shortwave and longwave radiation but also through the modification of temperature and water vapor profiles, wind circulation, and cloud properties (Boucher et al., 2013; Knippertz and Stuut, 2014). Because mineral dust absorbs shortwave and longwave radiation, it can trigger uneven radiative heating or cooling within the atmosphere, which can locally alter clouds and precipitation distributions (Wong et al., 2009; DeFlorio et al., 2014; Doherty and Evan, 2014; Huang et al., 2014; Amiri-Farahani et al., 2017). Additionally, spatial variability in dust loading and absorption can drive mesoscale or synoptic-scale circulation, further influencing the cloud and precipitation distributions (Chen et al., 2010; Perlwitz and Miller, 2010). These changes in thermodynamical states, clouds, and precipitation due to the presence of absorbing aerosols, such as mineral dust, effectively result in adjustments to the dust radiative effect (Boucher et al., 2013; Forster et al., 2021). Consequently, because coarse and super-coarse dust aerosols have substantial impacts on shortwave and longwave radiation (Section 4.1), they can have a significant influence on the adjustments to

the dust-radiation interactions. This section describes the adjustment to dust-radiation interaction through the impacts of coarse dust absorption on clouds and precipitation.

4.2.1. Impacts of coarse and super-coarse dust absorption on clouds

The adjustment to aerosol-radiation interactions through changes in cloud cover was originally referred to as a *semi-direct effect* (Boucher et al., 2013; Forster et al., 2021). An aerosol semi-direct effect was first postulated by Grassl (1975) and later described by Hansen et al. (1997) and Ackerman et al. (2000) using both observation and model simulations. As one of the absorbing aerosols in the atmosphere (Samset et al., 2018), dust semi-direct effects occur when the dust absorption alters the heating rates and changes the atmospheric stability leading to changes in cloud cover and its distribution (Doherty and Evan, 2014; Huang et al., 2014; Amiri-Farahani et al., 2017). The magnitude of the dust semi-direct effect and whether it results in a positive (warming) or a negative (cooling) radiative perturbation depends primarily on two factors: the relative positions of the dust and cloud layers within the atmospheric column and the amount of radiation absorbed by the dust layers (Meloni et al., 2005; Perlwitz and Miller, 2010; Amiri-Farahani et al., 2017). Consequently, because fine and coarse dust absorbs radiation differently in shortwave and longwave (see Section 4.1), the dust semi-direct effect also depends on the vertical distribution of the ratio between fine and coarse dust.

In addition, the sign of dust semi-direct effect, whether it has a positive or negative effect, depends on the relative positions of the dust and cloud layers within the atmospheric column (Huang et al., 2014; Amiri-Farahani et al., 2017). For low-altitude clouds, the current understanding in literature is that dust semi-direct effect is negative (cooling) when the dust layer lies above the cloud and positive (warming) when the dust layer lies within or below the cloud (Huang et al., 2014; Amiri-Farahani et al., 2017). When the aerosol is within or below the low-altitude cloud, the localized shortwave warming could reduce the relative humidity and the liquid water paths, resulting in destabilization of the layer and dissipation of the cloud cover and, consequently, a positive semi-direct effect (Huang et al., 2006; Amiri-Farahani et al., 2017). In contrast, when the absorbing aerosol is above the low-level cloud, the localized shortwave warming increases the buoyancy of the layer above the clouds and contributes to the enhancement of the lower tropospheric stability, resulting in increases in cloud cover and, therefore, a negative aerosol semi-direct effect (Doherty and Evan, 2014; Amiri-Farahani et al., 2017), though this may vary with aerosol, cloud, and boundary layer properties (Herbert et al., 2020). Over the North Atlantic Ocean, these mechanisms are used to explain the negative semi-direct effect during summer when more than 60 % of the Saharan dust resides above the low-level clouds, and the positive semi-direct effect during winter when about 88 % of the Saharan dust resides within or below the low-level clouds (Amiri-Farahani et al., 2017). For high-altitude clouds, changes in cloud cover and, therefore, dust semi-direct effect depend on dust-induced changes in available water vapor in the atmospheric column. For example, Perlwitz and Miller (2010) showed that, though increased moisture convergence (which tends to increase cloud cover) can overwhelm the warming effect produced by dust absorption (which tends to decrease cloud cover) during the summer, the dust absorption results in an overall annual-mean decrease in high cloud cover (see also Amiri-Farahani et al., 2019).

Regardless of the height of dust and cloud layers, the magnitude of dust semi-direct effect depends on dust absorption properties, where the ratio between fine and coarse dust is important. For example, Perlwitz and Miller (2010) showed that for sufficiently large dust aerosol optical depth, more dust absorption directly results in more low-level cloud cover over dust-dominating regions. In contrast, there are weak increases and sometimes reductions (especially over land) in low-level cloud cover for conditions of low dust aerosol optical depth and weak dust absorption (Perlwitz and Miller, 2010). For the same dust aerosol optical depth, the abundance of coarse and super-coarse dust aerosols

relative to the fine dust will result in more absorption of both shortwave and longwave radiation (see also Fig. 4 and Section 4) (Otto et al., 2007, 2011; Adebisi and Kok, 2020). Therefore, the influence of coarse and super-coarse dust aerosols on dust absorption suggests that their abundance in the atmosphere would enhance semi-direct effects, especially over dust-dominating regions.

In addition, the impact of coarse and super-coarse dust aerosols on semi-direct effects also depends on their vertical distribution (Otto et al., 2007; Ryder et al., 2019). Processes such as convective mixing may act against the gravitational removal of coarse dust, allowing for an increased presence of coarse dust in the vertical distribution, even after a long-range transport (e.g., van der Does et al., 2018a). For example, Yang et al. (2013) and Gasteiger et al. (2017) showed uniform vertical distributions of lidar-based depolarization ratio between approximately 2 and 5 km over the North Atlantic Ocean, suggesting a consistent observation of coarse dust in the upper part of the Saharan dust layer. Such vertical distribution of coarse and super-coarse dust aerosols could impact the overall distribution of dust absorption. Specifically, the vertical distribution of coarse and super-coarse dust aerosols could determine where dust warms the dust layer in the shortwave and cools it in the longwave (Carlson and Benjamin, 1980; Otto et al., 2007). Unlike the shortwave warming that may occur over the entire dust layer, the longwave cooling maximizes at the top of the dust layer and may result in longwave warming at the bottom of the layer or close to the surface (Chen et al., 2010; Ryder, 2021). For the case of dust aerosols above the low-level cloud, this additional dust longwave warming may complement the shortwave warming and lower-tropospheric stability at the top of the underlying low-level clouds and thus increasing the low-level cloud cover, consequently enhancing the dust semi-direct effects (e.g., Choobari et al., 2014). The full impact of longwave radiation on dust semi-direct effects is still an open question and may further depend on the separating distance between the dust-cloud layers, the underlying spectral surface albedo, and surface temperature (e.g., Otto et al., 2007).

Other than the uncertainties associated with the coarse dust abundance or its vertical distribution, the uncertainties in the estimates of dust semi-direct effects may also depend on the uncertainties in the cloud and thermodynamical processes (e.g., Stier et al., 2013). For example, Hill and Dobbie (2008) suggested that it is difficult to isolate the microphysical effects of aerosols, such as changes in the concentration of cloud condensation nuclei, from the estimates of aerosol semi-direct effects, especially in the case where the aerosols are within or near the low-level clouds. In addition, changes in atmospheric variables, such as specific humidity or temperature unrelated to the aerosol effects, can also influence the low-level clouds, therefore confounding the estimates of semi-direct effects (Perlwitz and Miller, 2010; Wong et al., 2009).

4.2.2. Impacts of coarse and super-coarse dust absorption on precipitation

Dust is a dominating source of aerosol-induced atmospheric energy absorption (Samset et al., 2018; Sand et al., 2021). As such, it is expected to affect precipitation - globally and regionally - through adjustments to dust-radiation interaction (Myhre et al., 2018; Richardson et al., 2018). While the underlying processes and energetic constraints that connect absorption to precipitation formation are well established, no constraint yet exists on the global mean impact of dust on precipitation, whether fine, coarse or super-coarse. Here, we discuss some of the key literature linking aerosol absorption and precipitation in general and use these known relations to provide a first-order estimate of the overall potential influence of dust absorption on precipitation in the present atmosphere. Because the abundance of coarse dust directly influences the overall dust absorption (Section 4.1), this inference suggests the impact of coarse and super-coarse dust absorption on precipitation.

Using a single climate model, Andrews et al. (2010) found indications of a linear correlation between the atmospheric absorption added to the climate system by a change in a climate driver, such as a doubling of CO₂ concentration or a large increase in aerosol amounts, and a reduction in global mean precipitation. Subsequent single and

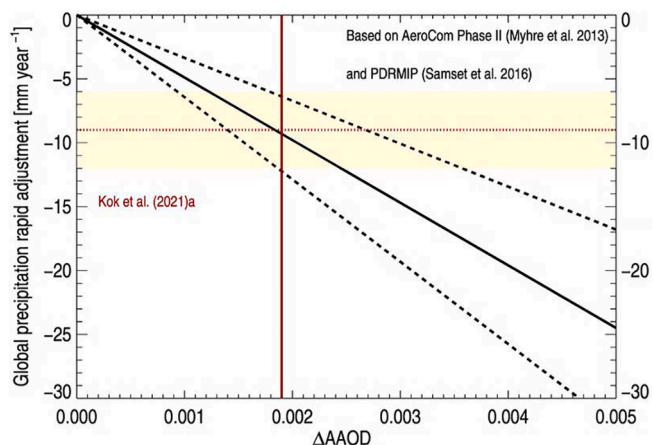


Fig. 12. A lower bound on the inhibition of global mean precipitation by dust-induced absorption. The black lines show the overall relationship between AAOD and precipitation reduction from rapid adjustments derived from multi-model studies, and the black dashed lines show the range of uncertainty. The red line shows the estimate of total dust SW AAOD shown in Fig. 9 based on (Kok et al., 2021a) and the resulting constraint (yellow shading).

multi-model studies have confirmed this relationship (Kvalevåg et al., 2013; Samset et al., 2016) and found that it holds for the global mean and is independent of the details of the forcing mechanism. This includes greenhouse gases, changes in irradiation, and aerosol concentrations. Consequently, the relation can be expected to apply equally to dust-induced absorption, even though dust aerosols (fine or coarse) have not so far been explicitly included. And while the absolute change in precipitation per unit of atmospheric absorption change (in Wm^{-2}) varies between models, their correlation is virtually model-independent (Samset et al., 2016; Smith et al., 2018). The underlying mechanism, as discussed in a range of studies (Myhre et al., 2018; Richardson et al., 2018; Smith et al., 2018), is the influence of absorption on the energy balance at precipitation formation where latent heat is released due to condensation. Essentially, absorption of radiation warms the air aloft, providing extra energy and therefore inhibiting condensation. Further, the influence of this additional heating on cloud formation and lapse rate (see Section 4.2) also affects the dynamical conditions underlying precipitation formation.

Because of the increase in the ratio of coarse-to-fine dust per unit volume, dust absorption can therefore be expected to have an inhibiting influence on global mean precipitation. The magnitude of this influence will depend on the absolute amount of dust-induced absorption, which, in turn, depends on the optical properties and atmospheric vertical profile of dust (Samset et al., 2018). It further depends on the geographical distribution of dust, as the efficiency of the absorption-precipitation interaction has been shown to be regionally dependent (Allen et al., 2019; Samset and Myhre, 2015; Sand et al., 2021).

Based on the above and following the method recently introduced in Samset (2022), a first estimate of the overall influence of dust absorption on precipitation (P) can be derived using the following relationship:

$$\Delta P = \frac{\Delta P}{\Delta R_{Abs}} \times \frac{\Delta R_{Abs}}{\Delta \tau_{abs}^d} \times \Delta \tau_{abs}^d \quad (1)$$

Here, $\Delta \tau_{abs}^d$ is the change in global mean absorbing aerosol optical depth due to dust (τ_{abs}^d), $\frac{\Delta R_{Abs}}{\Delta \tau_{abs}^d}$ is the relationship between atmospheric absorption (in Wm^{-2}) and τ_{abs}^d , and $\frac{\Delta P}{\Delta R_{Abs}}$ is the relationship between precipitation change and atmospheric absorption. The two latter relations can be estimated from the multi-model studies of PDRMIP (Precipitation Driver Response Model Intercomparison Project) (Samset et al., 2016) and AeroCom Phase II (Myhre et al., 2013), respectively, to arrive at the relation shown in Fig. 12. We have used $\frac{\Delta P}{\Delta R_{Abs}} = -9.33 \text{ mm y}^{-1}$

$1/\text{W m}^{-2}$ and $\frac{\Delta R_{Abs}}{\Delta \tau_{abs}^d} = 525 \pm 165 \text{ Wm}^{-2}$, respectively. The uncertainty on the first relation is suppressed, as it is estimated to be an order of magnitude smaller than the latter. Next, we combine the general relation of Eq. (1) with the coarse dust shortwave τ_{abs}^d estimate of 0.0019 from DustCOMM (Fig. 7) (Kok et al., 2021a). The result is an estimated precipitation inhibition due to rapid adjustments in dust-radiation interaction of $P = -10 \text{ mmy}^{-1}$. We consider this estimate to be a lower bound. Firstly, because it only includes the shortwave τ_{abs}^d . Secondly, an underestimate of the volume of effectively absorbing coarse and super-coarse dust aerosols would also imply an underestimate in total dust-induced τ_{abs}^d . Any surface temperature change resulting from dust absorption would add a positive contribution to the precipitation change; however, this effect is expected to be minor (Samset et al., 2016). We also note that since coarse and super-coarse dust particles have not been explicitly modeled, there may yet be a different coefficient, or even non-linear relationships, between absorption and precipitation relative to other, more commonly studied drivers of climate change.

Regionally, the impacts of coarse and super-coarse dust absorption on precipitation can be expected to be complex and heterogeneous. The specific physical mechanisms are, however, poorly studied. Several studies have reported dust impacts on parts of Asian and African precipitation and on monsoon characteristics (Huang et al., 2014; Jordan et al., 2018). No clear picture of the details of dust-absorption-precipitation interactions can be drawn from these studies, but there is a clear consensus emerging that dust may be of marked regional importance and that the topic is, therefore, in need of further research.

Overall, existing literature describes physical mechanisms that link dust-induced absorption to inhibition of global mean precipitation as part of the atmospheric rapid adjustments to the presence of absorbing aerosol. The absolute magnitude and regional details of this potentially very important process are, however, poorly constrained and therefore represent a clear knowledge gap when assessing the regional climate implications of atmospheric aerosols.

4.3. The role of coarse and super-coarse dust aerosols as cloud condensation nuclei and ice-nucleating particles

In addition to the impact of dust absorption on cloud amount and distribution, dust can act as cloud condensation nuclei (CCN) and ice-nucleating particles (INPs), influencing cloud microphysical properties. The ability of a dust particle to act as CCN and INPs depends not only on its mineral composition but also on the dust size and surface area distribution (Mahowald et al., 2014). In turn, the dust mineralogical composition can also vary as a function of particle size (e.g., Kandler et al., 2009; Atkinson et al., 2013), further separating the role of fine dust from that of coarse and super-coarse dust aerosols in acting as CCN or INP. Subsequently, the abundance of coarse and super-coarse dust aerosols can have substantial impacts on the properties and evolution of clouds, as well as the intensity and distribution of precipitation. We discuss here the role of coarse and super-coarse dust aerosols as CCN (Section 4.3.1) and INPs (Section 4.3.2) on the properties of clouds and precipitation.

4.3.1. The role of coarse and super-coarse dust aerosols as cloud condensation nuclei

The majority of CCN around the globe are submicron aerosol particles composed, at least in part, of soluble inorganic and organic materials. It is well known that increasing the concentration of this class of CCN leads to increased cloud droplet number concentration (CDNC) and that these clouds have a greater albedo and lifetime (Lohmann and Feichter, 2005). Mineral dust can also interact with warm (liquid) clouds, but due to its inherently different composition (being insoluble) and the fact that the size of dust particles extends to much greater sizes than typical CCN, dust particles have a distinct and complex effect on warm cloud microphysics. While freshly emitted dust can be largely

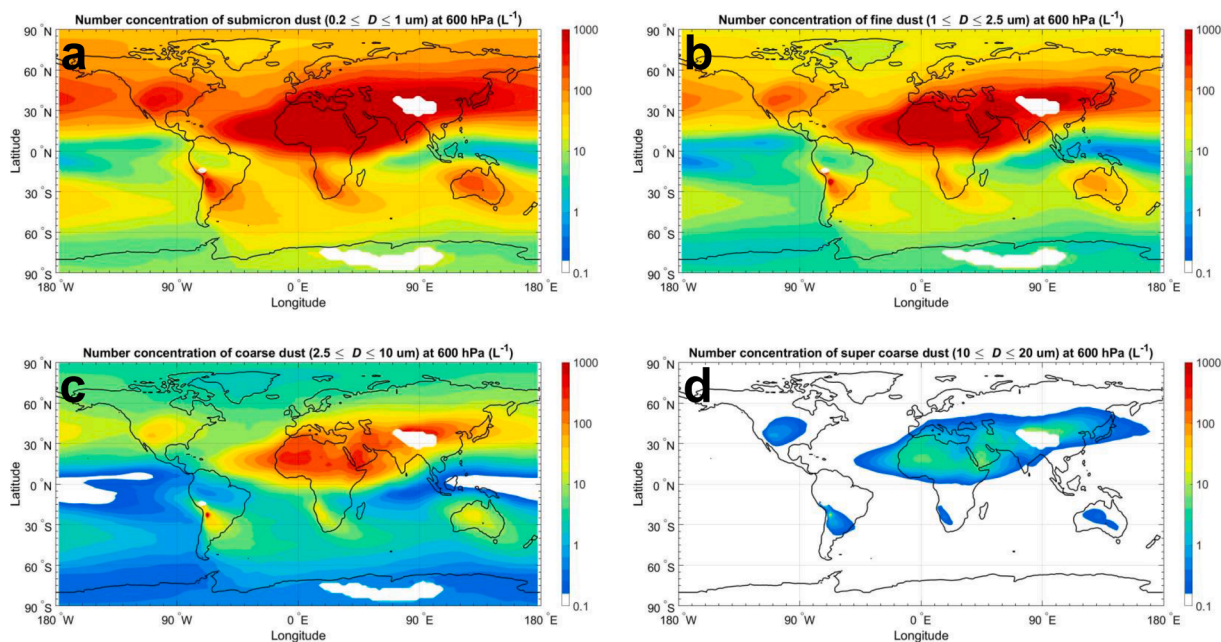


Fig. 13. The global dust number concentration for four dust size ranges – (a) submicron-fine dust ($0.2 \leq D \leq 1 \mu\text{m}$); (b) super-micron-fine dust ($1 \leq D \leq 2.5 \mu\text{m}$); (c) coarse dust ($2.5 \leq D \leq 20 \mu\text{m}$); (d) super-coarse dust ($10 \leq D \leq 20 \mu\text{m}$) – at 600 hPa from the DustCOMM dataset (see beginning parts of Section 4 for details).

devoid of soluble materials, it has been shown to have modest hygroscopic properties, and uptake of soluble material can enhance its CCN activity (Kumar et al., 2009; Nenes et al., 2014). Under the right conditions, the addition of desert dust to the atmosphere can therefore lead to an increase in the CDNC (Karydis et al., 2017). However, the uptake of condensable material, such as sulphuric acid or organics, onto the surface of mineral dust can also deplete the reservoir of material required to create other CCN, and therefore the presence of mineral dust can reduce the CCN concentration (Manktelow et al., 2010; Karydis et al., 2017; Zamora and Kahn, 2020). Karydis et al. (2017) suggest that dust enhances the CDNC over the African and Asian deserts, whereas, in polluted regions such as Europe, desert dust can deplete the CDNC. In addition to these effects, larger dust particles can activate at relatively low supersaturation, thus potentially inhibiting the activation of smaller CCN (Karydis et al., 2011). Larger aerosol can also produce cloud droplets that can be much larger than the bulk of cloud droplets initiating a collision coalescence process (Feingold et al., 1999). Since the main topic of this review is on coarse and super-coarse dust aerosols, we will focus on the specific role these particles play in clouds composed of liquid water (we discuss the role dust particles play in ice nucleation below).

Feingold et al. (1999) presented a case that relatively large soluble aerosol particles can create haze or cloud droplets that are substantially larger than droplets produced by standard CCN. These larger droplets fall faster than smaller droplets, thus creating conditions conducive to collision coalescence, where a falling droplet grows rapidly to drizzle sizes. This process is therefore thought to initiate precipitation sooner than it would otherwise occur (Blyth et al., 2003). These larger CCN are commonly (although not always) termed giant CCN (the term giant CCN in this context should not be confused with the term giant dust defined in Fig. 2). The effect of giant CCN on collision coalescence is largest for clouds forming in regions of high concentrations of standard CCN, such as polluted regions, whereas the effect is much smaller in clouds with low CDNC. There is considerable divergence in the literature over the size limit above which particles are considered to serve as giant CCNs. Indeed the size limit will be different when considering the giant CCN effect of suppressing the activation of smaller CCN or enhancing the coalescence process. Feingold et al. (1999) suggest that sea salt particles larger than $\sim 10 \mu\text{m}$ in diameter can initiate the collision coalescence

processes if their concentration is larger than about 0.1 to 10 L^{-1} . In contrast, Yin et al. (2000) consider particles larger than $2 \mu\text{m}$ diameter as giant CCN, and Mechem and Kogan (2008) place this limit at $1 \mu\text{m}$ diameter. It is thought that an important class of giant CCN is sea salt; however, dust is often found internally mixed with soluble material, and it has been suggested that it serves as a giant CCN (Levin and Ganor, 1996; Levin et al., 2005). In fact, Levin et al. (2005) found that the inclusion of efficient giant dust CCN enhanced collision coalescence and the resulting precipitation by as much as 37%. Clearly, large dust particles have the potential to initiate precipitation and alter cloud properties and lifetime.

To assess where in the world dust might serve as giant-CCN, we have plotted in Fig. 13 the global number concentration for four dust size ranges at 600 hPa from the DUSTCOMM dataset (see Section 4 and Kok et al., 2021a, b for details). As mentioned above, Feingold et al. (1999) found that at least 0.1 L^{-1} particles larger than $10 \mu\text{m}$ in diameter are needed to initiate precipitation. Thus, based on this, the regions with the greatest potential for dust to serve as giant CCN and influence cloud microphysical processes are close to the source regions since these larger aerosol particles have a greater fall speed. Hence, these regions include the African and Asian dust belt, but also, to a lesser extent, North America, South America, and Australia (Fig. 13d). We can also derive a concentration of particles larger than $10 \mu\text{m}$ from aircraft size distribution measurements. Integrating under the relevant portion of the size distributions reported by Ryder et al. (2018) from above the eastern tropical Atlantic, we find that the concentration of potential giant CCN was $\sim 1 \text{ L}^{-1}$, which is consistent with the model result (Fig. 13). The region where giant CCN is likely to be important is expanded to much of the globe if we consider all coarse mode particles as having the potential to serve as giant CCN (Fig. 13).

However, there are some important uncertainties and caveats in the simple analysis outlined above, and we should treat these numbers as an upper limit to the giant dust CCN concentration. Firstly, to serve as an efficient giant CCN, mineral dust particles need to become internally mixed with soluble material such as sulphate, organics, or sea salt. Indeed, it has also been argued that the uptake of sulphate onto dust is important for giant CCN (Levin et al., 1996). Hence, the ability of large dust particles to serve as giant CCN may be limited by the availability of soluble material. In addition, one would expect the largest dust particles

to be associated with intense dust activity. However, at times of high dust loading in locations such as the tropical Atlantic, convection is often suppressed because elevated dust is associated with hot-dry air (Prospero and Carlson, 1972; Carlson and Prospero, 1972). For this reason, regions with giant CCN may not be prone to convection, and the presence of the largest dust particles may not coincide with deep convective clouds. Nevertheless, there will be regions where dust interacts with clouds of varying depths (Levin et al., 2005; Stevens et al., 2016).

In summary, while there is a clear conceptual case for dust serving as a giant CCN and altering cloud properties and precipitation, there remain significant uncertainties. In particular, more work is needed to define the size range that we should consider as ‘giant’ in terms of CCN activity. The dependence on the mixing state with soluble material (through aging) and how this interacts with particle size should be explored. Also, the concentration of large dust particles that might serve as giant CCN is highly variable, challenging to measure, and carries substantial model uncertainty.

4.3.2. The role of coarse and super-coarse dust aerosols in cloud glaciation

Many clouds around the globe are sensitive to the formation of ice and are therefore affected by the aerosol particle types that catalyze ice formation (Cziczo et al., 2013; Storelmo, 2017; Ansmann et al., 2019a; Murray et al., 2021). There are a variety of aerosol types that can serve as ice-nucleating particles (INPs), and mineral dust from the world’s arid regions is thought to be one of the most important (Hoose and Möhler, 2012; Murray et al., 2012). The fact that desert dust is emitted in large quantities, transported globally, and that it has a relatively high ice-nucleating ability means it is an important INP type in cold clouds all around the planet from the surface to the top of the troposphere (Vergara-Temprado et al., 2017; Froyd et al., 2022).

Coarse, super-coarse, and giant dust particles may play an important role in cloud glaciation close to desert sources. In contrast, in regions remote from deserts, fine mode dust (0.05 to 2.5 μm) is thought to be most important for INP populations since it has a lifetime of weeks in the free troposphere, whereas the coarser mode has a much shorter lifetime. The tropical Atlantic is a location that is both rich in coarse mode dust and is influenced by deep convective clouds in which mixed-phase processes, including heterogeneous ice production on INP, play an important role in defining cloud properties (Hawker et al., 2021). While the air masses with the highest dust loadings are also the locations with the least convective activity, air in the eastern tropical Atlantic is generally dusty (Carlson and Prospero, 1972); hence dust is thought to play an important role in convective cloud systems in this region.

The impact of INPs and heterogeneous freezing (a process in which ice formation is mediated by insoluble particles) on convective clouds is complex and has been the topic of several modeling studies (Fan et al., 2010; Gibbons et al., 2018; Takeishi and Storelmo, 2018; Hawker et al., 2021). It has been shown that heterogeneous ice nucleation occurring in the mixed-phase cloud regime can reduce the amount of water available for homogeneous freezing, resulting in fewer and larger ice crystals in the high-altitude cirrus anvil. This is significant because the properties and lifetime of the anvil are important for a convective system’s cloud radiative effect since anvils cover a much larger area than the convective core and persist long after the convective core has dissipated (Hawker et al., 2021). The release of latent heat when liquid water is converted to ice can also invigorate convective clouds, resulting in the convective cores reaching higher altitudes (Gibbons et al., 2018). These studies show that it is not only the concentration of INP active at some temperatures that is important, but also the temperature dependence of the INP activation (Takeishi and Storelmo, 2018; Hawker et al., 2021). At low supercooling (around $-5\text{ }^\circ\text{C}$), nucleation by INPs drives the Hallett-Mossop ice multiplication process (Crawford et al., 2012), whereas, at lower temperatures, heterogeneous nucleation can compete directly with homogeneous freezing (Hawker et al., 2021). Hence, it is important to understand the concentration of INPs that become active right

through the full mixed-phase temperature range from just below 0 to around $-38\text{ }^\circ\text{C}$.

Heterogeneous ice nucleation on desert dust has been described using a number of approaches, each with its own advantages and disadvantages (Murray et al., 2012). Nucleation is fundamentally a time-dependent, probabilistic process, and to represent this time dependence, classical nucleation theory has been applied (Hoose et al., 2010; Zhao et al., 2021). This approach requires us to treat each unit surface area of dust as having an identical ice-nucleating ability. However, natural dust aerosols are made up of multiple minerals (Kandler et al., 2009), and even within each mineral class, nucleation probability across a surface is not uniform, instead occurring at specific active sites (Holden et al., 2019, 2021). This has led to stochastic models where classical nucleation theory is used, but the distribution of nucleating abilities is described using a probability distribution (Niedermeier et al., 2011; Broadley et al., 2012; Herbert et al., 2014). However, a simpler approach is to assume the time dependence of nucleation is second order compared to the site-to-site variability of nucleation probability across the surface. The evidence for nucleation occurring at specific sites on mineral surfaces is very strong (Holden et al., 2019), and the simplicity of neglecting the time dependence of nucleation is attractive; hence this so-called ‘singular’ approach has been widely used.

The singular ice-active site density approach has been used to describe both desert dust (Niemand et al., 2012; Ullrich et al., 2017; Reicher et al., 2018; Harrison et al., 2022) and the individual minerals in desert dust (Atkinson et al., 2013; Peckhaus et al., 2016; Harrison et al., 2019). Work over the last decade has demonstrated that the potassium-rich feldspars (K-feldspars) are the most active component of desert dust (Niedermeier et al., 2015; Harrison et al., 2019), a finding which contrasts with older reports where it was thought that the clay minerals dominated immersion mode freezing (Pruppacher and Klett, 2010). The advantage of linking INP concentration to K-feldspar surface area is that mineralogy is size dependent, and there is thought to be less feldspar and quartz in the fine fraction compared to the coarse fraction (Atkinson et al., 2013). The smaller fraction of ice-active minerals in the fine mode than in the coarse mode is consistent with measurements indicating the activity of dust decreases with particle size (Reicher et al., 2018). Hence, applying the same ice active site density to all sizes may overestimate the contribution of the fine-mode dust to the INP population.

In the eastern tropical Atlantic, it is thought that desert dust from Africa dominates the INP population (Price et al., 2018), and the emergence of detailed size distributions covering the full range of dust sizes allows us to assess the importance of the coarse, super-coarse, and giant dust to the INP population in this region. This calculation is based on the size distribution from the Saharan Air Layer (SAL) layer measurements in the AER-D (Ryder et al., 2018) (shown in black in Fig. 4) in combination with the temperature (T) dependent active site density (n_s) parameterization for K-feldspar from Harrison et al. (2019). For each size bin, i , the fraction activated at T was derived for particles of diameter, D , that had a surface area per particle, s , assuming they were spherical and using Eqn. (2)

$$f(T, i, D) = 1 - e^{-n_s(T)s(i,D)} \quad (2)$$

The concentration of dust particles that activate to ice at T , $N_T(T)$, was then $f(T, i, D)$ multiplied by the total dust concentration in that size bin, N_i . This analysis allows us to plot $N_{\text{INP}}(T)$ size distributions ($dN_{\text{INP}}(T)/d\log D$), plots that reveal which size ranges contribute most to the INP population for different temperatures. By summing $N_{\text{INP}}(T, i)$ over the size bins, we can produce the total $N_{\text{INP}}(T)$ over the whole mixed-phase temperature regime.

Mineral dust contains a variable quantity of K-feldspar, with desert dust particles typically containing between a few and a few tens of percent of feldspar (Atkinson et al., 2013; Perlwitz et al., 2015; Kandler et al., 2018; Harrison et al., 2022). In our calculations, we assume that the feldspar is externally mixed and that the surface area fraction is in

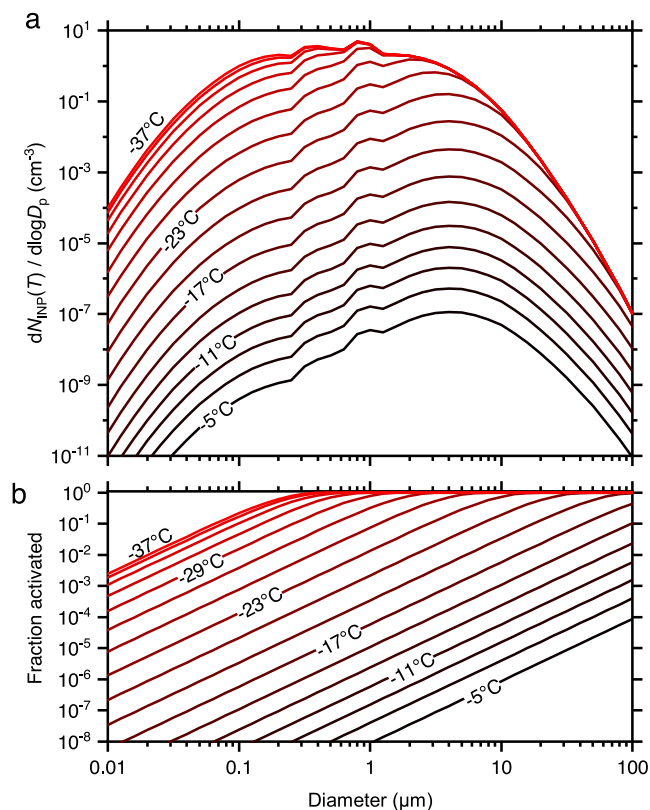


Fig. 14. Analysis of the size dependence of dust INPs. a) shows the INP size distribution for desert dust in the eastern tropical Atlantic based on the AER-D size distributions reported by Ryder et al. (2018). b) shows the fraction of K-feldspar-containing dust particles that can become active as a function of diameter and temperature. This is for the ‘20, 1%’ K-feldspar assumption. See Section 4.3.2 for details.

proportion to the mass fraction of feldspar. The external mixing assumption will lead to an underestimate in the INP concentration contribution for the larger particles. The amount of K-feldspar also increases with size so that there is around a factor of 10 more feldspars in the particles bigger than 10 μm than the particles in the fine mode (Nickovic et al., 2012; Perlwitz et al., 2015). To approximate this size dependence of the mineralogy, we assume that all particles bigger than 10 μm contain 20 % (2 %) K-feldspar and particles smaller than 2.5 μm contain 1 % (0.1 %) K-feldspar and assume a logarithmic decrease of this proportion between 10 and 2.5 μm (referred to as the 20, 1 % (2, 0.1 %) K-feldspar assumption; the values in brackets were used to test the sensitivity to these proportions).

The resulting plots are shown in Fig. 14 and Fig. 15. The INP size distributions in Fig. 14a show that the peak in the INP size distribution above temperatures of about -23°C is in the coarse mode, whereas as temperature decreases, the peak shifts to smaller sizes. This shift is a result of the activated fraction (Fig. 14b) equaling unity – where all particles are activated – for the larger sizes in the distribution. The temperature dependence of the contribution of the different modes is reinforced in Fig. 15a, where we have plotted the fraction of INP, which are from the fine, coarse, super-coarse, and giant modes. Across the full mixed-phase temperature range, the giant mode particles are too few to make a major contribution to the INP population. In contrast, the super-coarse, coarse and fine mode particles all make a substantial contribution. The relative contribution of the super-coarse and coarse mode decreases below about -23°C and the fine mode becomes more important.

The relative contribution of the different modes is a function of the size distribution and the assumptions made in this set of calculations,

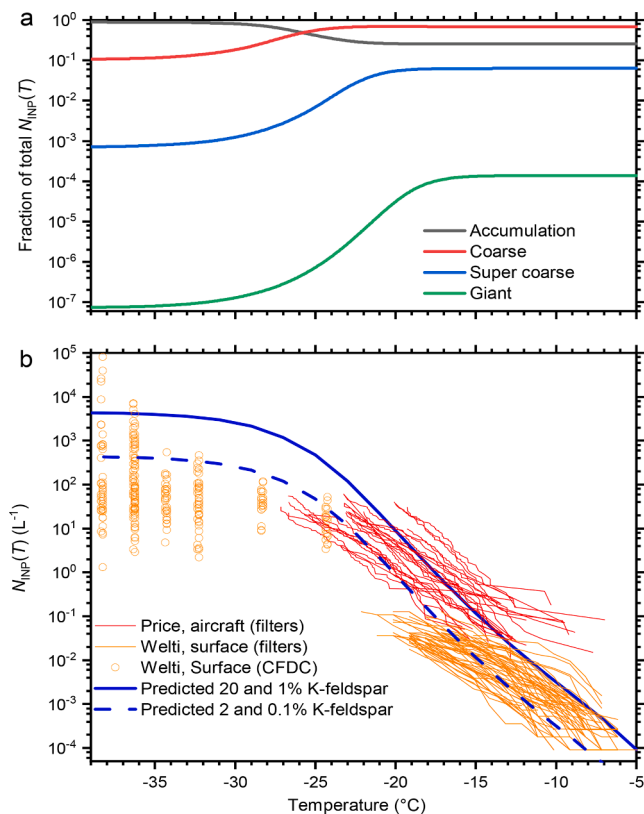


Fig. 15. The temperature dependence of the INP dust population and the contribution of the various size categories. a) the fractional contribution of the fine (accumulation) mode (0.05 to 2.5 μm), the coarse mode (2.5 to 10 μm), the super-coarse mode (10 to 62.5 μm), and the giant mode (62.5 to 100 μm). This is for the case where the particles bigger than 10 μm have 20 % K-feldspar and particles smaller than 2.5 μm have 1 % K-feldspar (see Section 4.3.2 for details). b) shows a comparison of the predicted total INP concentrations (N_{INP}) to the limited number of measurements in the eastern tropical Atlantic. Price et al. (2018) made airborne measurements in the SAL and boundary layer using a filter technique, whereas Welti et al. (2018) made measurements at the surface in Cape Verde using a filter technique and a continuous flow diffusion chamber (CFDC). The data from Price et al. (2018) were adjusted downwards by a factor of 2.5 to take into account sub-isokinetic inlet effects that have since been characterized (Sanchez-Marroquin et al., 2019). The solid blue line is for the case where particles bigger than 10 μm have 20 % K-feldspar and particles smaller than 2.5 μm have 1 % K-feldspar, whereas the dashed blue line is for a feldspar concentration 10 times smaller.

but they do illustrate that the coarse and super-coarse mode particles are critically important for defining the INP population in a region relatively close to the source. This should inform the sampling strategy employed in field campaigns. For example, employing a 2.5 μm size cut in the sampling system would lead to a substantial undercounting of the INP concentration, particularly for those INP active at temperatures above about -23°C .

We also compare our predicted total INP (integrating under the INP size distribution curve) with the available measurements in the eastern Tropical Atlantic. The AER-D measurements were made in the same set of flights on the same aircraft as the INP measurements reported by Price et al. (2018). Hence, we can make a direct comparison between these results with the ‘20, 1 %’ K-feldspar assumption. The agreement in both magnitude and slope is good. Also, Ryder et al. (2018) report dust variability in their measurements of about a factor of 15, which is comparable to the variability in the measurements of Price et al. (2018). We also plot the data of Welti et al. (2018), measured at the surface in Cape Verde and over a different period. These measurements indicate a lower INP concentration. There are multiple reasons why the INP

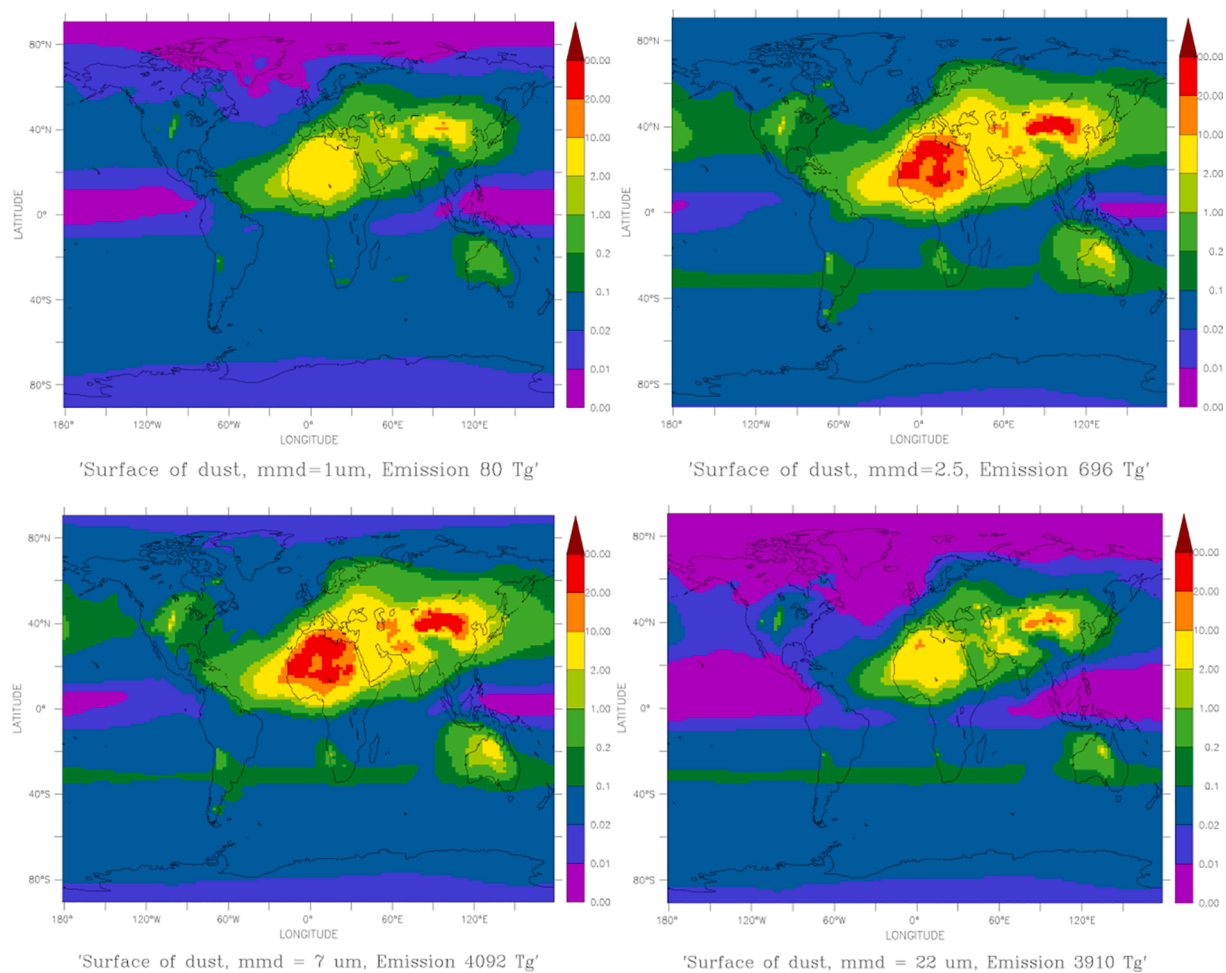


Fig. 16. Global maps of the annual mean of the total surface area per unit column of air of mineral dust calculated by the LMDZOR-INCA model in four modes represented by the following mean modal diameters. $1\ \mu\text{m}$, $2.5\ \mu\text{m}$, $7\ \mu\text{m}$, and $22\ \mu\text{m}$. Units are $\text{cm}^2\ \text{m}^{-2}$. These modes correspond rather well to the fine mode ($1\ \mu\text{m}$), coarse ($2.5\text{--}10\ \mu\text{m}$), and super-coarse ($10\text{--}62.5\ \mu\text{m}$) classes of the classification proposed earlier (Fig. 2). The giant dust particle fraction (greater than $62.5\ \mu\text{m}$) is not represented, as models still struggle to account for the transport of these very large particles. We use LMDZOR-INCA here because it has previously been used to investigate the uptake of reactive or non-reactive species on mineral dust (e.g., George et al., 2007; Ndour et al., 2008) and has recently been upgraded to represent the size distribution of mineral dust, including coarse particles (Checa-García et al., 2021).

concentration reported by Welti et al. (2018) was lower, not least that it was a different location and time (and at the surface) to the aircraft data reported by Price et al. (2018) and Ryder et al. (2018). The measurements of Welti et al. (2018) are consistent with the Ryder et al. (2018) average size distribution and a factor of 10 lower feldspar concentration (‘2, 0.1 %’ K-feldspar assumption).

Overall, this analysis indicates that coarse and super-coarse mode dust aerosols are very important for the INP concentration in the eastern tropical Atlantic. Dust in this location is within a few days of transport from the dust source regions in north Africa and we would anticipate the coarse and super-coarse modes to become less important on further transport as the largest particles in the size distribution are deposited.

4.4. Impacts of coarse and super-coarse dust aerosols on atmospheric chemistry

Mineralogy varies according to the parent soil from which dust originates. In addition, the size fraction of the aerosol considered exhibits very large mineralogical variations. Therefore, while airborne in the atmosphere, one important aspect of mineral dust is that it undergoes chemical aging by the uptake of reactive compounds in the gas phase, by photochemistry, and by in-cloud and off-cloud processing. These aspects, and the role of the coarse fraction size and mineralogy,

are discussed in this section.

Many field and laboratory studies (de Reus et al., 2000; Grassian, 2001; Usher et al., 2003; Bonasoni et al., 2004; Chan et al., 2005; Crowley et al., 2010; Shen et al., 2016; George et al., 2015; Tang et al., 2016, 2017; Zhou et al., 2015; Zein et al., 2014; Ponczek et al., 2019) show that dust aerosols provide with a reactive surface that removes and transforms various inorganic and organic trace gases and radicals, including nitrogen-containing compounds (NO_x , HNO_3 , N_2O_5 , HONO), sulphur dioxide (SO_2), and ozone (O_3). It is also a sink for volatile organic compounds (VOCs) such as formaldehyde (HCHO), acetone (CH_3COCH_3), glyoxal ($\text{H}_2\text{C}_2\text{O}_2$), and organic acids, H_2O_2 , and various radicals (OH, HO_2 and NO_3) (Bedjanian et al., 2013a, b; Karagulian et al., 2005; Lasne et al., 2018; Li et al., 2001; Liggio et al., 2005; Matthews et al., 2014; Ponczek and George, 2018; Romanias et al., 2016; Romanías et al., 2016; Wang et al., 2018; Wang et al., 2020a, b; Zein et al., 2014; Zeineddine et al., 2018, 2017). Additionally, mineral dust aerosols containing titanium and iron oxides are photo-chemically active substrates that can uptake of NO_2 and form the NO_3^- anion in the presence of light (Ndour et al., 2008, 2009), while also acting as a source of OH radical in wet conditions (Dupart et al., 2012). Chemical box models, global and regional climate models, all including the coarse and super-coarse fraction, show that those processes are capable of affecting the composition and the oxidative capacity of the atmosphere (Dentener

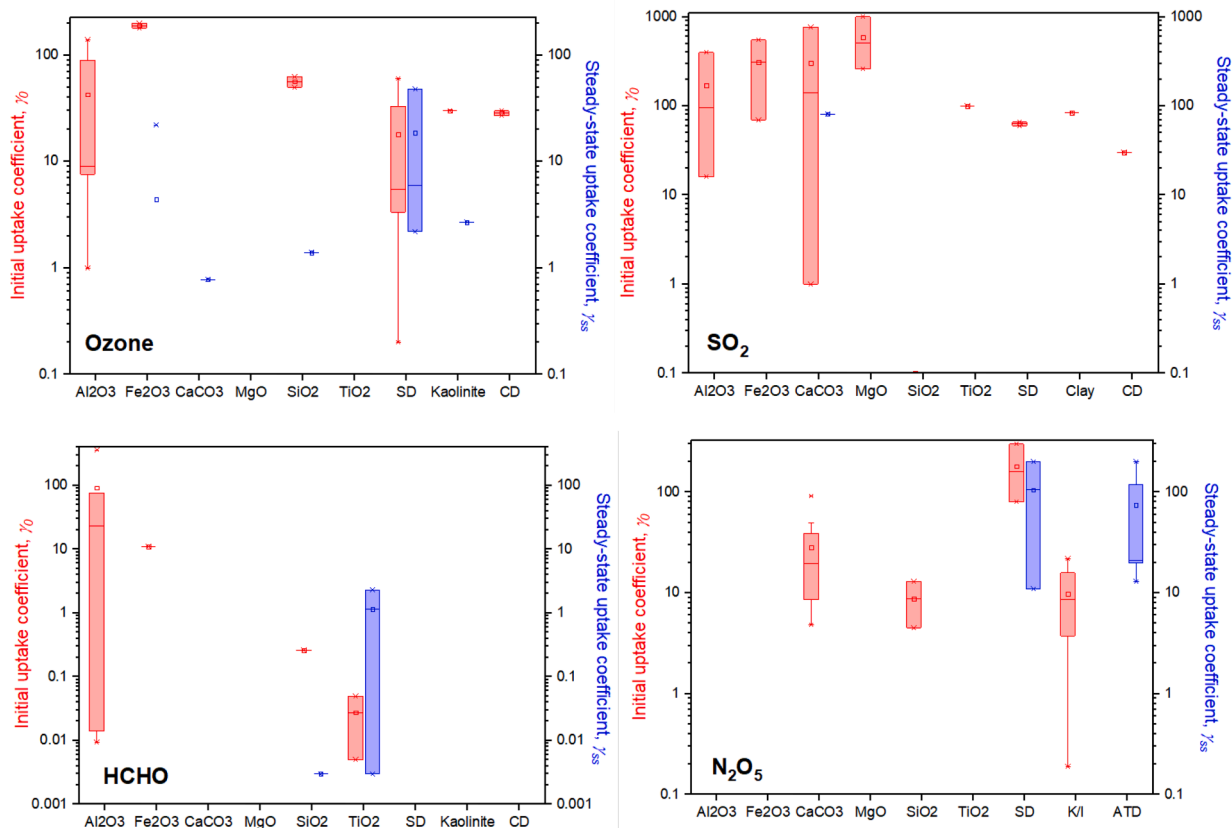


Fig. 17. Values of the initial uptake coefficients γ_0 , in red) and of the steady-state uptake coefficients (γ_{ss} , in blue) for four relevant reactive gas species and for a number of synthetic minerals or authentic dust samples. Values of γ_0 and γ_{ss} can either represent the uptake on the particle geometric area or the BET surface area, without distinction. SD stands for “Saharan dust”, CD for “Chinese dust”, K/I for “Kaolinite and Illite”. While values are reported in the supplementary document, the ones here have been multiplied for 10^{-6} for clarity.

et al., 1996; Zhang et al., 1994; Zhang and Carmichael, 1999; Bauer et al., 2004).

Heterogeneous processing and photochemistry involving mineral dust can also contribute to new particle formation in the atmosphere. Photo-catalysis can induce the desorption of gaseous OH radicals from the surface of mineral dust containing metal oxides, which then promotes the formation of new H_2SO_4 particles in the vicinity of the dust particles when SO_2 is present at atmospherically relevant humidity conditions (Dupart et al., 2012). This kind of mechanism is also proposed to explain the unexpected formation of secondary organic aerosol (SOA) in the presence of VOCs, as observed for dust episodes mixed with pollution in the remote atmosphere (Nie et al., 2014).

On the other hand, the condensation of reactive gaseous species on coarse mineral dust particles is a mechanism for transferring the mass of secondary aerosols from the fine to coarse fraction. Coarse mineral dust particles can accumulate coatings that contain sulphates, nitrates or organic compounds that would preferentially be found in the accumulation particle mode (Carlos-Cuellar et al., 2003; Falkovich et al., 2004, 2001, p. 200; Fan et al., 1996; Koçak et al., 2007; Li-Jones and Prospero, 1998; Okada and Kai, 1995; Russell et al., 2002; Sobanska et al., 2003; Sullivan et al., 2007; Trochkin et al., 2003; Zhou et al., 1996). In addition, many studies based on single-particle analysis show that mineral dust can be internally mixed with sea salt (Andreae et al., 1986; Deboudt et al., 2010; Denjean et al., 2015; Kaaden et al., 2009; Niemi et al., 2005; Niimura et al., 1998; Okada et al., 1990; Reid et al., 2003b; Zhang et al., 2003a, 2003b), soot and organic carbonaceous particles (Arimoto et al., 2006; Deboudt et al., 2010; Falkovich et al., 2004, 2001; Formenti et al., 2011b; Hand et al., 2010; Kandler et al., 2009; Matsuki et al., 2010; Parungo et al., 1994, 1992; Russell et al., 2002).

Ultimately, atmospheric processing has an impact on the properties

of mineral dust. Chemical aging can modify the dust hygroscopicity (e.g., Li-Jones et al., 1998; Laskin et al., 2005; Tobo et al., 2010), henceforth its capability of acting as cloud or ice condensation nuclei (e.g., Levin and Ganor, 1996; Kulkarni et al., 2015; Kumar et al., 2011; Sullivan et al., 2009; Tang et al., 2016; Krueger et al., 2003) as well as its solubility in water, altering its fertilization capabilities for the oceans (e.g., Meskhidze et al., 2005; Paris et al., 2011; Shi et al., 2012; Kandler et al., 2020).

The size of mineral dust particles, directly and indirectly, its chemical aging, and the impacts on atmospheric chemistry that result from it. The removal of atmospheric gases by solid-phase particles requires an initial collision of a gas molecule X with the condensed phase. The pseudo-first-order removal rate $\frac{d[X]_g}{dt}$ can be expressed as:

$$\frac{d[X]_g}{dt} = -\frac{\gamma \bar{c}(X) S_A [X]_g}{4} \quad (3)$$

where $[X]_g$ is the concentration of X in the gas phase (molecules cm^{-3}), $\bar{c}(X)$ the average molecular speed of the gas molecules (cm s^{-1}), γ is the uptake coefficient of the compound X , representing the probability of non-reactive and reactive uptake between the chemical species X and the surface of the condensed phase and S_A is the surface area of condensed phase per volume of the gas phase, cm^{-1} .

We illustrate the annual mean of the geographical distribution of the surface area of mineral dust in Fig. 16 (Di Biagio et al., 2020). The figure shows the distribution of the surface area of coarse and super-coarse particles in the atmosphere, and the extent to which they are available for heterogeneous processing. In particular, it shows the predominance of the available surface of coarse and super-coarse particles in those areas of the world (e.g., Arabian Peninsula, East Asia) where mixing

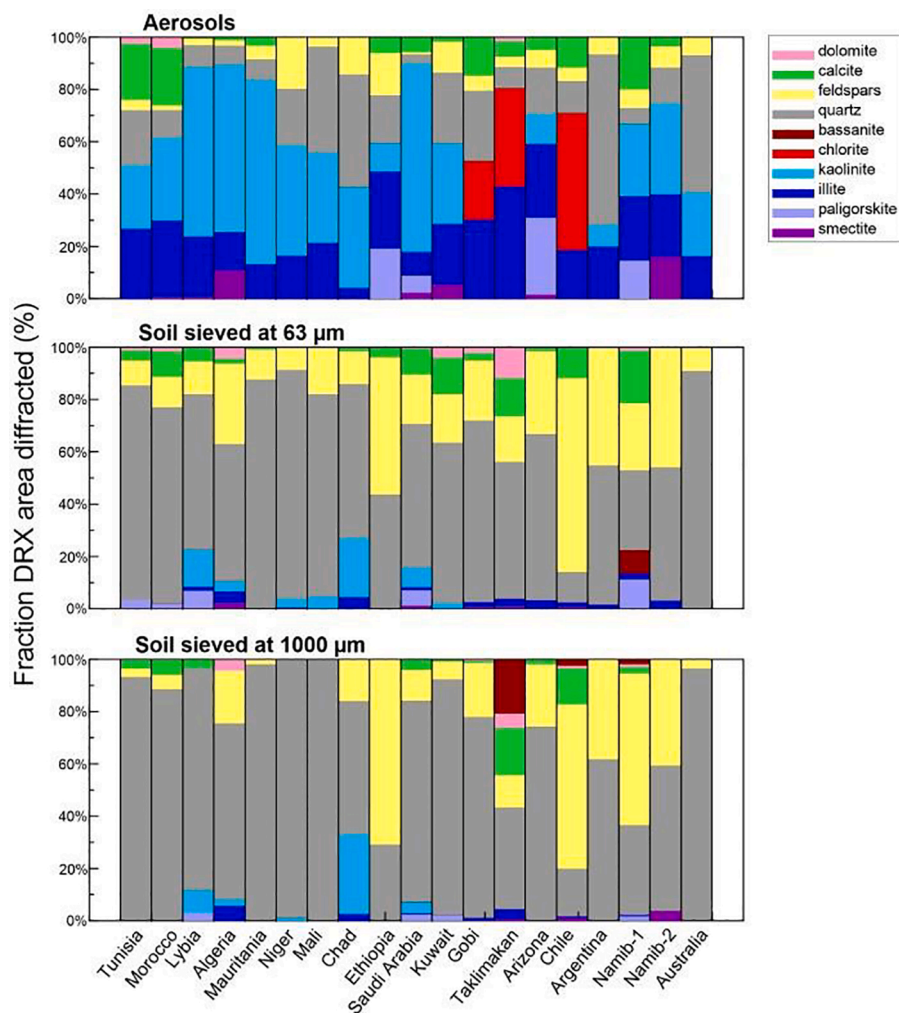


Fig. 18. Mineralogical composition of the suspended aerosol particles of size smaller than $10\ \mu\text{m}$ in aerodynamic diameter (top panel) compared to that of the parent soils sieved at $63\ \mu\text{m}$ and $1000\ \mu\text{m}$, respectively (mid- and low-panel). The aerosol was generated by mechanical shaking from the parent soil sieved at $1000\ \mu\text{m}$, suspended in a large simulation chamber, and extracted on polycarbonate filters. Both the aerosol and the soil fractions were analyzed by X-ray diffraction. Data represent the percent surface diffracted by each identified mineral. All details about the methodology and evaluation of size ranges are found in Di Biagio et al. (2019, 2017).

with intense anthropogenic emissions is expected (e.g., Pósfai et al., 2013; Semeniuk et al., 2015; Pan et al., 2017; Xia et al., 2022). The surface area of the coarse and super-coarse mode is also large in the Mediterranean sea and in western Africa, towards the Gulf of Guinea, where additional mixing with seasonal biomass burning may also occur (e.g., Bonasoni et al., 2004; Johnson et al., 2008; Osborne et al., 2008; Prasad et al., 2010; Abdelkader et al., 2015). Furthermore, because of the known difficulties of models in transporting particles larger than $20\ \mu\text{m}$ at distances (see Section 5.2.2), the features discussed above should be regarded as lower limits and concentrations could be significantly higher.

Mineralogical composition varies strongly with the surface area as well as the aerodynamic diameter of the dust particle (c.f. Section 2.1). Mineral dust consists of a complex mixture of minerals whose proportions vary according to the nature of the parent soil, as well as the particle size (Claquin et al., 1999; Kandler et al., 2009; Nickovic et al., 2012; Journet et al., 2014). At emission, the size-dependence of the dust composition is determined by the size-fractionation that occurs by the saltation and sandblasting of the grains erodible soils by wind (e.g., Journet et al., 2014; Perlwitz et al., 2015). The relative abundance of clays (majority of illite and kaolinite) is higher in the fine fraction, while quartz (SiO_2) and calcium carbonate (CaCO_3) are more abundant in the coarse, super-coarse, and giant fractions (e.g., Lafon et al., 2006; Kandler et al., 2007; Chou et al., 2008; Kandler et al., 2009; Formenti et al., 2011b, 2014; Kandler et al., 2020). Ti- and Fe-oxides are ubiquitous in fine and coarse fractions (Lafon et al., 2006; Kandler et al., 2007). During transport, as discussed above, the composition of each modal

class changes by chemical aging and gravimetric deposition of larger particles, enhancing the relative importance of clay minerals compared to carbonates and quartz (e.g., Weinzierl et al., 2017).

Those different minerals react differently toward trace gases. We summarize the values taken by the uptake coefficients for minerals other than Al- and Fe- oxides, calcium carbonates and natural and model soils (Saharan dust and Arizona test dust) in Fig. 17. Details of these values and those not shown in Fig. 17 can be found in the supplementary document, based on reviews, including by Usher et al. (2003), Crowley et al. (2010), and Tang et al. (2017). Analyses of these values (Fig. 17 and supplementary document) are not straightforward because of the many variables that might influence the resulting value of the uptake coefficient. These are the environmental conditions of the experiments (relative humidity, temperature, gas phase concentration or surface pre-treatment i.e. thermal pre-treatment, pre-exposure to oxidants, etc.), the state of the mineral dust (sieved soil, synthetic or natural mineral or soil), and the evaluation of its available surface for uptake/reaction, either the geometric area or the total sample surface area (e.g., the Brunauer–Emmett–Teller (BET) surface area), representing the maximum available surface area, including internal pore volume and bulk surface area of granular material (Chen et al., 2020).

As summarized in Fig. 17, the uptake on quartz (SiO_2), the major constituent of mineral dust at emission is understudied. At the steady state, the uptake capacity of quartz is very low with respect to HCHO (0.003×10^{-6}), and low for O_3 . On the contrary, SiO_2 is relevant to the uptake of N_2O_5 . The other major mineral in the coarse and super-coarse fraction, calcium carbonate (CaCO_3), is extremely relevant for the

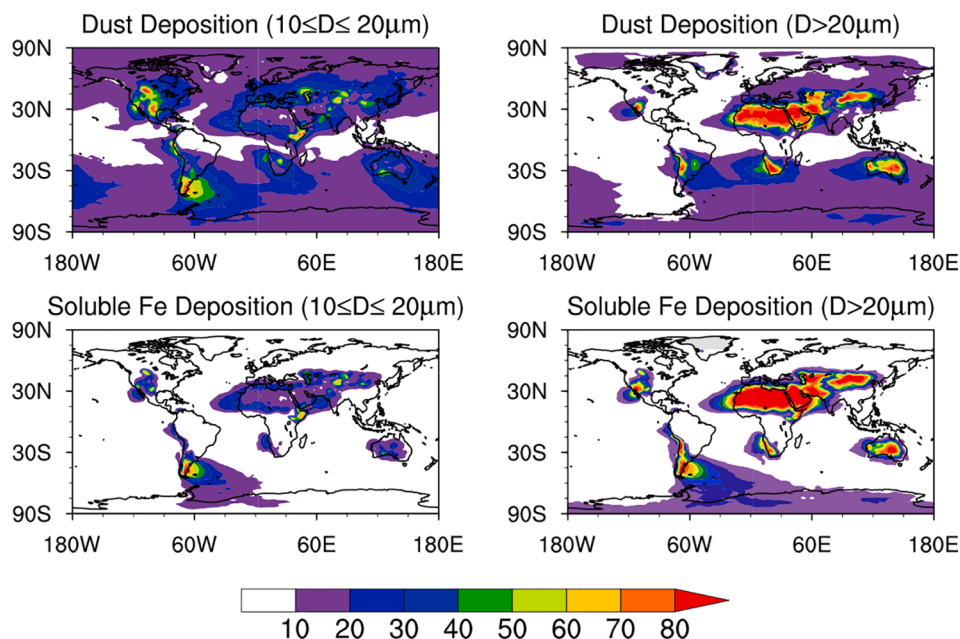


Fig. 19. Fraction of the dust (a and b) and soluble iron (c and d) deposition estimated in a sensitivity study that is between 10 and 20 μm in diameter (a and c) and greater than 20 μm in diameter (b and d). The solubility of iron in dust $<10 \mu\text{m}$ comes from the intermediate solubility mechanisms of Hamilton et al. (2019), while the solubility of iron in dust $>10 \mu\text{m}$ is assumed to be 0.45 % (Luo et al., 2008; Longo et al., 2016).

uptake of N_2O_5 and moderately or little to that of SO_2 and O_3 . While HNO_3 reactivity is not discussed here, these facts are consistent with the fact that nitrate formation occurs preferentially on calcium carbonate particles (e.g., Sullivan et al., 2007; Fairlie et al., 2010). No data of the uptake of CaCO_3 with formaldehyde are reported in the above-cited reviews, which, on the contrary, document that the uptake on aluminum oxide (Al_2O_3) should not be neglected. A few values of the uptake coefficients of ozone on Al_2O_3 are obtained for different size fractions, but a trend on its size dependence cannot be established. Considering the geometric surface distribution, the reported initial uptake coefficient for SO_2 ranges from 16 to 400×10^{-6} , of the same order of magnitude as for ozone, HCHO, and N_2O_5 . These tendencies are also observed with respect to authentic dust samples (Saharan dust, Arizona dust and Chinese dust or loess), but the actual values can differ by order of magnitudes (and no data for the uptake of HCHO are available).

To improve on our understanding of how uptake coefficients evolve during dust atmospheric cycle, and to specifically constrain these coefficients for the coarse and super-coarse fractions which account for most of the available reactive surface, we adopt here Tang et al. (2017)'s recommendation, and we further extend it. Tang et al. (2017) and Urupina et al. (2021) suggested the investigation of the reactivity of the authentic dust sources (or mineralogical equivalent soils), instead of those of individual minerals, to account for the right proportions and competitive effects of the different mineral phases. Indeed, as an example, Abou-Ghanem et al. (2020) showed that natural TiO_2 minerals do not behave like the commercially available TiO_2 that was extensively used by Ndour et al. (2009, 2008). Additionally, and to the best of our knowledge, there is no systematic measurement of the uptake coefficient per size class to date (e.g., Usher et al., 2003; Tang et al., 2017). Therefore, we recommend that to investigate more atmospheric relevant dust surfaces, the uptake capability or reactivity of dust should be investigated on size-segregated fractions, and whenever possible, on airborne mineral dust rather than on deposited soils.

This recommendation is supported by the differences that exist between the mineralogical composition in the airborne aerosol particles, including the coarse fraction, in the atmosphere, and that of the corresponding soil fractions. Fig. 18 shows this difference for soil mineralogy of soil fraction sieved up to 63 μm and 1000 μm , and for the mineralogy

obtained for airborne atmospheric dust particles. We recommend that future studies of reactive and non-reactive uptake of coarse mineral dust evolve towards the analysis of the aerosol fractions of airborne particles more than soil. In addition, new studies should take advantage of the synergy of recent developments, such as the use of large atmospheric simulation chambers where the airborne dust aerosol can be generated in a realistic manner, including at atmospheric relevant sizes and at transport time scales (e.g., Di Biagio et al., 2014). First results from recent experiments indicate that atmospheric chamber experiments are efficient in probing the changes in the mineral dust aerosol properties due to interactions with the gas phase, while the determination of uptake coefficients remains challenging as the aerosol surface versus surface of the chamber is relatively low (P. Formenti and M. Romanias, pers. comm.). Additionally, hyperspectral measurements from space, both in the UV/visible and the infrared ranges, such as the incoming NASA EMIT (Earth Surface Mineral Dust Source Investigation) mission (<https://earth.jpl.nasa.gov/emit/>) (Green et al., 2020) and the AERO-IASI method of Cuesta et al. (2015), respectively, provide with novel capabilities of probing the composition of dust sources and airborne mineral dust at the global scale and better constrain their mineralogy worldwide.

We recommend that future laboratory investigations with soils use sieved fractions only. Indeed, the comparison of the mineralogy of the 63- μm soil fraction reported in Fig. 18 and that of the aerosols in dust storms reported by Kandler et al. (2009) suggests that the 63 μm -sieved soil fraction could represent the composition of super-coarse particles. While sieving soils at 10 μm could be challenging for laboratory uptake studies, as the dust mass would be low, we recommend at least sieving the soils at 20 μm to capture the uptake of the coarse particle fraction. In addition, Fig. 18 suggests that the individual minerals investigated to date are insufficient to understand the reactivity of the soil samples. For example, no study has been done, to our knowledge, on feldspars which make up for a significant fraction of soils. Furthermore, no large-scale targeted projects have addressed the reality and the significance of the impact of mineral dust and its coarse fraction to atmospheric chemistry since the MINeral dust And TROpospheric Chemistry (MINATROC; e.g., de Reus et al., 2005). These are needed in various mixed environments, urban and remote, as opportunistic observations might fail in providing

the full set of observational parameters needed to characterize the air masses and initiate chemical box models. Finally, size segregated dust measurements are a requirement to evaluate the relative significance of the dust coarse fractions.

4.5. Impacts of coarse and super-coarse dust aerosols on biogeochemistry

Desert dust aerosols can supply important nutrients, especially iron and phosphorus, for land and ocean biogeochemistry (Duce and Tindale, 1991; Jickells and Moore, 2015; Jickells et al., 2005; Maring and Duce, 1990; Martin et al., 1991; Okin et al., 2004; Swap et al., 1992).

Some ocean systems have high nutrient, and low chlorophyll (HNLC; low chlorophyll or low productivity) conditions, which are postulated to be caused by iron limitation (Martin et al., 1991). In situ fertilization experiments have shown that the Equatorial Eastern Pacific, parts of the Southern Ocean, and during some seasons, the North Pacific are subject to iron limitation (de Baar et al., 2005; Boyd et al., 2007). While there are sedimentary and hot-spot sources in the ocean as well as effects from upwelling that are important for surface iron ocean budgets (Blain et al., 2001; Boyd et al., 2007; Moore and Braucher, 2008), observational analyses (Cassar et al., 2007; Lam and Bishop, 2008) and ocean biogeochemical modeling studies suggest that atmospheric inputs of iron are important in some regions (Krishnamurthy et al., 2009; Tagliabue et al., 2014; Mahowald et al., 2018). Nitrogen fixing organisms have higher iron requirements, thus linking the nitrogen and iron cycles in the ocean, and increasing the importance of the atmospheric inputs of iron (Capone et al., 1997; Moore et al., 2006, 2013). However, because the particles sediment through the surface ocean layers, not all iron is available, and most studies focus on the soluble iron fraction as more bioavailable (Baker et al., 2013). Desert dust particles tend to be less soluble than combustion iron (Ito et al., 2021b), although this varies with the mineralogy and source of the particles (Chuang et al., 2005; Guieu et al., 2005; Journet et al., 2008; Schroth et al., 2009), and desert dust particles can be made more soluble by atmospheric processing by acids (Meskhidze et al., 2005; Johnson and Meskhidze, 2013; Longo et al., 2016; Mahowald et al., 2018).

Sensitivity studies conducted using the model simulations described at the beginning of Section 4 and in Meng et al. (2022), suggest that the super-coarse fraction may represent an important contribution (>30 %) to the desert dust deposition over some ocean regions, especially close to the coasts of the major dust sources (Fig. 19). Interestingly, the super-coarse mode appears to be a relatively more important part of the dust deposition in the southern hemisphere than over the North Atlantic (Fig. 19), where much of the data has been collected (Ryder et al., 2019, 2013b, 2013a). The importance of this size fraction in these less-studied regions should be measured directly.

Dust deposition can serve as an important ballast for organic materials in the ocean mixed layer, causing organic particles to coagulate with the mineral particles, become heavier, and to move more quickly out of the ocean mixed layer, thus by itself this dust input to the ocean may modify the removal rate of carbon or nutrients from the mixed layer (Armstrong et al., 2001). Thus, missing this source of deposition may miss some of these interactions in models, although much of the deposition greater than 10 μm diameter occurs close to coastal regions, where riverine sources of sediment or nutrients make the budgets more difficult to understand (e.g., Seitzinger et al., 2005). Notice that including dust particles with a diameter up to 20 μm in models reduces this missing deposition (Fig. 19a vs Fig. 19b).

For the ocean iron problem, the soluble fraction is most important, so we combine this study with soluble iron modeling studies for the size fraction of particles <10 μm (Hamilton et al., 2019), and the assumptions that super-coarse mode dust aerosols have an iron amount of 3.5 % and iron solubility of 0.45 % – which is likely to be on the high side of observations (Luo et al., 2008; Sholkovitz et al., 2012; Longo et al., 2016). Using these assumptions, we obtain the result that for soluble iron, the super-coarse fraction is less important, and usually only important in

Table 2

Summary of the limitations in observational retrievals and modeling of coarse dust particles.

Observation of coarse dust particles	
Passive ground-based remote-sensing retrievals	<ul style="list-style-type: none"> • Very limited spatial coverage; misses most smoke and dust plumes • Relatively high AOD is required to distinguish particle type • Derived properties are column-effective – can be diluted if multiple modes of different types are present or properties such as size distribution vary vertically • Enhanced optical models for different dust types are needed; ellipsoids are usually assumed • Cloud contamination can prevent or compromise retrievals
Passive satellite retrievals	<ul style="list-style-type: none"> • Relatively high AOD required to distinguish particle type, especially over land • Retrievals require near-IR channels for coarse dust sensitivity • Multi-angle and/or polarization offers some dust discrimination capability; alternatively, particle size is used as a dust proxy, especially over water • UV absorption used to identify coarse dust is sensitive to aerosol layer height • Thermal-IR retrievals are sensitive to temperature profile, aerosol elevation, moisture, surface emissivity • Derived properties are column-effective – can be diluted if multiple modes of different types are present • Enhanced optical models for different dust types are needed; assumptions vary by algorithm • Cloud contamination can compromise retrievals
Lidar retrievals	<ul style="list-style-type: none"> • Enhanced optical model (inversion model) for irregularly shaped particles is lacking. • Size-dependent separation by means of the depolarization lidar technique is restricted (or fixed) to particles with diameters < 1 μm and greater than 1 μm. • Possible interference by other depolarizing aerosol types (pollen, fresh smoke, dry marine particles)
Modeling of coarse dust particles	
Emission	<ul style="list-style-type: none"> • Measurements of super-coarse and giant dust are difficult to make because their substantial inertia causes large fractional losses in inlets to particle samplers • Substantial terminal velocity of super-coarse and giant dust makes it difficult to determine flux emitted by eroding soil • Complex and poorly understood processes might determine the emission of super-coarse and giant dust • Numerical diffusion can affect deposition schemes in models • Limited understanding of how the fractional contributions of super-coarse and giant dust to the emission flux changes with wind speed, atmospheric stability, and soil conditions.
Transport	<ul style="list-style-type: none"> • Numerical models tend to be too diffusive, creating leakage of dust particles, for example, through inversion layers. • Processes associated with vertical mixing through subgrid-scale, parameterized processes (e.g., shallow and moist convection) are not well represented • Many transport processes depend on particle size, such that errors in the emitted size distribution can propagate into transport processes.
Deposition	<ul style="list-style-type: none"> • Insufficient knowledge of size distribution and shapes, and thus aerodynamic behavior of particles • Insufficient knowledge of electrical effects • Insufficient knowledge of microphysical detail in wet removal processes • No explicit representation of individual convective storms

coastal regions, where there may be other sources of iron, such as riverine or sedimentary (Tagliabue et al., 2014). But notice that in some important parts of the southern Hemisphere, the soluble iron inputs from the greater than 10 μm dust fraction could be up to 80 % close to South America and South Africa. Indeed, one can also speculate, that for specific dust events during dust storms, super-coarse dust particles may be important near North Africa and the Arabian Sea. Notice that including both particles up to and larger than 20 μm may be required for these regions (Fig. 19c vs Fig. 19d).

Atmospheric deposition of phosphorus from North African dust has been speculated to be important for the long-term productivity of the Amazon (Swap et al., 1992). Some studies have suggested some sensitivity of ocean biota, especially nitrogen fixation to atmospheric deposition of phosphorus close to dust source areas (Mahaffrey et al., 2003), and on the longer term, large fluxes of phosphorus in dust may help fertilize the ocean (Falkowski et al., 1998). Modeling and stoichiometric analyses do not suggest most ocean basins are sensitive to phosphorus deposition from the atmosphere (Krishnamurthy et al., 2010; Okin et al., 2011), suggesting this super-coarse mode may not be important for phosphorus, however, this analysis leaves open the option that the super-coarse mode could be important during specific dust storm events.

5. Limitations in observation and modeling of coarse and super-coarse dust aerosols

Despite the impacts of coarse and super-coarse dust aerosols on the Earth's system, their long-term observations in the atmosphere and their representation in numerical models remain challenging. First, we discuss in Section 5.1 the strengths and limitations in the remote-sensing observation of coarse and super-coarse dust aerosols in the atmosphere. Specifically, we focus here on retrievals of dust size distribution from remote-sensing observations, such as those of the AEROSOL ROBOTIC NETWORK (AERONET), lidar and space-based satellites. For instruments that directly measure dust sizes in the ocean, above the ground, and in the atmosphere, see Section 3 above. Second, we discuss in Section 5.2 the limitation in simulating the emission, transport, and deposition of coarse and super-coarse dust aerosols in climate models. A summary of the discussion points is given in Table 2. Although the table and subsequent discussion broadly focus on coarse dust, most of the highlighted limitations in observation and modeling also apply to other dust sizes, including fine dust.

5.1. The strengths and limitations in the retrieval of coarse and super-coarse dust aerosols from remote-sensing observation

Remote-sensing platforms provide long-term observations of aerosol amounts, along with some constraints on particle microphysical properties. Satellites offer frequent, extensive coverage from stable platforms, whereas ground-based instruments can capture varying conditions on very short timescales at certain locations. However, deriving detailed, size-resolved aerosol properties from these observational platforms remains challenging, as retrievals rely on inversion algorithms that are generally underdetermined, requiring underlying assumptions, and are subject to uncertainties in input parameters as well as in the measurements themselves. Further, most remote-sensing instruments are not optimized for coarse-dust observation, and as such, there are added limitations associated with the retrievals of these aerosol particles, even for techniques that offer some sensitivity (Dubovik et al., 2000; Mamouri and Ansmann, 2014; Kahn and Gaitley, 2015). In the sections below, we discuss some of the strengths and limitations of observing airborne coarse dust properties with remote-sensing instruments.

5.1.1. Ground-based remote-sensing retrievals of coarse dust and super-coarse dust aerosols

Most ground-based remote-sensing platforms exist as part of an

observational network that uses similar instrumentation and retrieval algorithm, allowing for regionally and globally representative datasets that is useful for validation studies and climate research. These remote-sensing platforms include AERONET (AEROSOL ROBOTIC NETWORK; Holben et al., 1998), SKYNET (Sky Radiometer Network; Nakajima et al., 2020), SONET (Sun-sky Radiometer Observation Network; Li et al., 2018), and CARSNET (China Aerosol Remote Sensing Network; Che et al., 2019). Because the datasets from these different platforms use a retrieval algorithm similar to that of AERONET, they exhibit similar strengths and limitations (e.g., Nakajima et al., 2020). We focus our attention here on discussing the strengths and limitations of AERONET, because it has the most extensive network and produces the most widely-used datasets among those listed above.

The ground-based AEROSOL ROBOTIC NETWORK (AERONET) instruments measure two classes of variables: the spectrally resolved direct solar intensity at 340, 380, 440, 500, 675, 870, 940, and 1020 nm wavelengths, and the directional sky radiance distribution at 440, 675, 870 and 1020 nm (Holben et al., 1998). The spectrally resolved direct solar intensity is used to compute the column aerosol optical depth (AOD) at each wavelength except 940 nm. Due to their high accuracy, these AOD measurements have been widely used as the ground truth for evaluating spaceborne remote-sensing retrieval results (Kahn et al., 2010; Levy et al., 2013; Tesche et al., 2013; Sogacheva et al., 2020) and global aerosol models (Huneeus et al., 2011; Gliß et al., 2021). In addition, the spectral sky radiance intensities and AODs are used to retrieve column-effective aerosol size distributions and complex refractive indices (Dubovik and King, 2000; Sinyuk et al., 2020).

Although the ground-based AERONET direct-sun AOD retrievals are among the highest quality atmospheric aerosol measurements made with remote sensing, identifying dust components, and retrieving their microphysical properties from AERONET data is more challenging. The AERONET level 2.0 aerosol single-scattering albedo and refractive index results are viewed as confident only for AOD greater than 0.4 at 440 nm wavelength (Holben et al., 2006). Given that such high AOD is common only for aerosol plumes, this requirement tends to skew the retrieved optical properties toward conditions of high aerosol loading (Andrews et al., 2017). The extinction Ångström exponent generally decreases with decreasing volume fraction of coarse aerosol in the column (Schuster et al., 2006). Kim et al. (2011) found that for North African dust, the extinction Ångström exponent between 440 and 870 nm in AERONET data had a value below 0.2. So, to further help distinguish coarse-mode events, especially those that are dust-dominated, some studies suggest applying an upper bound on the Ångström exponent well below unity (Holben et al., 2001; Dubovik et al., 2006). Yet, when multiple aerosol types reside in the atmospheric column, interpreting the Ångström exponent in terms of particle size is ambiguous. For example, dust and fine-mode carbonaceous particles (such as black carbon and brown carbon) tend to mix, either externally or internally, in dusty polluted regions such as northern India and eastern China (Eck et al., 2010). Additional filtering criteria have been suggested to help distinguish dust and other aerosol types in AERONET data. Russell et al. (2010) showed that due to greater light absorption in the near-ultraviolet than the mid-visible wavelength range, the absorption Ångström exponent (AAE) between 440 and 870 nm for coarse-mode mineral dust in AERONET retrievals generally exceeds 1.5 and uniquely exceeds about 2 among common aerosol types; Schuster et al. (2016b) demonstrated that relatively large particle size also contributes to the dust AAE values. Schuster et al. (2016b) also distinguish mineral dust from carbonaceous particles by requiring a retrieved imaginary refractive index < 0.0042 within the wavelength range from 675 to 1020 nm.

The presence and identification of clouds can also be a challenge for AERONET retrievals, particularly so for dust aerosol. AERONET processing algorithms include automatic cloud screening in producing Level 1.5 data in near-real-time (Giles et al., 2019). Recently, Evan et al. (2022) found that for a site close to a dust source in North America the AERONET algorithm regularly misclassified dust as clouds in 85 % of

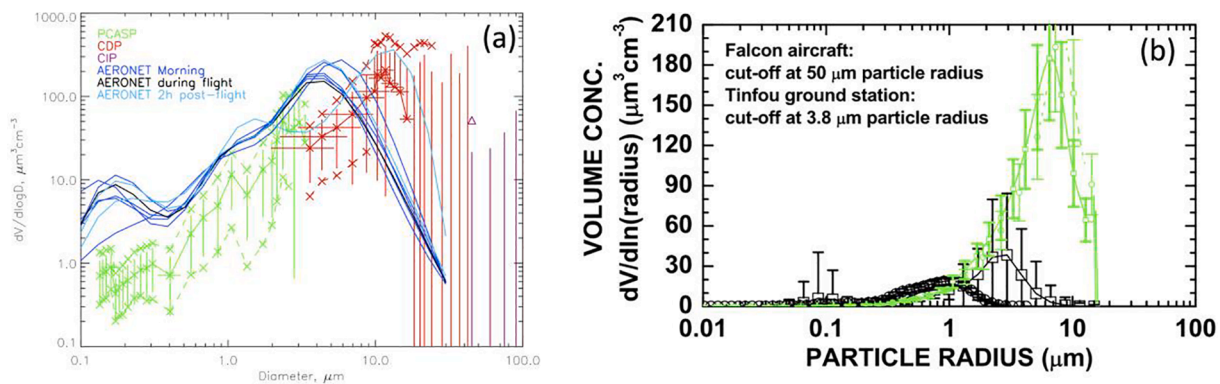


Fig. 20. AERONET-retrieved dust size distributions are substantially finer than near-coincident aircraft measurements. (a) The dust volume size distribution ($dV/d\log D$) as a function of particle diameter (D) acquired during the Fennec campaign close to the Zouerate AERONET site (Ryder et al., 2015), where aircraft data show the median size distribution measurements across altitudes from 80 m to 5.5 km. (b) The dust size volume distribution ($dV/d\ln R$) as a function particle radius (R) during the SAMUM campaign above the Ouazazate-airport AERONET site (Müller et al., 2010). The second figure (b) includes the AERONET values (black squares), in-situ measurements taken on the ground (back circles), which exclude particles larger than 3.8 μm radius, and in-situ aircraft measurements at 3247 m (green circles) and 4853 m (green boxes) altitude. Images are adapted, with permission, from Ryder et al. (2015) and Müller et al. (2010).

dusty cases and 95 % of cases when AOD was greater than 0.1, principally due to the high AOD variability. Besides reducing dust-storm AOD by a factor of 2 in these cases, such findings have implications for the coarse dust size distribution retrieved at AERONET sites close to dust sources, where AOD is likely to have high temporal variability. In these cases, a large proportion of retrievals may be removed from the record due to misclassification of dust as clouds, further hampering the effort to constrain coarse dust size distribution close to emission.

A lack of realistic dust optical models has been a persistent issue for all aerosol remote-sensing techniques. The look-up table for the Version 1 AERONET retrieval algorithm assumed spherical dust particles (Dubovik and King, 2000). This assumption creates an artificial fine mode component in the retrieved dust size distribution as well as an unrealistic spectral change in the real part of the retrieved dust refractive index (Dubovik et al., 2002). The Version 2 AERONET algorithm adopts a mixture of spheroids to model dust optics, which resolves the main issues with the Version 1 algorithm and helps distinguish non-spherical dust from the preponderance of spherical particles in the atmosphere (Dubovik et al., 2006). However, to reach agreement at all wavelengths, different shape distributions are retrieved at different wavelengths (Dubovik et al., 2006), indicating that the spheroid shape distribution does not adequately represent actual atmospheric dust particles (Nousiainen and Kandler, 2015; Huang et al., 2020). In addition, the maximum possible diameter in AERONET size distribution retrievals is 30 μm (Fig. 20) and the tails of the size distributions are constrained to very small magnitudes (Hashimoto et al., 2012), with large errors (Dubovik et al., 2000). For comparisons between aircraft and AERONET retrievals, it is important that the aircraft data are sampled and averaged vertically, as AERONET retrievals aggregate aerosol over the entire atmospheric column. Comparisons are further complicated logistically by potential flight limitations very close to AERONET sites, as well as the occurrence of good atmospheric conditions for comparisons, which must include (1) cloud-free skies, (2) homogeneously distributed aerosol in both the horizontal and the vertical, as aircraft sample more space than the single column above the AERONET site, and preferably (3) reasonable dust loadings. Future work on precise one-to-one comparisons is also needed in addition to more realistic dust optical models (Fig. 20).

5.1.2. Passive satellite instrument retrievals of coarse and super-coarse dust aerosols

Broad-swath, single-view, multi-spectral imagers such as the Moderate resolution Imaging Spectroradiometer (MODIS) are most effective at distinguishing fine-mode-dominated from coarse-mode-dominated aerosol over dark water. This sensitivity has been used to separate

coarse-mode “dust” aerosol air masses from fine-mode smoke, pollution, and other aerosol air mass types over the Atlantic Ocean (Kaufman et al., 2005). An empirical partitioning of aerosol types, for example, to account for the contributions of dust to fine mode and of sea salt to coarse mode, helps improve the identification of dust components with this approach (Kaufman et al., 2005; Yu et al., 2009).

Multi-angle, multi-spectral imaging allows for better surface-atmosphere separation, and also helps distinguish the scattering-angle dependence of spherical particle reflectance from that of non-spherical particles, of which dust is the primary atmospheric component (Kalashnikova and Kahn, 2006; Kahn and Gattley, 2015). As the Multi-angle Imaging SpectroRadiometer (MISR) instrument flies aboard NASA’s Terra satellite together with MODIS, the more sensitive MISR multi-angle dust retrievals have been used to refine the interpretation of the MODIS fine mode versus coarse dust particle distinctions, to then take advantage of the much greater MODIS spatial-temporal coverage over the northeast Atlantic region (Guo et al., 2013). MISR multi-angle imagery is also used to derive plume heights and the associated wind vectors geometrically, and such observations can help locate dust sources over the Middle East and North Africa (Yu et al., 2018).

UV imagers such as the Total Ozone Mapping Spectrometers (TOMS), the Global Ozone Monitoring Experiment (GOME), the Ozone Mapping Instrument (OMI), and Ozone Mapping and Profiler Suite (OMPS) are sensitive to the shortwave light-absorption properties of many mineral dust types. They have the advantage of low sensitivity to surface reflectance in most cases, and so can offer good retrievals over land, but the estimates of aerosol column amount are qualitative and also depend on the aerosol layer height (Herman et al., 1997; Prospero et al., 2002; Torres et al., 2007). Imaging from MODIS using the “Deep Blue” technique has also mapped dust plumes in North Africa (Ginoux et al., 2010). Distinguishing dust from other UV-absorbing aerosol species requires observations at longer wavelengths, input from aerosol transport modeling, or context-related constraints from other sources.

Although satellite aerosol retrieval algorithms detect the total column AOD for all particle sizes at whatever wavelength is measured, they are most sensitive to those particles for which the variable $\times \left(= \frac{2\pi r}{\lambda} \right) \sim 1$, where r is the particle radius and λ is the wavelength of observation. MODIS, VIIRS, and other visible and near-infrared (VNIR) imagers use wavelengths no longer than about 1.6 μm (and only 876 nm for MISR) to characterize aerosols (e.g., Levy et al., 2013), so they are most sensitive to particles no larger than about 2.5 μm in diameter. (Note that the MODIS dark target algorithm uses a 2.3 μm channel to help characterize the surface for their aerosol retrievals). In practice, the exceptions are passive sounding instruments that sample the thermal infrared (TIR)

spectrum between about 3.7 and 15.5 μm , such as NASA's Atmospheric InfraRed Sounder (AIRS) and EUMETSAT's Infrared Atmospheric Sounding Interferometer (IASI), along with infrared imagers such as the European Space Agency's Spinning and Enhanced Visible and InfraRed Imager (SEVIRI). Particle extinction cross-sections diminish greatly as $\times \ll 1$, so measurements at these longer wavelengths are preferentially sensitive to particles greater than 2.5 μm in diameter, compared to the smaller particles that are generally more abundant in the atmospheric column. Such large particles dominate mainly in dust plumes.

Accordingly, both AIRS and IASI have been used to track large-scale transports of particles from major dust source regions across the ocean during both day and night (DeSouza-Machado et al., 2006; Cuesta et al., 2015, 2020). Dust sources have been mapped over the North African deserts with SEVIRI, which observes the region every 15 min from its geostationary vantage, allowing nascent sources to be pinpointed before the ensuing plume obscures the surface over larger areas (Schepanski et al., 2007). The TIR retrievals require having the atmospheric temperature profile, which can introduce uncertainties (e.g., Brindley et al., 2012), but also allows the aerosol layer height to be estimated. Near-source retrievals face additional challenges, in part because the temperature and emissivity of dusty land surfaces are often poorly constrained, making it difficult to account for the surface contribution to the top-of-atmosphere signal, and in part, because multiple scattering due to relatively high particle concentrations, combined with the challenge of modeling non-spherical particle scattering properties, further increase retrieval uncertainty. A comparison of VNIR AOD retrievals from MISR and MODIS and TIR retrievals from IASI and SEVIRI over North Africa shows that MODIS and IASI tend to perform best at lower AOD, whereas the SEVIRI TIR method performs best at higher AOD, and SEVIRI along with MISR perform best over bright surfaces, when compared to AERONET. In addition, sensitivity to surface emissivity, elevation, and moisture also affect the performance of different techniques (Banks et al., 2013).

In general, passive aerosol remote sensing can be affected by cloud contamination, which is especially problematic for instruments with coarse pixel resolution, such as most space-based UV imagers to date. Surface characterization can introduce substantial uncertainty for VNIR aerosol retrievals, especially over bright land surfaces, such as deserts. For dust, in particular, passive remote sensing is also limited by a lack of good optical models for mineral dust. This is due to the difficulty in modeling light-scattering by non-spherical particles, the complexity of dust particle shapes, a lack of information about particle indices of refraction at all wavelengths, and the diversity of mineral dust types from major sources. Collecting adequate samples of airborne dust for laboratory measurements is also challenging, due to the low efficiency of aircraft particle collection inlets. Modeling non-spherical dust optical properties is an area of current research (Legrand et al., 2014; Granados-Muñoz et al., 2016; Lee et al., 2017; Saito et al., 2021).

5.1.3. Lidar retrievals of coarse and super-coarse dust aerosols

One of the difficulties of ground-based AERONET and satellite passive-remote-sensing instruments is the inability to characterize the vertical distribution of aerosol properties. The combination of vertical dust profiling with lidar and spectrally resolved observations with sun and sky photometers, preferably in networks such as AERONET (Holben et al., 1998), MPLNET (Micro-Pulse Lidar NETwork) (Welton, 2001), and EARLINET (European Aerosol Research Lidar Network) (Pappalardo et al., 2014), seems to be an ideal addition to space-borne monitoring of dust outbreaks and (intercontinental) long-range dust transport. Retrieval techniques such as LiRIC (Lidar and Radiometer Inversion Code) (Chaikovskiy et al., 2016) and GARRLiC (Generalized Aerosol Retrieval from Radiometer and Lidar Combination) (Lopatin et al., 2013) have been developed and are summarized in a recent article of

Lopatin et al. (2021). The GARRLiC algorithm is integrated into the GRASP (Generalized Retrieval of Atmosphere and Surface Properties) approach (Dubovik et al., 2011, 2014) and inverts both photometric and lidar observations.

An important limitation of all these combined techniques results from the use of the spheroidal shape model to describe the irregular shape of natural dust particles in forward modeling approaches in the framework of the GARRLiC/GRASP data analysis. The simulated spectra (355–1064 nm) of dust backscatter, lidar ratio and depolarization ratio disagree with the lidar observations of dust optical properties at exactly 180.0° (Müller et al., 2010, 2012; Shin et al., 2018; Saito et al., 2021; Haarig et al., 2022). Sophisticated modeling studies comparing the impact of very different shape models on the lidar observations corroborate the results from laboratory and field studies (Gasteiger et al., 2011; Lindqvist et al., 2014; Kemppinen et al., 2015; Järvinen et al., 2016; Saito et al., 2021). This is a source of uncertainty that must be overcome by introducing more realistic dust shape models into the GARRLiC/GRASP computations. The use of the spheroidal model can be regarded as a first (but important) step only on the way toward an adequate, more realistic consideration of the complex dust shape characteristics in dust optical property forward modeling. Further limitations of these combined lidar-photometer methods arise from the fact that clear skies during the sun photometer observations are required; even a thin cirrus deck prohibits any trustworthy dust retrieval. Furthermore, complex vertical aerosol layering and complex mixtures of aerosols varying with height (i.e., different mixtures in the boundary layer and in lofted layers above) cannot be resolved. Examples are discussed by Tsekeri et al. (2017).

The traditional polarization lidar technique (presented in an easy-to-follow way by Tesche et al. (2009) combined with the recently introduced POLIPHON (Polarization Lidar Photometer Networking) extension (Mamouri and Ansmann, 2016, 2017) provides an alternative approach to precisely monitor dust layers, to retrieve height profiles of dust mass, volume, and surface area concentration, and to estimate cloud-relevant properties such as cloud condensation nucleus and ice-nucleating particle concentrations. Active remote sensing allows height-resolved dust observations even under cloudy conditions, so that field studies of aerosol-cloud interactions that focus on the role of dust in cloud evolution and precipitation processes, an important contribution to weather and future climate predictions, become possible (e.g., Ansmann et al., 2019a). The POLIPHON method is fully based on measured dust input parameters (dust depolarization ratio, dust lidar ratio). No dust shape model is required.

In the promising polarization lidar technique, a laser transmits linearly polarized laser pulses and collects the co- and cross-polarized lidar return signal components. The ratio of cross-to-co-polarized particle backscattering is denoted as the particle linear depolarization ratio (PDR). Ensembles of non-spherical desert dust particles cause a large depolarization ratio of about 0.3 at 532 nm and can easily be detected and separated from non-dust particles such as spherical marine, haze, and biomass-burning smoke aerosols that produce low depolarization ratios (PDR < 0.05). The latest dust-related applications, using the spaceborne CALIPSO polarization lidar, are presented by Marinou et al. (2017) and Proestakis et al. (2018). In the separation of dust and non-dust aerosol (Tesche et al., 2009), a PDR of 0.31 for dust and 0.03 for non-dust is assumed. The CALIPSO aerosol typing approach (Kim et al., 2018), which distinguishes dust layers (showing PDR > 0.2), dusty marine aerosol over the Oceans (PDR from 0.075 to 0.2), and polluted dust (mainly over land, PDR from 0.075 to 0.2), can produce only a rough identification of dust-containing aerosol layers.

Recently, the application spectrum of the polarization lidar technique was broadened by introducing a method for estimating the dust mass concentration profiles for particles that are finer than 1 μm and

those that are coarser than 1 μm (Mamouri and Ansmann, 2014, 2017). The method makes use of the laboratory studies of Sakai et al. (2010) and Järvinen et al. (2016) which were corroborated by modeling studies (Gasteiger et al., 2011; Saito et al., 2021). In the laboratory studies it was found that fine-dust-dominated particle ensembles cause particle depolarization ratios of about 0.14–0.18 at 532 nm (Sakai et al., 2010; Järvinen et al., 2016) and dust dominated by coarse mode leads to dust depolarization ratios close to 0.39–0.4 (Sakai et al., 2010). Near-dust-source lidar observations also point to a high coarse-mode-related depolarization ratio close to 0.4 at \sim 532 nm (Burton et al., 2015; Veselovskii et al., 2016; Hofer et al., 2020; Hu et al., 2020). Similar contrasting features hold for the other important laser wavelengths of 355 and 1064 nm. Note again that the measured overall (fine + coarse) 532 nm dust PDRs are typically around 0.3 (Freudenthaler et al., 2009; Groß et al., 2011; Tesche et al., 2011; Groß et al., 2015; Haorig et al., 2017; Hofer et al., 2020). All this information can now be used to estimate fine and coarse dust fractions. A first example was shown by Ansmann et al. (2017). It was found that the removal of dust from the atmosphere was too strong for large transport paths in the simulations and the modeled fine-to-coarse dust ratio (in terms of mass concentration and light extinction) was much too high in the models compared to the observations.

After separating dust and non-dust aerosol components based on optical properties, conversion into mass, volume, and surface area concentrations remain to be carried out, by using conversion factors derived from long-term AERONET climatologies collected at desert stations (Ansmann et al., 2019b). The POLIPHON methodology can be applied at all three aerosol lidar wavelengths (355, 532, and 1064 nm). The POLIPHON methodology has been fully tested and applied in several field campaigns (Ansmann et al., 2017; Mamouri and Ansmann, 2017; Mamali et al., 2018; Marinou et al., 2019). Extensive comparisons with in situ aircraft observations of dust size distributions, fine and coarse dust volume concentrations, and dust and non-dust fractions as they are available from several field campaigns in Morocco (2006), Cabo Verde (2008), Barbados (2013) and Cyprus (2017) are required as a next step. Furthermore, additional laboratory and modeling studies (for all three laser wavelengths) regarding the fine-mode and coarse-mode depolarization and lidar ratios are desirable.

Uncertainties in dust monitoring arise from the fact that several non-dust aerosol components can depolarize linearly polarized laser light. These aerosol types are dry marine particles (in the upper part of the marine boundary layer) (Haorig et al., 2017), wildfire smoke in the upper troposphere and lower stratosphere (Burton et al., 2015; Haorig et al., 2018; Hu et al., 2020), pollen aerosol in the boundary layer (Shang et al., 2020; Bohlmann et al., 2021), and volcanic ash. This additional contribution to the particle depolarization ratio can be erroneously interpreted as a dust contribution. An additional aerosol fluorescence channel may help to overcome such biases, because in contrast to dust particles, pollen and wildfire smoke produce a significant aerosol fluorescence backscatter signal (Veselovskii et al., 2021, 2020).

5.2. The limitations in modeling coarse and super-coarse dust aerosols

Because of the limitations in the in-situ and remote-sensing observation of coarse and super-coarse dust aerosols in the atmosphere (Sections 3 and 5.1), constraining dust processes in models that account for accurate representation of coarse dust properties have been a difficult task. Several recent studies that compared global model simulations against measurements showed that most models underestimate the abundance of coarse and super-coarse dust aerosols in the atmosphere (Ansmann et al., 2017; Adebisi and Kok, 2020; Meng et al., 2022; Drakaki et al., 2022). This underestimation is largely attributed to inadequate representation of the emission, transport, and deposition of coarse and super-coarse dust aerosols. In this section, we discuss the issues and limitations in modeling coarse and super-coarse dust emission, transport and deposition processes (Sections 5.2.1 and 5.2.2).

5.2.1. Limitations in modeling emission of coarse and super-coarse dust aerosols

Dust of all sizes is emitted predominantly through the process of saltation, in which strong winds pick up sand-sized particles (\sim 75–500 μm) that undergo ballistic trajectories (Gillette, 1979; Shao et al., 1993; Kok et al., 2012). The energetic impacts of these particles on the soil bed rupture the interparticle bonds that glue most dust-sized particles in soils to surrounding particles, resulting in the emission of fine, coarse and super-coarse dust aerosols. The resulting vertical flux of dust thus depends on the properties of the soil bed, the turbulent wind, and the presence of obstacles that shelter the soil bed from the full force of the wind by absorbing a portion of the wind momentum (Raupach et al., 1993; Marticorena and Bergametti, 1995; Shao, 2001; Menut et al., 2013; Kok et al., 2014; Comola et al., 2019).

The size distribution of the emitted dust flux depends in large part on the patterns in which interparticle forces between particles rupture due to the impacts of saltating particles. For fine and coarse dust ($D \leq 10 \mu\text{m}$), theory and measurements indicate that the emitted size distribution is consistent with what would be expected if most dust is emitted through the fragmentation of brittle soil aggregates (Kok, 2011a; Huang et al., 2021; Meng et al., 2022). Moreover, measurements from around the world indicate relatively small variability in the emitted dust size distribution due to differences in wind speed (Gillette et al., 1974; Kok, 2011b; Shao et al., 2020; Wang et al., 2021), atmospheric stability (Khalfallah et al., 2020), fetch length (Dupont et al., 2015; Fernandes et al., 2019), and soil properties (Alfaro and Gomes, 2001; Shao, 2001; Kok, 2011a; Wang et al., 2021). Indeed, these variations are largely within the systematic error between different experimental data sets (Kok et al., 2017), which considerably simplifies the parameterization of the emitted dust size distribution in global models. However, more measurements are needed to better understand and parameterize the emitted size distribution of fine and coarse dust.

The emission of super-coarse and giant dust ($D > 10 \mu\text{m}$) is considerably more uncertain than that of fine and coarse dust ($D \leq 10 \mu\text{m}$). This is because of both difficulties in obtaining accurate measurements and because the emission process is more complex. Super-coarse and giant dust particles are difficult to measure because their substantial inertia causes large fractional losses in inlets and during subsequent transmission to particle samplers (Hinds, 1999; von der Weiden et al., 2009; Ryder et al., 2013b). Consequently, there are fewer measurements of emitted dust size distributions for super-coarse and giant dust than for finer dust (Fig. 21). However, over the past decade or so, substantially more measurements of super-coarse and even giant dust have been made (Table 2 and Section 3), especially by research aircraft using wing probes, which are not affected by inlet losses (Ryder et al., 2013b; Rosenberg et al., 2014; Ryder et al., 2019; Sanchez-Marroquin et al., 2019) although they may be affected to a lesser extent by airflow and shattering (Spanu et al., 2020).

In addition to the difficulties in measuring super-coarse and giant dust, the physics of their emission is also more complex. As mentioned above, theory and measurements suggest that the emission of finer dust is dominated by brittle fragmentation processes for soils with sufficient fine particle content to form brittle soil aggregates (excluding, for instance, emissions from sand dunes; Huang et al. 2019; Swet et al. 2020). However, for super-coarse and giant dust, the contribution of other processes could become more important, which could also cause the emitted dust size distribution to depend more strongly on soil properties and wind speed than it does for finer dust. These additional processes include aerodynamic lifting (Klose and Shao, 2012; Klose et al., 2014) and ejection (without fragmentation) of discrete soil particles by saltating particles (Kok, 2011a). Furthermore, super-coarse, and giant dust have substantial terminal fall speeds of the order of 0.5–50 cm/s, which complicates the calculation of the emitted dust size distribution from measurements of the gradient in the size-resolved dust concentration near the surface (Gillette et al., 1972; Shao, 2008; Dupont et al., 2015; Fernandes et al., 2019). Additionally, the large gravitational

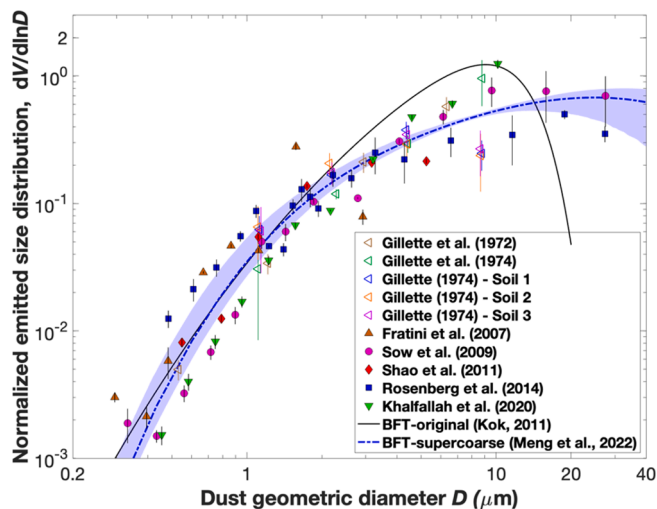


Fig. 21. Compilation of measurements of the size distribution of emitted dust aerosols. Different markers denote observations of the emitted dust size distribution from different studies, which were processed and corrected to geometric diameter as detailed in Huang et al. (2021). Vertical error bars denote the standard error of measurements under various wind events at a given soil (see Kok et al., 2017). Shown for comparison are the parameterization of the size distribution of emitted dust aerosols obtained using brittle fragmentation theory (BFT-original; Kok, 2011a,b) and the updated brittle fragmentation theory parameterization that accounts for emission of super-coarse dust (BFT-super-coarse; Meng et al. 2022). The updated parameterization reproduces measurements of the large contribution to the emission flux by super-coarse dust; however, very few measurements are available. Blue shading denotes the 68 % confidence interval. All curves are normalized to yield unity when integrated over the 0.1–20 μm diameter range. After Meng et al. (2022).

settling velocity of coarse dust impedes its vertical transport out of the near-surface layer. Consequently, aircraft measurements indicate that topography can strongly enhance the vertical transport of super-coarse and (especially) giant dust particles (Rosenberg et al., 2014). Large Eddy Simulations confirm this finding and indicate that the enhanced vertical transport of super-coarse and giant dust occurs because of a number of factors, including upward flow on the uphill slope driving vertical transport and increased vertical dispersion in the wake of crests (Heisel et al., 2021). Most of these processes affecting the emission and vertical transport of super-coarse and giant dust are not represented in current model parameterizations of dust emission, which likely underestimate the emission of super-coarse dust (Huang et al., 2021; Kok et al., 2021a), although an updated parameterization of the emitted dust size distribution using brittle material fragmentation seems to at least partially resolve this problem (Meng et al., 2022). Nonetheless, more studies are required to understand, parameterize, and model the emission of super-coarse and giant dust.

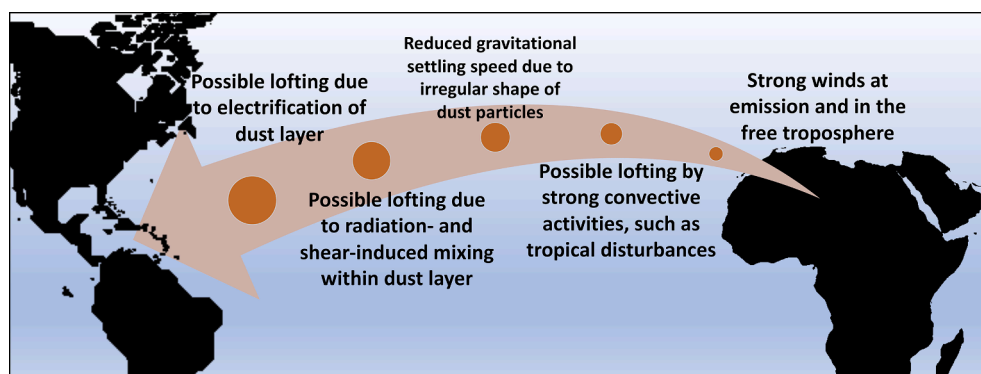


Fig. 22. Schematic summarizing some conditions that contribute to long-range transport of coarse and super-coarse dust aerosols from North African dust sources. These conditions could also apply to long-range transport from other major dust sources. While not included in the figure, frontal motions, and large overturning circulations such as the Walker and monsoon cells can also influence long-range dust transport, but they are reasonably well-resolved in most regional and climate models. Note that the arrow suggests only the transport of North African dust over the Atlantic Ocean and not the succession of processes or conditions highlighted in the image.

5.2.2. Limitations in modeling transport and deposition of coarse and super-coarse dust aerosols

Model underestimation of coarse and super-coarse dust particles is relatively larger after long range transport than when close to dust sources (e.g., Adebisi and Kok, 2020; Drakaki et al., 2022; Meng et al., 2022), evidencing that models predict coarse dust to fall out of the atmosphere more quickly than observed (e.g., Maring et al., 2003; Ansmann et al., 2017; Weinzierl et al., 2017; Drakaki et al., 2022; Meng et al., 2022). Traditionally, dust particles in the coarse to giant size range are expected to sediment quickly (e.g., Seinfeld and Pandis, 2006). Therefore, these particles can only stay in the atmosphere for longer periods and be subject to long-range transport, if some mechanisms counteract the gravitational force on them (e.g., Fig. 22).

Such mechanisms, that result in ascending motions and counteracting the gravitational force on dust particles, can occur at various spatial scales. For example, radiation-induced or shear-induced turbulence and vertical mixing can occur at the scale between ~ 10 – 100 m both in the boundary layer or in the elevated dust layer (e.g., Gutleben et al., 2020; Ryder, 2021). In addition, other mechanisms from dust shape, electrical forces in regions of substantial dust loading, moist convective activities (~ 10 km), frontal circulations (~ 100 km) to large overturning circulations such as the Hadley, Walker and monsoon cells (~ 1000 km) can influence dust long-range transport. For mechanisms of larger spatial scales (order of km), their impacts on long-range transport may strongly depend on the dust source and season. For example, higher-latitude sources such as the Taklimakan and Gobi deserts are often affected by springtime cold fronts associated with extratropical cyclones, allowing a relatively fast transport into upper-tropospheric levels (e.g., Wiacek et al., 2010). In contrast, for lower-latitude sources, such as the southern Sahara and Sahel, dust emission is more commonly caused by the strong winds associated with the pressure gradients at the equatorward edge of subtropical highs, particularly in the winter half of the year (e.g., Knippertz, 2014). For this case, lifting of dust particles to upper-tropospheric levels mostly occurs in connection with summertime deep convection (e.g., Wiacek et al., 2010) and with deep dry convection over large deserts such as the Sahara.

In the following subsection, we focus on the processes that currently have the largest knowledge gaps and associated model limitations, simplifications, or omissions. We initially review uncertainties related to particle settling (Section 5.2.2.1). Subsequently, we discuss the potential role of turbulence (Section 5.2.2.2), moist convection (Section 5.2.2.3), and electrical forces (Section 5.2.2.4) to sustain large dust particles in the atmosphere and their current representation in models. In contrast, we do not discuss the frontal motions and large overturning circulations such as the Walker and monsoon cells in this article, because they are reasonably resolved by the meteorological components of most dust models and are therefore unlikely to contribute to the disagreements between models and observations on long-range transport of large dust particles.

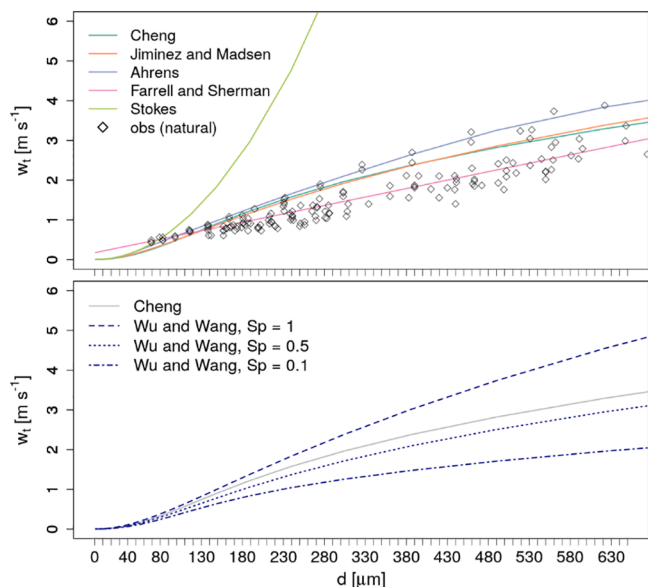


Fig. 23. (top) Particle terminal velocity w_t [m s^{-1}] as a function of particle diameter D [μm] based on experimental data (diamonds; Farrell and Sherman, 2015 and references therein) and on the theoretical or empirical relationships (lines) from Stokes (1851), Cheng (1997), Jiménez and Madsen (2003), Ahrens (2000), and Farrell and Sherman, (2015) using (where applicable) $\rho_a = 1.2 \text{ kg m}^{-3}$, $\rho_p = 2650 \text{ kg m}^{-3}$, $\nu = 1.45 \times 10^{-5} \text{ m}^2 \text{ s}^{-1}$, and $g = 9.81 \text{ m s}^{-2}$; (bottom) Impact of particle shape on w_t , obtained using the empirical expression from Wu and Wang (2006) with Corey shape factors $S_p = 1, 0.5$, and 0.1 .

5.2.2.1. Sedimentation and settling velocity. Sedimentation is a decisive process for the atmospheric lifetime of dust. The settling velocity, equilibrium fall velocity or terminal fall velocity w_t , of airborne particles is defined as the particle-to-fluid relative velocity under steady-state conditions – that is, when fluid drag forces balance the gravitational forces and the particle experiences no acceleration (Shao, 2008; Dey et al., 2019). It can be derived from the equation of motion of spherical particles in a fluid and is given by

$$w_t = \left(\frac{4\sigma_p g D}{3C_D} \right)^{\frac{1}{2}} \quad (4)$$

where $\sigma_p = \frac{\rho_p - \rho_a}{\rho_a}$ is the particle-to-fluid relative density with particle density, ρ_p , and fluid (air) density, ρ_a , g is gravitational acceleration, D particle diameter, and C_D is the drag coefficient. The latter depends on the particle Reynolds number, $Re_p = \frac{w_t D}{\nu}$, where ν is the fluid kinematic viscosity. For small Re_p , C_D decreases as $C_D(Re_p < 1) = \frac{24}{Re_p}$ (Stokesian regime), a relationship that is applicable to small dust particles ($D \lesssim 10 \mu\text{m}$). For larger Re_p , the relationship with C_D changes (transitional regime) until C_D is approximately constant for $Re_p > 10^3$ (Newtonian regime). The exact dependency between C_D and Re_p in the transitional regime has not been determined yet and experimental data show a considerable spread (e.g. (e.g., Dey et al., 2019; their Fig. 4), in particular considering different particle types (e.g. spheres versus non-spherical natural particles). As a consequence, w_t for coarse, super-coarse, and giant particles with varying particle properties is also subject to considerable uncertainty.

Most experiments on particle settling have been conducted in water. Farrell and Sherman (2015) compiled and quality-controlled the results from the few experiments that have been conducted in air using natural particles (sand; Fig. 23, top). While for $D \lesssim 100 \mu\text{m}$ the experimental data give consistent results, scatter starts to increase for larger diameters. For $D = 450 \mu\text{m}$, the approximate size of the largest particles found after long-range atmospheric transport (Betzer et al., 1988; van der Does

et al., 2018a), the observed w_t ranges between about 1.5 and 3.5 m s^{-1} , which is also reflected in the empirical relationships from Cheng (1997), Jiménez and Madsen (2003), and Ahrens (2000), reviewed by Dey et al. (2019), and Farrell and Sherman (2015). The latter predicts w_t based on D alone and compares to the observed data relatively well. This simple form can, however, also be disadvantageous, as it prevents the expression from being applied to other fluid conditions, e.g., for other planetary atmospheres. The theoretical Stokes-relationship is only applicable for small particles ($D \lesssim 10 \mu\text{m}$), but is shown here for larger particles also for illustrative purposes.

Most dust models do not currently include particles larger than 20 μm (Kok et al., 2021a) and therefore the large majority make use of the Stokes approximation. Only a few apply a correction for large particles. For example, Zender et al. (2003) use a time-invariant correction factor $C_{St} = \frac{w_t}{w_{t,St}}$ with $w_{t,St} = w_t(C_D = \frac{24}{Re})$, which is computed for each particle-size class at model start for characteristic atmospheric temperature and pressure values. Miller et al. (2006) apply a correction to particle diameter and in addition, introduce a dependency of w_t on turbulence intensity (the effects of turbulence on settling are explained below; Section 5.2.2.2). Klose et al. (2021) deploy empirical correction factors that reduce w_t for large particles to compensate for deviations from the Stokes approximation, as well as for numerical diffusion and other unaccounted factors. Tanaka and Chiba (2005) use a different approach and parameterize C_D in Eq. (4) using the empirical expression from Morsi and Alexander (1972). For small particles, models typically apply the Cunningham slip correction (Cunningham, 1910), which accounts for reduced resistance of viscosity if the particle size is of similar magnitude as the mean free path of air molecules (Zender et al., 2003; Tanaka and Chiba, 2005; Pérez et al., 2011).

The relationships shown in Fig. 23 (top) were derived for natural particles (mainly quartz sand grains), which makes them representative for particles that do not deviate far from spherical shape. Nonspherical and/or irregular particle shape leads to increased drag forces impacting on the particle and hence to a change in w_t . A common representation of particle shape is the Corey shape factor, $S_p = \frac{a_s}{(a_i^2 a_l)^{1/2}}$, where a_s , a_i , and a_l denote the shortest, intermediate, and longest axes of a particle respectively (Corey et al., 1949; Dietrich, 1982; Dey et al., 2019). Dietrich (1982) suggested that a typical coarse sand particle corresponds to $S_p \approx 0.7$. Wu and Wang (2006) related the empirical coefficients in the expression from Cheng (1997) to S_p (Fig. 23, bottom panel). The results suggest that shape can have a considerable effect on w_t in particular for particles larger than 100 μm . Expressions that take into account other measures of roundness are also available (e.g., Camenen, 2007). Indeed, some of the giant particles analyzed after long-range atmospheric transport exhibit considerable non-sphericity (Betzer et al., 1988; van der Does et al., 2018a). Ginoux (2003) calculates small reductions in settling velocities for coarse dust when assuming prolate spheroids with aspect ratios of ~ 2 , and only finds significant differences when aspect ratios are greater than ~ 5 , in comparison to spheres. Mallios et al. (2020) also show that the decrease in settling velocities scales with aspect ratio, and that vertically-oriented prolate spheroids have lower settling velocities than horizontally-oriented ones (by $\sim 23\%$ for particles of $\sim 10 \mu\text{m}$).

The description of settling for coarse to giant dust aerosols in models can also be limited by the performance of the numerical schemes used to resolve sedimentation across the vertically discretized grid. Models typically use upwind sedimentation schemes (Ginoux, 2003; Pérez et al., 2011; Rémy et al., 2019), which are conservative, positive definite, and computationally efficient but numerically diffusive. Indeed, (zero order) upwind schemes assume that both the terminal velocity and the concentration of particles are constant within the grid cell, which creates severe numerical diffusion because particles transported downward from a grid cell to the underlying one are available for transport further down during the same time step. This makes the result not only diffusive but also dependent on the time step and vertical resolution. Higher-

order methods that consider subgrid-scale vertical gradients as moments (e.g., Prather, 1986) are accurate and non-diffusive but are not used because their implementation in models is technically complex (Benduhn and Lawrence, 2013) and computationally expensive. Ginoux (2003) compared a simple explicit upwind scheme and a non-diffusive scheme that conserves the second-order moments of the spatial distribution in a dust model and showed that considering non-sphericity for dust particles is of second order compared to the impact of numerical diffusion. The diffusive treatment of sedimentation caused an underestimation of the dust mass loading by a factor 2 and of the mass of particles above $\sim 6 \mu\text{m}$ by up to two orders of magnitude in some locations. Therefore, the numerical treatment of sedimentation is critical and may be among the first aspects to address in most models to properly represent the long-range transport of coarse to giant dust aerosols. Some less diffusive, yet computationally efficient schemes have been proposed in the literature and may be considered (e.g., Kerkweg et al., 2006).

Inaccuracies in the sedimentation of coarse and super-coarse dust particles due to numerical diffusion can be further exacerbated by the common model simplifications in the representation of the dust particle size distribution (Mann et al., 2012). The dust size distribution in models is usually represented according to either a set of discrete size sections or bins (sectional approach) (Gelbard et al., 1980) or overlapping lognormal modes covering different parts of the particle size spectrum (modal approach) (Whitby, 1981), and less commonly through the method of moments (McGraw, 1997). High-resolution sectional approaches remain the most accurate but are computationally expensive because models must deal with many other types of aerosols in addition to dust, along with an increasing amount of microphysical processes determining aerosol properties that need to trace both mass and number. Using coarse-resolution sectional approaches leads to numerical diffusion in size space (Weisenstein et al., 2007) and is therefore undesirable. To reduce the computational burden, the modal approach is the most popular, but the usual simplifications apply, for example fixing the standard deviation of the modes, which causes biases in the sedimentation rates. This is particularly important for coarse to giant dust which is usually poorly represented with one single mode only (e.g., Vignati et al., 2004; Jones et al., 2022; Mann et al., 2010).

5.2.2.2. Turbulence. Turbulence in the atmosphere is most prevalent in the boundary layer. It can be triggered either thermodynamically by buoyancy, most commonly by the daytime solar heating of the surface, or mechanically by wind shear, most commonly in the vertical direction. As dust emission requires strong winds near the surface, this process is almost always accompanied by high levels of turbulence. Boundary layer turbulence is not a fully irregular process but – depending on stability and wind – coherent structures such as rolls or eddies can form. Similar to the re-circulation in convective storms discussed below (Section 5.2.2.3), these could, in principle, lead to multiple uplifts of large particles keeping them suspended for much longer than in a statistical average. However, the lifetimes of eddies are short (few hours at best) and the depth of the layer shallow (few km at best), leading to quickly decreasing probabilities for “lucky” large particles to survive. Despite all this, the fact that even giant particles are occasionally found over the open tropical Atlantic during winter, when convection and frontal uplift are absent and the dust layer is usually restricted to the lowest 2 km, suggests that a highly turbulent layer during a strong wind period alone can keep those large particles lofted for at least two days (van der Does et al., 2018a). Turbulence occasionally also occurs away from the surface, i.e., in areas of strong shear in the vicinity of jet streams or in layers of vertical instability in the free troposphere. An example for such a phenomenon was recently discussed in Gutleben et al. (2020) and Ryder (2021), where studies find evidence that long-wave radiative effects of water vapor in the mid-level Saharan air layer (SAL) over the Atlantic Ocean can cause destabilization and vertical mixing, which could contribute to keeping at least a small number of

particles aloft for longer than expected from simple arguments.

Turbulence can affect the vertical movement of dust particles in multiple ways. Models most generally represent vertical diffusion of dust assuming that, as other scalars, it follows fluid particles in the same turbulent field and should therefore be influenced by the same eddy diffusivity. However, turbulence can also directly affect settling velocity, i.e., the particle-to-fluid relative velocity, due to gravity and inertia. These effects, which are generally not considered in models, depend on relative turbulence intensity, σ/w_t , with σ being the velocity scale of the fluid (Nielsen, 1993; Stout et al., 1995; Kawanisi and Shiozaki, 2008; Dey et al., 2019). For $\sigma/w_t \gg 1$ (i.e., small particles and relatively strong fluid motions), particles tend to follow vortex trajectories (“vortex trapping”), which reduces their effective settling velocity. For $\sigma/w_t \approx 1$, particles are swept from vortex to vortex, leading to an increased downward motion (“fast tracking”). In the case of $\sigma/w_t \ll 1$, particles cross the turbulent eddies during their fall, experiencing repeated upward fluid motion for which they need longer to pass than for the downward motion (“loitering”) (Nielsen, 1993; Good et al., 2014). In addition, the increasing nonlinear behavior of the drag coefficient with the slip velocity can lead to an additional reduction in w_t in the upward flow (nonlinear drag) (Good et al., 2014). The latter effects may be most relevant for giant dust particles. More recently, the phenomenon of turbulent thermal diffusion (TTD) has been proposed based on theory (Elperin et al., 1996) and laboratory experiments (Elperin et al., 2006), although it has not been implemented in any widely used model yet. It is argued that due to inertia, particles within the eddies drift out and accumulate in regions between the eddies, which is where the pressure of the turbulent fluid is maximized. This results in a non-diffusive flux of particles in the direction of the heat flux in turbulent stratified flows. TTD scales with the temperature gradient and the eddy diffusivity coefficient as well as the particle size and density. One regional modeling study over Europe has evaluated the influence of TTD upon the fate of tropospheric aerosols (Sofiev et al., 2009), showing an increase of 5–15 % in the transport of coarse particles outside of the modeled domain, depending on the season. The relative effect of TTD on coarse particles is much stronger than that on fine aerosols because its contribution scales with the square of particle size.

When it comes to vertical diffusion, models typically follow two approaches: 1) local closure schemes that consider only adjacent vertical model levels and 2) non-local closure schemes that consider multiple levels to represent the effects of vertical mixing in the PBL. In local schemes, the turbulent dust flux is proportional to the local dust gradient and the eddy diffusivity. This is typically well suited for the free atmosphere and the PBL for neutral and stable conditions as the length scale of the eddies is typically smaller than the domain over which turbulence extends. The majority of models additionally consider non-local closure schemes for the PBL, which have been shown to better represent unstable and convective conditions, i.e., when the largest eddies can be of similar size to the depth of the PBL itself, and can transport heat upward despite localized stability maxima (Deardorff, 1972). In these schemes the non-local eddy diffusivity represents turbulent properties characteristic of the PBL. Models may underestimate the altitude of coarse particles in the PBL, i.e., before they are subject to long-range transport, due to limitations in PBL mixing schemes and/or the omission of phenomena such as the effect of subgrid-scale topography upon their vertical mixing (e.g., Rosenberg et al., 2014; Heisel et al., 2021). This could be the case, e.g., for the very deep mixing layer over the Sahara in summer (Garcia-Carreras et al., 2015). Likewise, for example, as the SAL progresses from the mixing layer to the elevated mixed layer above the marine boundary layer over the Atlantic Ocean, models may have issues representing vertical mixing. While free tropospheric local schemes may capture the shear-induced mixing in the SAL, buoyancy-induced mixing, referred to as self-lofting (e.g., Das et al., 2021), may be underrepresented due to underestimated dust absorption and underestimation of water vapor (Gutleben et al., 2020; Ryder, 2021). The former could be the result of dust size underestimation (Adebisi and Kok, 2020) and

widespread omission of LW scattering in models' radiation schemes. Another possibility is that models may not be accounting for potential non-local mixing or, if they do, might produce large errors because the structure of thermal turbulence is quite different from that in the PBL for which the non-local schemes are typically developed.

5.2.2.3. Moist convection: Strong winds associated with moist convection are a powerful mechanism to lift dust particles from the surface and transport them to great heights (Knippertz, 2014). The most prominent example is West African haboobs (Marshall and Ryder, 2021), which occur over the summertime Sahel and southern Sahara. Due to the specific atmospheric conditions in this region (thermodynamic profiles, wind shear), moist convection can organize into several hundreds of kilometers long, fast westward propagating squall-line systems (e.g., Fink and Reiner, 2003). Evaporation at the rearward, stratiform side of the storms leads to cooling, downward acceleration, and finally, a potent cold pool that undercuts the leading convection to run ahead of the system, where new convective cells can be triggered if stability is conducive. The arrival of such a cold pool is typically characterized by an abrupt jump in wind speed, temperature, moisture and visibility, creating an impressive moving wall of dust (e.g., Lafore et al., 2017). Idealized, high-resolution simulations by Takemi (2005) show that particles of 10 μm can be transported to the tropopause in such storms, both ahead and behind the leading edge but mostly towards the rear. It is conceivable that large particles could then subside and re-enter the main updraft with the rearward inflow jet, which would allow for multiple uplift cycles, as these systems have typical lifetimes of 12 h and far more than a day in extreme cases (e.g., Fink and Reiner, 2003). Once over the ocean, dust particles also experience deep uplift in tropical cyclones (Sauter and L'Ecuyer, 2017). If particles are not rained or washed out by the intense rainfall, a re-circulation – e.g., up in the eyewall, out in an outflow jet, and back in by the low-level convergent flow – would be possible, particularly as typical system lifetimes are much longer than for squall lines (van der Does et al., 2018a), however, estimate that, even under optimal conditions, at least four convective updrafts would be required for a 100 μm particle to reach the open tropical Atlantic, where such particles have been observed.

Some studies have shown the importance of convective parameterization and the subsequent scavenging for the vertical dust structure in models (Tost et al., 2010) and also for the accurate representation of dust-generating winds (Garcia-Carreras et al., 2021), which might impact the emitted size distribution. Most current dust models are too coarse to allow the explicit representation of deep convection. Most models use the traditional mass-flux schemes (Arakawa and Shubert, 1974), which are afflicted by substantial structural, parameter and process uncertainties. It has been shown that this leads to a serious misrepresentation of haboobs and thus an underestimation of the associated dust emission (Heinold et al., 2013; Pantillon et al., 2016). Due to a lack of convective organization in models, convection also tends to be more short-lived and of lower intensity, greatly reducing the potential for re-circulation of particles in a system. Tropical cyclones are represented at least in some dust models but are usually much weaker if the resolution is not fine enough.

5.2.2.4. Electrical forces: Atmospheric charging affects the dynamics of dust particles, with a vertical electrical force being able to potentially compensate for a particle's weight (Ulanowski et al., 2007). Laboratory experiments indicate that strong electric fields can keep particles suspended at higher elevations and increase the concentration of larger particles (Toth et al., 2020). Using balloon measurements, Renard et al. (2018) found large particles (>40 μm) persisting over long distances over the Mediterranean region and speculated that this was due to particle charge counteracting gravitational settling. Whether an electric field prolongs a particle's lifetime in the atmosphere depends on its polarity and the atmospheric electric field. The fair weather electric field

(order $\sim 10^2 \text{ V m}^{-1}$) is downward-directed and thus drives negatively charged particles upward, but its direction can reverse in disturbed weather (dust storm, thunderstorms), when electrical fields can increase by 2–3 orders of magnitude (Harrison et al., 2016; Nicoll et al., 2020; Daskalopoulou et al., 2021). The initial charge generated at dust emission is lost within hours (Nicoll et al., 2011), but triboelectrification, i.e. particle charging through collision in a turbulent layer with high dust concentrations, can lead to significant charge far from dust sources (Harrison et al., 2018). van der Does et al. (2018a, b) estimate the effect of charging on particle fall speed using typical numbers from the literature. In fair weather conditions the effect on particles of >10 μm is small but may become significant for larger background electrical fields. By accounting for the two distinct charging mechanisms, i.e. ion attachment and contact electrification, and assuming stagnant conditions, Mallios et al. (2022) estimate that the electrical force is more than one order of magnitude less than gravity in a 1D model, with no impact on the particles settling process. The uncertainty in these estimates, however, are large, as there are no published in-situ measurements of individual particle charges away from the surface (e.g., Nicoll et al., 2011). Another largely unexplored factor of uncertainty is the impact of particle composition with some evidence that quartz particles may charge more easily than clay minerals (Harrison et al., 2016 and references therein). A final complicating factor is that electrical fields are often enhanced in the vicinity of thunderstorms, where charge promotes the removal of dust by cloud droplets (Nicoll et al. 2011), such that convection and charging could work against each other. Given the many fundamental gaps in our knowledge in this area, electrical forces are so far not represented in any widely used dust model and therefore remain one of the great unknowns in our attempts to realistically represent the transport of coarse, super-coarse, and giant dust particles in numerical models.

6. Summary and recommendations

This review focuses on the role and impacts of large dust particles in the Earth system. While dust particle sizes span more than three orders of magnitude in diameter (Mahowald et al., 2014), the definitions and classifications of the diameter range representing coarse dust particles are not consistent across the literature (Section 2). Specifically, different studies used different dust size ranges to define coarse-mode dust aerosols (e.g., Wentworth, 1922; Whitby, 1978; Seinfeld and Pandis, 2006; Mahowald et al., 2014), which often depend on the diameter type used (e.g., Reid et al., 2003a, b; see also Section 2). To allow for consistency in future studies and across different disciplines, this review proposes a uniform classification for coarse dust particles using geometric diameters between 2.5 μm and 10 μm (Fig. 2). Furthermore, we also propose the term “super-coarse dust” and “giant” for particles with a geometric diameter between 10 and 62.5 μm , and above 62.5 μm , respectively (Fig. 2). This is because there are now several lines of observational evidence that dust particles with a diameter greater than 10 μm consistently undergo long-range transport beyond what can be explained by gravitational settling theory (e.g., Betzer et al., 1988; Jeong et al., 2014; Weinzierl et al., 2017).

These lines of observational evidence that show long-range transport of coarse to giant dust aerosols in the atmosphere include evidence from ground-based, deposition, and airborne measurements (Section 3 and Table 1). For example, coarse to giant dust particles have been measured across the Atlantic Ocean and over North America, South America, Europe, and Iceland at several ground-based in-situ and dust-deposition stations (e.g., van der Does et al., 2018a, b; Kramer et al., 2020; Barkley et al., 2021; Varga et al., 2021). In addition, measurements have also documented coarse to giant dust aerosols across the Pacific Ocean and over Asia (e.g., Betzer et al., 1988; Jeong et al., 2014). Because these observations have shown that giant dust particles can travel for thousands of kilometers (Fig. 3; e.g., van der Does et al., 2018a, b), similar transport processes can facilitate coarse and super-coarse dust particles

to travel even farther in the atmosphere. Indeed, observations now suggest the abundance of coarse and super-coarse dust particles (Fig. 4) (e.g., Ryder et al., 2019) that accounts for a substantially higher fraction of the global dust mass load than simulated in climate models (Fig. 6).

Because coarse and super-coarse dust aerosols dominate the global dust mass, they can have substantial impacts on several aspects of the Earth system (see Fig. 1). This review highlights how important coarse and super-coarse dust aerosols are to radiation, clouds, precipitation, atmospheric chemistry, and biogeochemistry. Specifically, when compared to fine dust particles (diameter, $D \leq 2.5 \mu\text{m}$) that produce a net negative direct radiative effect (cooling effect) at the top of the atmosphere (TOA), coarse and super-coarse dust aerosols produce a net positive direct radiative effect (warming effect) at TOA (Section 4.1 and Fig. 11). This is because coarse and super-coarse dust aerosols warm the climate by absorbing shortwave (SW) radiation and extinguishing longwave (LW) radiation, which dominate its scattering of SW radiation that tend to cool the climate. Furthermore, because coarse and super-coarse dust aerosols absorb SW and LW radiation, coarse dust interactions with clouds and precipitation also influence the effective dust-radiation interactions (see Section 4.2). In particular, adjustments to dust-radiation interaction occur because absorption by coarse and super-coarse dust aerosols can modify temperature and water vapor profiles which influence the distribution of clouds and precipitation and subsequently the overall radiative effect (Boucher et al., 2013; Knippertz and Stuu, 2014). Since coarse and super-coarse dust aerosols absorb more SW and LW radiation than fine dust, their abundance, and spatial distribution, therefore, determine whether the overall dust direct radiative effect is to warm or cool the global climate system.

In addition to the radiative impacts, coarse and super-coarse dust aerosols also significantly influence clouds, atmospheric chemistry, and biogeochemistry. Specifically, when coarse and super-coarse dust particles are chemically aged, they can get activated as cloud condensation nuclei at relatively low supersaturation, and therefore they can initiate precipitation sooner than it would otherwise occur (Section 4.3.1) (e.g., Feingold et al., 1999; Levin et al., 2005). At higher altitudes, coarse and super-coarse dust particles are also easily activated when compared to fine dust, and therefore they contribute a substantial fraction of the activated ice-nucleating particles (INPs), especially at temperatures above $-23 \text{ }^\circ\text{C}$ (Section 4.3.2; see also Fig. 14 and Fig. 15). Furthermore, the ability of given mineral dust to undergo chemical aging by the uptake of reactive compounds in the gas phase, by photochemistry, and by in-cloud and off-cloud processing depend on the surface area. As a result, coarse and super-coarse dust aerosols account for most of the available reactive surfaces for atmospheric processing (Section 4.3.2). For land and ocean biogeochemistry, coarse and super-coarse dust aerosols represent a critical contribution to the deposited dust particles since it supplies important nutrients such as iron and phosphorus (Section 4.4). Although coarse and super-coarse dust particles have strong impacts closer to major dust-source regions where they dominate the dust mass loading, the evidence of their long-range transport and abundance in the atmosphere suggests that their impacts likely extend beyond previously estimated (e.g., Fig. 1).

There are major challenges in observing coarse and super-coarse dust particles in the atmosphere and considerable limitations in simulating them in climate models (Table 2). Specifically, in-situ measurements are limited in the spatiotemporal coverages, and the remote-sensing instruments on the ground- or space-based platforms that can have continuous observations of atmospheric aerosols area are associated with uncertainties in their retrieval of size-resolved dust properties (Section 5.1). Because of the limitations in observing systems, constraining coarse to giant dust processes in climate models has been a major challenge. Specifically, most climate models underestimate coarse and super-coarse dust load in the atmosphere, and this underestimation can be associated with poorly-resolved or poorly-understood processes that result in too-little emission or too-fast deposition of these particles in climate models (Sections 5.1 and 5.2).

Table 3

Despite our understanding of the importance of coarse and super-coarse dust aerosols, there remain significant uncertainties and unresolved questions. We provide some recommendations here which, in our view, are critical to further understand the role of coarse and super-coarse dust aerosols in the Earth's climate system. The table describes 'What' is needed and 'How' it can be achieved.

What	How
Need to use consistent terminology of dust size classification in examining dust impacts on the Earth system.	Adhere to the dust size classification proposed in this review article (see Section 2.2).
Need improvements of existing instruments and development of new ones to accurately measure coarse dust particles in the atmosphere	Such improvements in instrumentation may include better sampling and transmission efficiency through an improved inlet and reduced pipework.
Need to obtain extensive airborne and ground-based measurements of dust size distribution to constrain dust properties in remote-sensing retrieval algorithms and model simulations.	Conduct consistent airborne field campaign measurements of dust and establish a network of permanent ground stations with state-of-the-art instruments in different dust-dominated regions, influenced by various dust sources, and where collocation with ground- and space-based remote-sensing observations are possible.
Improve limitations of dust observation in multi-angle visible, infrared (IR), and UV-absorption passive remote-sensing aerosol retrieval techniques.	Develop next-generation satellite passive remote-sensing instruments for aerosol monitoring with multi-angle observations spanning the UV to IR, with polarization sensitivity, allowing better aerosol-type discrimination under a broader range of observing conditions.
Need accurate global-scale characterization of size-resolved dust vertical distribution and occurrence with high vertical and temporal resolution to complement satellite remote sensing of aerosols.	Develop the next generation of aerosol lidar and ceilometers with polarization-sensitive channels so that a very sensitive detection and monitoring of dust outbreaks can be possible.
Identify the physical processes acting in the atmosphere which allow coarse, super-coarse, and giant dust particles to undergo long-range transport.	Perform targeted observations of dust size distributions at emission and during transport and combine them with different models to investigate, identify, and quantify the most important physical processes influencing size-resolved dust transport.
Constrain size-dependent mineralogy of mineral dust in the soil and the atmosphere	Obtain spatiotemporal observations of soil mineralogy and improve dust emission theories to estimate the emitted distribution of coarse and super coarse minerals and mineral aggregates.
Constrain direct radiative effects in the shortwave and longwave spectra, accounting for the realistic range of dust particle sizes in the atmosphere.	Use in-situ, laboratory, and remote-sensing measurements to constrain size-resolved dust optical properties in shortwave and longwave spectrum, and account for realistic dust's longwave scattering.
Investigate the broader climate responses to coarse dust, notably rapid adjustments to absorption and its effects on regional precipitation	Build on validated Earth System Model implementations of coarse dust, perform idealized perturbation simulations to isolate Effective Radiative Forcing, influences on radiative fluxes and clouds, and precipitation processes.
Quantify the cloud condensation and ice nucleating abilities of mineral dust as a function of particle size	Obtain observational constraints on size-segregate dust aerosols, and model realistic scenarios to understand the role of dust as cloud condensation and ice-nucleating particles as a function of size.
Quantify vertical transport of coarse to giant dust particles through deep convective clouds and tropical cyclones.	Measure these particles consistently in in- and outflow regions using adequate aircraft sensors.
Compare the chemical, elemental, or mineralogical composition of natural dust with uptake efficiency for different dust size classes.	Perform kinetic measurements to screen the uptake of atmospheric relevant probe gas molecules (organics, or inorganic species) with an exhaustive list of natural samples originating from different arid regions and with variable chemical compositions.

(continued on next page)

Table 3 (continued)

What	How
Improve measurements of size-resolved dust deposition, including the iron and soluble iron content in deposited coarse and super-coarse dust particles.	Establish a network of stations along major dust transport pathways to measure dust deposition and include studies of size-speciated iron and soluble iron in regions likely impacted by super-coarse mode, especially in the Southern Ocean.
Implement and evaluate coarse dust emissions, transport, and physical interactions in Earth System Models	Build on implementations in dedicated aerosol models, evaluate as part of multi-model intercomparison projects such as AeroCom, and include coarse dust physics goals in research projects, such as CMIP (Coupled Model Intercomparison Project)

Because coarse and super-coarse dust aerosols are an essential component of the Earth system, there is still a need for many additional studies in characterizing their impacts on several aspects of the Earth system. To facilitate these future studies, we offer some recommendations which are highlighted in Table 3. Overall, we conclude that an accurate representation of coarse and super-coarse properties is critical to understand the overall impacts of dust aerosols on the Earth system.

CRedit authorship contribution statement

Adeyemi A. Adebisi: Conceptualization, Formal analysis, Visualization, Methodology, Project administration, Supervision, Writing – original draft. **Jasper F. Kok:** Conceptualization, Data curation, Formal analysis, Visualization, Methodology, Supervision, Writing – original draft. **Benjamin J. Murray:** Data curation, Formal analysis, Visualization, Writing – original draft. **Claire L. Ryder:** Data curation, Formal analysis, Visualization, Writing – original draft. **Jan-Berend W. Stuut:** Formal analysis, Visualization, Writing – original draft. **Ralph A. Kahn:** Visualization, Writing – original draft. **Peter Knippertz:** Formal analysis, Visualization, Writing – original draft. **Paola Formenti:** Data curation, Formal analysis, Visualization, Writing – original draft. **Natalie M. Mahowald:** Data curation, Formal analysis, Visualization, Writing – original draft. **Carlos Pérez García-Pando:** Data curation, Formal analysis, Visualization, Writing – original draft. **Martina Klose:** Data curation, Formal analysis, Visualization, Writing – original draft. **Albert Ansmann:** Formal analysis, Writing – original draft. **Bjørn H. Samset:** Data curation, Formal analysis, Visualization, Writing – original draft. **Akinori Ito:** Resources, Writing – review & editing. **Yves Balkanski:** Formal analysis, Visualization, Writing – original draft. **Claudia Di Biagio:** Formal analysis, Visualization, Writing – original draft. **Manolis N. Romanias:** Formal analysis, Visualization, Writing – original draft. **Yue Huang:** Resources, Writing – review & editing. **Jun Meng:** Resources, Writing – review & editing.

Declaration of Competing Interest

The authors declare that they have no known competing financial interests or personal relationships that could have appeared to influence the work reported in this paper.

Data availability

Data used for most figures can be found in cited references in the caption.

Acknowledgements

A.A.A. was supported by Department of Energy's Research Development and Partnership Pilot program grant DE-SC0023033, the

University of California – Merced, and the University of California Office of the President. JFK acknowledges funding from the National Science Foundation, United States (NSF) grants 1856389 and 2151093 and the Army Research Office (cooperative agreement number W911NF-20-2-0150). CLR received funding from NERC independent research fellowship grant (NE/M018288/1). CPG-P acknowledges support from the European Research Council under the European Union's Horizon 2020 research and innovation programme (grant # 773051; FRAGMENT) and the AXA Research Fund through the AXA Chair on Sand and Dust Storms at the Barcelona Supercomputing Center. MK received funding through the Helmholtz Association's Initiative and Networking Fund (grant agreement no. VH-NG-1533). NMM acknowledges support from the US Department of Energy: DE-SC0021302. MNR acknowledge funding from CLIMDO project funded by ANR under contract (ANR-19-CE01-0008) and Labex CaPPA, funded by ANR through the PIA under contract ANR-11-LABX-0005-01, BHS acknowledges funding from the Research Council of Norway (grant nr 324556, ARIDITY). AI acknowledges funding from JSPS KAKENHI Grant Number 20H04329. BJM acknowledges support from the European Research Council (648661 MarineIce) and the Natural Environmental Research Council (NE/T00648X/1) and also thanks Alan Blyth (University of Leeds) for comments on text he contributed. RAK is supported in part by the NASA ACMAP program and by the NASA Earth Observing System Terra and MISR projects. The views and conclusions contained in this document are those of the authors and should not be interpreted as representing the official policies, either expressed or implied, of any of the funding agencies or the US Government.

Appendix A. Supplementary data

Supplementary data to this article can be found online at <https://doi.org/10.1016/j.aeolia.2022.100849> and the DustCOMM data for dust with diameter greater than 20 μm is available at <https://doi.org/10.15144/S4059V>.

References

- Abdelkader, M., Metzger, S., Mamouri, R.E., Astitha, M., Barrie, L., Levin, Z., Lelieveld, J., 2015. Dust–air pollution dynamics over the eastern Mediterranean. *Atmos. Chem. Phys.* 15, 9173–9189. <https://doi.org/10.5194/acp-15-9173-2015>.
- Abou-Ghanem, M., Oliynyk, A.O., Chen, Z., Matchett, L.C., McGrath, D.T., Katz, M.J., Locock, A.J., Styler, S.A., 2020. Significant variability in the photocatalytic activity of natural titanium-containing minerals: implications for understanding and predicting atmospheric mineral dust photochemistry. *Environ. Sci. Technol.* 54, 13509–13516. <https://doi.org/10.1021/acs.est.0c05861>.
- Ackerman, A.S., Toon, O.B., Stevens, D.E., Heymsfield, A.J., Ramanathan, V., Welton, E. J., 2000. Reduction of tropical cloudiness by soot. *Science* 288, 1042–1047. <https://doi.org/10.1126/science.288.5468.1042>.
- Adebisi, A.A., Kok, J.F., 2020. Climate models miss most of the coarse dust in the atmosphere. *Sci. Adv.* 6, eaaz9507. <https://doi.org/10.1126/sciadv.aaz9507>.
- Ahrens, J.P., 2000. A fall-velocity equation. *J. Waterw. Port Coast. Ocean Eng.* 126, 99–102. [https://doi.org/10.1061/\(asce\)0733-950x\(2000\)126:2\(99\)](https://doi.org/10.1061/(asce)0733-950x(2000)126:2(99)).
- Albani, S., Mahowald, N.M., Perry, A.T., Scanza, R.A., Zender, C.S., Heavens, N.G., Maggi, V., Kok, J.F., Otto-Bliesner, B.L., 2014. Improved dust representation in the community atmosphere model. *J. Adv. Model. Earth Syst.* 6, 541–570. <https://doi.org/10.1002/2013MS000279>.
- Alfaro, S.C., Gomes, L., 2001. Modeling mineral aerosol production by wind erosion: Emission intensities and aerosol size distributions in source areas. *J. Geophys. Res.* Atmos. 106, 18075–18084. <https://doi.org/10.1029/2000JD900339>.
- Allredge, A.L., Silver, M.W., 1988. Characteristics, dynamics and significance of marine snow. *Prog. Oceanogr.* 20, 41–82. [https://doi.org/10.1016/0079-6611\(88\)90053-5](https://doi.org/10.1016/0079-6611(88)90053-5).
- Allen, R.J., Amiri-Farahani, A., Lamarque, J.F., Smith, C., Shindell, D., Hassan, T., Chung, C.E., 2019. Observationally constrained aerosol–cloud semi-direct effects. *NPJ Clim. Atmos. Sci.* 2, 1–12. <https://doi.org/10.1038/s41612-019-0073-9>.
- Amiri-Farahani, A., Allen, J.R., Neubauer, D., Lohmann, U., 2017. Impact of Saharan dust on North Atlantic marine stratocumulus clouds: Importance of the semidirect effect. *Atmos. Chem. Phys.* 17, 6305–6322. <https://doi.org/10.5194/acp-17-6305-2017>.
- Amiri-Farahani, A., Allen, R.J., Li, K.-F., Chu, J.-E., 2019. The semidirect effect of combined dust and sea salt aerosols in a multimodel analysis. *Geophys. Res. Lett.* 46, 10512–10521. <https://doi.org/10.1029/2019GL084590>.
- Anderson, J.R., Buseck, P.R., Patterson, T.L., 1996. Characterization of the Bermuda tropospheric aerosol by combined individual-particle and bulk-aerosol analysis. *Atmos. Environ.* [https://doi.org/10.1016/1352-2310\(95\)00170-4](https://doi.org/10.1016/1352-2310(95)00170-4).

- Spectroradiometer (MODIS). *J. Geophys. Res. Atmos.* 114 <https://doi.org/10.1029/2008JD010648>.
- Yu, H., Chin, M., Yuan, T., Bian, H., Remer, L.A., Prospero, J.M., Omar, A., Winker, D., Yang, Y., Zhang, Y., Zhang, Z., Zhao, C., 2015. The fertilizing role of African dust in the Amazon rainforest: a first multiyear assessment based on data from Cloud-Aerosol Lidar and Infrared Pathfinder Satellite Observations. *Geophys. Res. Lett.* 42, 1984–1991. <https://doi.org/10.1002/2015GL063040>.
- Yu, Y., Kalashnikova, O.V., Garay, M.J., Lee, H., Notaro, M., 2018. Identification and characterization of dust source regions across North Africa and the Middle East Using MISR satellite observations. *Geophys. Res. Lett.* 45, 6690–6701. <https://doi.org/10.1029/2018GL078324>.
- Zamora, L.M., Kahn, R.A., 2020. Saharan dust aerosols change deep convective cloud prevalence, possibly by inhibiting marine new particle formation. *J. Clim.* 33, 9467–9480. <https://doi.org/10.1175/JCLI-D-20-0083.1>.
- Zein, A.E., Romanias, M.N., Bedjanian, Y., 2014. Heterogeneous Interaction of H2O2 with Arizona Test Dust. *J. Phys. Chem. A* 118, 441–448. <https://doi.org/10.1021/jp409946j>.
- Zeineddine, M.N., Romanias, M.N., Gaudion, V., Riffault, V., Thévenet, F., 2017. Heterogeneous interaction of isoprene with natural gobi dust. *ACS Earth Space Chem.* 1, 236–243. <https://doi.org/10.1021/acsearthspacechem.7b00050>.
- Zeineddine, M.N., Romanias, M.N., Riffault, V., Thévenet, F., 2018. Heterogeneous interaction of various natural dust samples with isopropyl alcohol as a probe VOC. *J. Phys. Chem. A* 122, 4911–4919. <https://doi.org/10.1021/acs.jpca.8b02034>.
- Zender, C.S., Bian, H., Newman, D., 2003. Mineral Dust Entrainment and Deposition (DEAD) model: Description and 1990s dust climatology. *Journal of Geophysical Research* 108, 4416–4416. [10.1029/2002JD002775](https://doi.org/10.1029/2002JD002775).
- Zhang, Y., Carmichael, G.R., 1999. The role of mineral aerosol in tropospheric chemistry in East Asia—a model study. *J. Appl. Meteorol. Climatol.* 38, 353–366. [https://doi.org/10.1175/1520-0450\(1999\)038<0353:TROMAI>2.0.CO;2](https://doi.org/10.1175/1520-0450(1999)038<0353:TROMAI>2.0.CO;2).
- Zhang, D., Iwasaka, Y., Shi, G., Zang, J., Matsuki, A., Trochkin, D., 2003a. Mixture state and size of Asian dust particles collected at southwestern Japan in spring 2000. *J. Geophys. Res. Atmos.* 108 <https://doi.org/10.1029/2003JD003869>.
- Zhang, L., Kok, J.F., Henze, D.K., Li, Q., Zhao, C., 2013. Improving simulations of fine dust surface concentrations over the western United States by optimizing the particle size distribution. *Geophys. Res. Lett.* 40, 3270–3275. <https://doi.org/10.1002/grl.50591>.
- Zhang, Y., Sunwoo, Y., Kotamarthi, V., Carmichael, G.R., 1994. Photochemical oxidant processes in the presence of dust: an evaluation of the impact of dust on particulate nitrate and ozone formation. *J. Appl. Meteorol. Climatol.* 33, 813–824. [https://doi.org/10.1175/1520-0450\(1994\)033<0813:POPITP>2.0.CO;2](https://doi.org/10.1175/1520-0450(1994)033<0813:POPITP>2.0.CO;2).
- Zhang, D., Zang, J., Shi, G., Iwasaka, Y., Matsuki, A., Trochkin, D., 2003b. Mixture state of individual Asian dust particles at a coastal site of Qingdao, China. *Atmos. Environ.* 37, 3895–3901. [https://doi.org/10.1016/S1352-2310\(03\)00506-5](https://doi.org/10.1016/S1352-2310(03)00506-5).
- Zhao, C., Liu, X., Leung, L.R., Johnson, B., McFarlane, S.A., Gustafson, W.I., Fast, J.D., Easter, R., 2010. The spatial distribution of mineral dust and its shortwave radiative forcing over North Africa: modeling sensitivities to dust emissions and aerosol size treatments. *Atmos. Chem. Phys.* 10, 8821–8838. <https://doi.org/10.5194/acp-10-8821-2010>.
- Zhao, C., Chen, S., Leung, L.R., Qian, Y., Kok, J.F., Zaveri, R.A., Huang, J., 2013. Uncertainty in modeling dust mass balance and radiative forcing from size parameterization 13, 10733–10753. <https://doi.org/10.5194/acp-13-10733-2013>.
- Zhao, X., Liu, X., Burrows, S.M., Shi, Y., 2021. Effects of marine organic aerosols as sources of immersion-mode ice-nucleating particles on high-latitude mixed-phase clouds. *Atmos. Chem. Phys.* 21, 2305–2327. <https://doi.org/10.5194/acp-21-2305-2021>.
- Zhou, M., Okada, K., Qian, F., Wu, P.-M., Su, L., Casareto, B.E., Shimohara, T., 1996. Characteristics of dust-storm particles and their long-range transport from China to Japan — case studies in April 1993. *Atmos. Res.* 40, 19–31. [https://doi.org/10.1016/0169-8095\(95\)00023-2](https://doi.org/10.1016/0169-8095(95)00023-2).
- Zhou, L., Wang, W., Hou, S., Tong, S., Ge, M., 2015. Heterogeneous uptake of nitrogen dioxide on Chinese mineral dust. *J. Environ. Sci.* 38, 110–118. <https://doi.org/10.1016/j.jes.2015.05.017>.